STARS

Electronic Theses and Dissertations, 2004-2019

2017

Coupling Infrastructure Resilience and Flood Risk Assessment for a Coastal Urban Watershed

Justin Joyce
University of Central Florida

COUPLING INFRASTRUCTURE RESILIENCE AND
FLOOD RISK ASSESSMENT
FOR A COASTAL URBAN WATERSHED

by

JUSTIN JOYCE
B.S. University of California, Irvine, 2012

A thesis submitted in partial fulfillment of the requirements
for the degree of Master of Science
in the Department of Civil, Environmental and Construction Engineering
in the College of Engineering and Computer Science
at the University of Central Florida
Orlando, Florida

Summer Term
2017

Major Professor: Ni-Bin Chang

ABSTRACT

This thesis sheds light on coupling potential flood risk and drainage infrastructure resilience of low-lying areas of a coastal urban watershed to flood hazards and subsequent multi-scale impacts of those hazards via detailed modeling frameworks. Physically based models along with statistical models are employed to highlight the complexity for characterizing flood risk while evaluating such risk under various levels of adaptive capacity from traditional flood management techniques to low impact development (LID), as a first step to conduct resilience assessment. Findings indicate that the coupling flood risk and infrastructure resilience is achievable by the careful formulation of flood risk associated with a resilience metric, which is a function of the hazard(s) considered, vulnerability and adaptive capacity. The results also give insights into improving existing methodologies for municipalities in flood management practices such as incorporating multi-criteria flood risk evaluation that includes resilience.

ACKNOWLEGMENTS

TABLE OF CONTENTS

LIST OF FIGURES

exposure). Normalized spatial risk for (e) LID & Dredging, (f) LID & Wall, (g) Dredging and

Wall and (h) LID, Dredging and Wall during Tropical Storm Debby on June 24th, 2012 Hour 18

LIST OF TABLES

CHAPTER 1: INTRODUCTION

1.1. <u>Impact of Flooding on Urban Areas</u>

Flood impacts over the past two decades has affected 2.3 billion people resulting in an estimated total damage cost of US $662 billion (UNISDR, 2015). The future impact and severity of such events will be exacerbated by the increasing concentration of the population in cites, with the UN-Habitat (2012) predicting that more than 70% of the world's population will live in cities by 2050. According to the National Oceanic Atmospheric Administration (NOAA), about 3.2 billion people worldwide live and work along the coast just 200 km wide, and a two-thirds of the global population are within 400 km of a coastline (NOAA, 2016). Within the United States., it is projected that by the year 2025, nearly 75% of Americans are expected to live in coastal counties (NOAA, 2016b). This causes a reason for concern such that populations are increasing closer to pathways that hold immense bodies of water which can be disturbed by changes in climate.

Future climate change impacts are expected to include a warmer atmosphere, a warmer and more acidic ocean, higher sea levels, and larger changes in precipitation patterns (Solomon et al.,2007; US EPA, 2014). Coastal regions are among the most vulnerable to these climate changes particularly when considering sea level rise, including its impacts on low-lying coastal areas, and warmer oceans which have been projected to result in stronger intensity of tropical cyclones which could be associated with greater rainfall (Knutson et al., 2010). Although, tropical cyclones represent one aspect of causes to flooding, they represent events that cause many hazards simultaneously such as rainfall runoff and storm surges, which can inundate large regions that are increasing urbanized. Examples of such impacts include Hurricane Katrina in

2005 and Hurricane Sandy in 2012 which were the costliest flood events in the US, with

respective damage costs of US $108Bn (Knabb et al. 2005) and $72Bn (Blake et al., 2013)

affecting two major urban areas New Orleans and New York City, respectively. With these

factors in mind, coastal urban regions in particular are increasingly at risk to flooding.

   1.2. <u>Defining Flood Risk</u>

       Risk, qualitatively, can be described as the likelihood of a hazard or hazards occurring

with an associated loss or negative impact. Risk in this sense is the combined effect of

probability (likelihood) and consequences from likelihood. Determination of such likelihood(s)

and consequences is dependent upon the nature of the risk considered, the number of variables

involved and the relationships between such variables considered (i.e., interdependency). For

flood risk, the determination of likelihood and associated consequences is heavily dependent

upon the hazard(s) considered which are typically multivariate in nature (Chebana and Ouarda,

2011) and could be interdependent (Wahl et. al, 2012). Flood risk is also dependent upon the

level of vulnerability to the hazard(s) considered or the propensity or predisposition to be

adversely affected or susceptibility to harm (IPCC, 2014). Flood risk, broken down further, is

also dependent on the level of exposure which is influenced by both the hazard(s) considered and

level of vulnerability. For instance, flood exposure is dependent upon the spread of hazardous

effects given the vulnerability such as proximity to waterbodies and/or physical condition of

drainage outfalls.

       Risk, however, is not static in general and particularly for flooding. Assumptions of static

or fixed risk have implications for decision-makers who typically seek to protect constituents

using fixed risk in protection measures (Sun et al., 2010; Lin et. al, 2012). The problem in fixed risk assessment is that the hazard(s) considered in flooding are highly variable (i.e., rainfall) within a given period and particularly in the future when greater uncertainty exists. Risk also is variable with the ability to recover from considered hazard(s). This ability to recover from potentially harmful or negative impacts can be associated with a particular level of resilience.

1.3. <u>Incorporating Resilience within Flood Risk Framework</u>

The concept of resilience has expanded from its origins in material science and engineering to ecological resilience (Holling, 1973) and eventually to other disciplines such as the social sciences (social resilience) and psychology (psychological resilience). When considering infrastructure systems, such as drainage under flooding, resilience is the ability of such systems to absorb disturbance (i.e. flooding) and recover after a disturbance has occurred or an ability to continue functionality under adverse conditions (Omer, 2013).

Coupling flood risk and engineering resilience is by no means an easy task. DeBruijn (2005) defined resilience, in terms of flood risk management, as the ability of a system to recover from floods. Quantitatively, this can be represented via several indicators such as the amplitude or magnitude of the reaction to disturbances, the graduality of reaction(s) under increasing disturbances and recovery rate (DeBruijn, 2005). A resilient system results in a lower amplitude of reaction to disturbances, low graduality of reaction to increasing disturbances and a higher recovery rate. Analogously this can be tied to three types of capacity of resilience, proposed by Francis and Bekera (2014), which include absorptive capacity, adaptive capacity and restorative capacity. The absorptive capacity allows for adequate buffering to absorb or contain hazard

effects while adaptive capacity is the ability to adjust or provide the necessary changes in response to adverse impacts such as when absorptive capacity has been exceeded. Restorative capacity is the ability to return to normal function or improved level of performance after a disturbance.

As with many systems, however, the absorptive capacity can fluctuate with changes in hazards such as the case when considering future flood risk. With this considered, adaptive capacity can be seen as "bridge" to restorative capacity and eventually resilience when absorptive capacity has been exceeded. Adaptive capacity can be understood as the capacity to cope and adapt to adverse effects or, from a systems approach, the extent to which a system can modify its circumstances to move to a less vulnerable condition (Luers et al., 2003). Adaptive capacity also encompasses the ability to plan, prepare for, facilitate and implement adaptation options (Klein et al., 2003) which first depend upon the nature of the disturbances or potential disturbances. Subsequently additional factors such as scale of adaptation (individual to systemic), policy, and constraints must also be considered. Klein et al. (2003) has argued the use of adaptive capacity as an umbrella concept that includes the ability to prepare and plan for hazards, as well as to implement technical measures before, during and after a hazard event. All the while, the strategy for adaptive capacity must be flexible with respect to both risk and resilience (DeBruijn, 2005) such as to the reduce rigidity in case of disruptive events (Park et al., 2013).

While adsorptive capacity can provide an "initial gauge" of toward resilience, when exceeded, failure is imminent unless adaptive measures are taken. This is particularly concerning for system design based upon a particular risk event as opposed to adapting system design to

various levels of risk. Essentially as Park et al. (2013) argued, the risk-based approach considers developing resistance to identified threats as opposed to resilience-based approaches which embrace uncertainty and failure to possible threats via anticipation and adaptation. However, in this regard, risk and resilience cannot be applied individually but must work together. Risk provides a starting point for identifying potential problems or threats at hand; however, resilience considers how progression can be maintained in the face of potential disturbances or threats.

1.4. <u>Flood Risk and Resilience in Policy and Planning</u>

Determining flood risk for urban areas under complex earth system processes poses a challenge with uncertainties often depending upon the context and sequence of preceding events. With respect to policy and planning at municipal levels, effective flood risk management through risk assessment requires consideration of alternative future scenarios with respect to flooding impact, probability of occurrence along with solutions for improving resilience.

Detailed flood control assessment covering both risk and resilience aspects at a local level is scarce. With demand for flood adaptation strategies and mitigation actions within policy and planning increasing, new opportunities can be had for incorporating useful flood risk and resilience assessment framework to formalize and implement future flood management by balancing risk assessment, resilience and adaptive measures. This is important from the advantage point of national policies related to flood risk and insurance. The National Flood Insurance Program (NFIP) aims to reduce the impact of flooding on private and public property by providing affordable insurance to property owners. The Community Rating System (CRS) of the NFIP is a voluntary program that encourages communities to adopt and enforce flood

management practices which exceed NFIP requirements as an incentive for reducing flood insurance premiums. Recommended flood management practices under CRS include flood protection measures such as structural projects along with drainage system maintenance.

1.5. Research Objectives

The objective of this thesis will demonstrate how to couple flood risk and flood resilience for a case study of a urbanized watershed by the following: (1) Expanding upon the concept of flood risk as by classifying potential flooding hazards (Chapter 2), (2) expanding upon the concept of resilience as it pertains to drainage infrastructure (Chapter 3) and (3) how to merge the concepts of flood risk and infrastructure resilience via consideration of a risk formulation and methodology which couples resilience (Chapter 4). Chapter 4 will address results of such coupling of flood risk and resilience and provide a discussion of how the results of such coupling of flood risk and resilience can aid stakeholders and/or decision-makers such as municipalities and legislators in decision making policy toward flood risk via decision criteria and metrics. Chapter 4 also concludes with overall benefits of resolving resilience within a risk framework and its implications in policy and planning.

1.6. Limitations

This work conducted within this thesis is limited to a coastal urban watershed near Tampa Bay, Florida. Some aspects of the methodology frameworks presented in this thesis are limited to the policies of municipalities governing the coastal urban watershed.

1.7. <u>References</u>

Blake, E., Kimberlain, T., Berg, R., Cangialosi, J., and Beven II, J. 2013. Tropical cyclone report: Hurricane Sandy, National Hurricane Center, National Oceanic and Atmospheric Administration, Miami, FL.

Chebana F, Ouarda, T.B.M.J., 2011: Multivariate quantiles in hydrological frequency analysis. *Environmetrics*, 22:63-78.

De Bruijn, K.M., 2005: Resilience and flood risk management. A systems approach applied to lowland rivers. PhD thesis. Delft University of Technology, Delft, The Netherlands.

Francis, R., & Bekera, B. (2014). A metric and frameworks for resilience analysis of engineered and infrastructure systems. Reliability Engineering and System Safety, 121, 90 - 103.

IPCC, 2014: Summary for Policymakers. In: Climate Change 2014: Impacts, Adaptation, and Vulnerability. Part A: Global and Sectoral Aspects. Contribution of Working Group II to the Fifth Assessment Report of the Intergovernmental Panel on Climate Change [Field, C.B., V.R. Barros, D.J. Dokken, K.J. Mach, M.D. Mastrandrea, T.E. Bilir, M. Chatterjee, K.L. Ebi, Y.O. Estrada, R.C. Genova, B. Girma, E.S. Kissel, A.N. Levy, S. MacCracken, P.R. Mastrandrea, and L.L. White (eds.)]. Cambridge University Press, Cambridge, United Kingdom and New York, NY, USA, pp. 1-32.

Holling, C.S., 1973: Resilience and stability of ecological systems. Annual review of ecology and systematics, 1–23.

Klein R.J.T, Nicholls R.J., and Thomalla F.T., 2003: Resilience to natural hazards: how useful is this concept? *Environ Hazards* 5:35–45. doi:10.1016/j.hazards.2004.02.001

Knabb, R., Rhome, J. and Brown, D., 2005: Hurricane Katrina : August 23-30, 2005, Tropical Cyclone Report.

Knutson, T.R. et al., 2010: Tropical Cyclones and Climate Change, *Nature Geosci 3.3*: 157-163.

Lin, N., K. Emanuel, M. Oppenheimer, and E. Vanmarcke (2012), Physically based assessment of hurricane surge threat under climate change, Nature Climate Change, 2(6):462–467

Luers, A.L., Lobell, D.B., Sklar, L.S., Addams, C.L, Matson, P.A., 2003: A method for quantifying vulnerability, applied to the agricultural system of the Yaqui Valley, Mexico. *Global Environmental Change* 13:255-267.

NOAA, 2016. The Coastal Population Explosion. Available online at [http://oceanservice.noaa.gov/websites/retiredsites/natdia_pdf/3hinrichsen.pdf]

Omer. M., 2013: The resilience of networked infrastructure systems. World Scientific.

Park, J., Seager, T. P., Rao, P. S. C., Convertino, M. and Linkov, I., 2013: Integrating Risk and Resilience Approaches to Catastrophe Management in Engineering Systems. Risk Analysis, 33: 356–367. doi:10.1111/j.1539-6924.2012.01885.x

Solomon, S., Qin, D., Manning, M., Alley, R. B., Berntsen, T., Bindoff, N. L., Chen, Z., Chidthaisong, A., Gregory, J. M., Hegerl, G. C., Heimann, M., Hewitson, B., Hoskins, B. J., Joos, F., Jouzel, J., Kattsov, V., Lohmann, U., Matsuno, T., Molina, M., Nicholls,

N. Overpeck, J., Raga, G.,Ramaswamy, V., Ren, J., Rusticucci, M., Somerville, R,
Stocker, T. F., Whetton, P., Wood, R. A.,and Wratt, D. (2007). Technical Summary. In:
Climate Change 2007: The Physical Science Basis. Contribution of Working Group I to
the Fourth Assessment Report of the Intergovernmental Panel on Climate Change
[Solomon, S., D. Qin, M. Manning, Z. Chen, M. Marquis, K.B. Averyt, M. Tignor and
H.L. Miller (eds.)]. Cambridge University Press, Cambridge, United Kingdom and New
York, NY, USA

Sun, S.A., Djordjevic, S., and Khu, S. T., 2010: Decision making in flood risk based storm sewer
network design. NOVATECH, 1-10.

UNISDR, 2015. The Human Coast of Weather Related Disasters 1995-2015, UNISDR, Geneva,
Switzerland.

UN-Habitat, 2012. State of the World's Cities 2012/2013, Prosperity of Cities: State of the World's
Cities.

US EPA (2014). Future Climate Change. Available online [http://www.epa.gov/climatechange/
science/future.html]

Wahl, T., Mudersbach, C. and Jensen, J., 2012: Assessing the hydrodynamic boundary
conditions for risk analyses in coastal areas: a multivariate statistical approach based on
Copula functions. *National Hazards and Earth Syst. Science*, 12, 495–510.

CHAPTER 2: IMPACT OF HURRICANES, STORM TIDAL SURGE, SEA LEVEL RISE AND PRECIPITATION VARIABILITY ON FLOOD ASSESSMENT IN A COASTAL URBAN WATERSHED

2.1. <u>Introduction</u>

The Tampa Bay Region in Florida, faces threat to several types of flood hazards including high tide events and rainfall runoff from storm events. Consideration of these potential flood impacts requires the need for developing an integrated modeling system that can communicate much needed information to government agencies to make informed decisions on potential flooding of their constituent areas and its effects on local policy.

Combining these present hazards with future climate change scenarios such as storm surges associated with a major tropical cyclonic event, tropical cyclone associated rainfall and SLR (Tampa Bay Climate Science Advisory Panel, 2015) make the Tampa Bay region particularly vulnerable to flooding. The Tampa Bay region is already experiencing SLR when considering NOAA gage tidal records (NOAA, 2016). While the region has been spared a direct-hit by a major hurricane since 1921 (National Weather Service, 2015), the possible impacts of a hurricane making landfall in Tampa Bay has been the hot topic of discussion for researchers and agencies alike [Weisberg and Zheng (2006); Weisberg and Zheng (2008); Tampa Bay Regional Planning Council (2009); Huang et al. (2010)]. These current and future hazards can contribute to potential flooding in low-lying inland areas within the region. These concerns have also been reflected on the policy level with modifications to Florida's comprehensive planning law [Florida Statute Sect. 163.3178(2)(f)] in 2015, pertaining to coastal management, that highlights requirements in development and redevelopment efforts to reduce the flood risk by considering

"high-tide events, storm surge, flash floods, stormwater runoff, and the related impacts of sea-level rise." Development and redevelopment efforts to reduce flood risk, however, cannot be made without considering the elements of risk.

Risk in this context can be described as the likelihood of a flood hazard occurring with an associated loss or negative impact. Hazards can be thought of as physical manifestations or occurrences of adverse events and exposure as the elements that are negatively affected by hazards. Vulnerability can be summarized as the propensity or predisposition to be adversely affected (IPCC, 2014). Flood inundation mapping can be a useful tool for not only determining extent of flooding due to hazards considered but can also be useful in highlighting vulnerable areas and determining exposure. Extent of flood inundation, however, can vary with a particular storm surge hazard or hazards considered along with hydrologic and hydraulic interactions.

Weisberg and Zheng (2006) investigated the storm surge responses of the Tampa Bay region and its sensitivities to point of landfall, direction and speed of approach, and intensity of cyclonic events to delineate the worst case scenario tropical cyclone amongst those factors. Weisberg and Zheng (2008) also investigated the storm surge response of the Tampa Bay region to hypothetical direct hit by a Hurricane Ivan-like storm. This was followed by investigations by Huang et al. (2010) on coupling surge and waves for determining impact of a hypothetical Hurricane Ivan-like hurricane making landfall near Tampa Bay. While the studies mentioned previously provide starting point for analyzing storm surge in Tampa Bay region, what is not apparent in those above-mentioned studies is how these responses could potentially interact with climate change impacts such as SLR. Condon and Sheng (2012) evaluated coastal inundation hazard in Southwest Florida for present and future climates, using a high resolution storm surge

modeling system, CH3D-SSMS, and an optimal storm ensemble with multivariate interpolation, while accounting for climate change impacts such as SLR scenarios. However, what was not included in the analysis was hurricane associated rainfall. Tang et al. (2013) coupled a three-dimensional coastal ocean model FVCOM with a two-dimensional shallow water model to simulate hydrodynamic flooding from coastal ocean water while applying a topography-based hydrologic method to estimate inland flooding due to precipitation. However, neither drainage networks nor subsurface interactions were included in the analysis. Cheng et al. (2010) demonstrated a coupled coastal watershed and nearshore oceanic model to characterize stormwater interactions at both the surface and subsurface levels due to storm surge and rainfall along with accounting for drainage networks via one-dimensional (1-D) stream-river networks, two-dimensional (2-D) overland regimes, and three-dimensional (3-D) subsurface media model (i.e., pWASH123D). Thompson and Frazier (2014) deterministic hazard extents under combined storm surge, inland precipitation and SLR for use in vulnerability assessments to depict coastal hazard inundation in Sarasota County, Florida. However, the analysis did not account for subsurface interactions and outputs of the storm surge and SLR scenarios were combined with the rainfall scenarios via overlay analysis rather than via model integration (Table 1a). There are several major hydrological models for possible combinations in flood assessment (Table 1b). Of these models, only WASH123D and HydroGeosphere were coupled or integrated with oceanic models to reflect the impact driven by storm surge with inherent numerical complexities.

Table 2-1: Literature Review of Relevant Studies

Hazard Considered	Hydrologic Interaction	Hydraulic Interaction	Modeling System	Reference
Storm Surge	No	No	3D Finite-volume coastal ocean model (FVCOM)	Weisberg and Zheng (2006), Weisberg and Zheng (2008), Huang et al. (2010)
Storm Surge+ SLR	No	No	Storm surge modeling system (CH3D-SSMS)	Condon and Sheng (2012)
Storm Surge+SLR	Yes, rainfall	No	Coupled 3D ocean model (FVCOM) and 2D shallow water model	Tang et al. (2013)
Storm Surge	Yes, rainfall and subsurface	Yes, 1D-channel flow	Coupled 2-D ADvanced CIRCulation (ADCIRC) model for oceanic, coastal, and estuarine waters and WAterSHed systems of pWASH123D model	Cheng et al. (2010)

Hazard Considered	Hydrologic Interaction	Hydraulic Interaction	Modeling System	Reference
Storm Surge+SLR	Yes, rainfall	Yes, 1D-channel flow	Sea, Lake, and Overland Surges from Hurricanes (SLOSH) model and the Interconnected Channel and Pond Routing(ICPR) model	Thompson and Frazier (2014)

Table 2-2: Major hydrological models for possible combinations in flood assessment

Models	Algorithms & Products	Advantages	Disadvantages	Reference
HEC-HMS/RAS	1D physically based watershed model	•sediment transport • water quality analysis	• no groundwater component • no 2-D flow regime	Bedient et al., 2000; Knebl et al., 2005
HydroGeosphere	3D physically based watershed model	• coupling surface and groundwater • flexible mesh	• operational complexity	Brunner and Simmons, 2012

Models	Algorithms & Products	Advantages	Disadvantages	Reference
WASH123D	3D physically based watershed model	• coupling surface and groundwater • flexible mesh • can be coupled with storm surge model	• operational complexity	Yeh et al., 2005
FLO2D	2D physically based watershed model	• simulate flood flow, debris flow, and mudslides	• no groundwater component	Hübl and Steinwendtner, 2001; Canuti et al., 2002
Sobek	2D physically based watershed model	• can simulate 1D channel and 2D flood flow with sewer systems	• no groundwater component	Deltares System, 2014
GSSHA™	2D physically based watershed model	• can simulate 1D channel, 2D flood flow, and groundwater system	• no sewer systems component	Downer and Ogden, 2004

Models	Algorithms & Products	Advantages	Disadvantages	Reference
TELEMAC	2D physically based watershed model	• can simulate 2D flood flow	• no sewer systems component	Hervouet, 2007
ICPR v4	3D physically based watershed model	• can simulate 2D/3D flood flow with groundwater interactions • flexible mesh • can be integrated with storm surge model	• sewer systems component can only be approximated by an equivalents way	Streamline Technologies, Inc., 2015

2.1.1. Chapter Objectives

The objective of this chapter is to derive deterministic flood inundation maps for a coastal urban watershed in the Tampa Bay region by accounting for simultaneous hazards of a combined storm tide and storm surge from varying scenarios of hurricanes under SLR and rainfall while reflecting both drainage systems and subsurface interactions within the target year 2030. This study utilizes an integration of a coupled hydrodynamic circulation and wave driven model, ADvanced CIRCulation (ADCIRC) and Simulating WAves Nearshore (SWAN) (Dietrich et al.,

2011), and a hydrological/hydraulic watershed model, the Interconnected Channel and Pond Routing (ICPRv.4) software (Streamline Technologies, 2015) to carry out flood hazard mapping.

2.2. <u>Study Area</u>

The focus of this chapter is the Cross Bayou Watershed Tampa Bay region of Florida located within Pinellas County (Figure 1). The Cross Bayou Watershed of Pinellas County was selected as a case study due to its sensitivity to current coastal flooding hazards such as high tide events and rainfall runoff along with future hazards such as sea level rise. The Cross Bayou watershed encompasses approximately 31 km^2 (7,697 acres). An important feature of the watershed is a 16.9 km (10.5-mile) long Cross Bayou Canal (Figure 2) which divides the watershed in half and connects to both Tampa Bay and Boca Ciega Bay on its northeastern and southwestern ends, respectively. Water within the canal can flow in either direction depending upon tidal conditions. Areas immediately surrounding the Cross Bayou Canal are low-lying with higher elevations found for both the northwest and the southeast regions of the watershed.

Figure 2-1:Extent of Tampa Bay Region with Cross Bayou Watershed
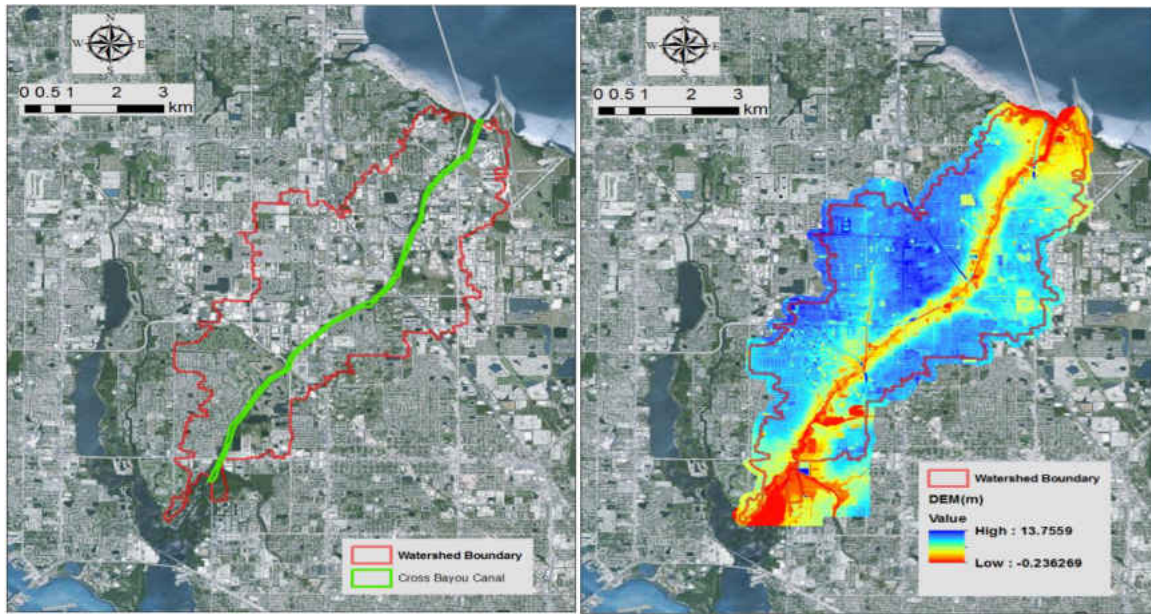
(a)   (b)

Figure 2-2: Extent of Cross Bayou Canal within the Cross Bayou Watershed (a) and digital elevation map of the watershed in meters (b)

2.3. <u>Methodology</u>

2.3.1. Hazard Framework

The study framework is divided into two phases. Phase 1 consists of setting up and running a coupled hydrodynamic circulation and wave driven model, including the ADCIRC and SWAN models (Dietrich et al., 2012) for the purposes of obtaining total water levels (i.e., storm surge, astronomic tide levels and waves). Results obtained from Phase 1 will be inputs into a hydrodynamic stormwater and hydrologic model - the ICPR v.4 software (Streamline Technologies, 2015) in Phase 2 with possible iterative interactions.

2.3.1.1. *Phase I and II Boundary*

Outputs from the coupled ADCIRC+SWAN model such as total water levels are useful as tidal boundary conditions in the ICPR model in modeling tidal conditions within the Cross Bayou Canal. The boundary between the ADCIRC+SWAN model and the ICPR takes place at two specific locations (Figure 3) where the Cross Bayou Canal meets with Boca Ciera Bay southwest of the watershed and where the Cross Bayou Canal meets with Tampa Bay northeast of the watershed. It is at these two locations that the ADCIRC+SWAN model pass information such as total water levels to ICPR. The opposite effect, ICPR passing information to ADCIRC-SWAN such as water fluxes was considered via incorporation of ADCIRC river influx boundary conditions (see Appendix). However, under tropical storm conditions, ICPR fluxes did not impact ADCIRC-SWAN levels at the boundary and are assumed to not affect possible storm surge. As a result, a mainland boundary with no incoming normal flow was applied for ADCIRC-SWAN while total water levels are passed to ICPR via an external utility (Figure 4) which converts ADCIRC+SWAN output at varying time-steps to necessary formatting for processing in the ICPR model.
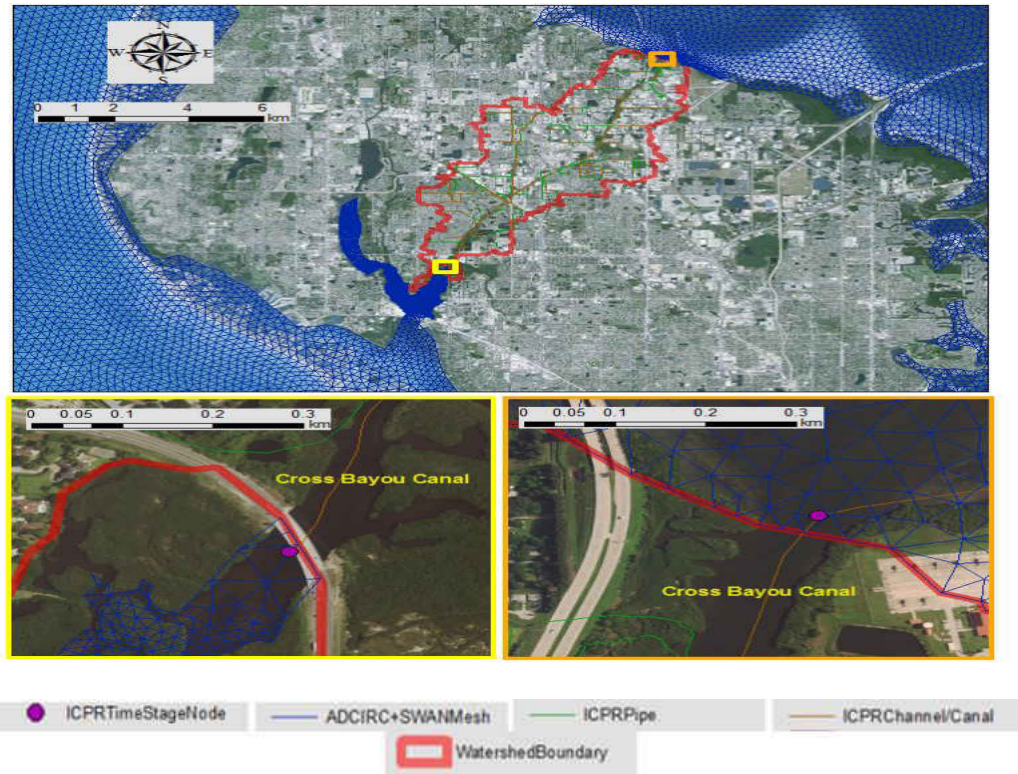
Figure 2-3: Extent of ADCIRC+SWAN mesh (top) with extent of ICPR Cross Bayou Watershed boundary and interface points of ICPR and ADCIRC+SWAN models (bottom)
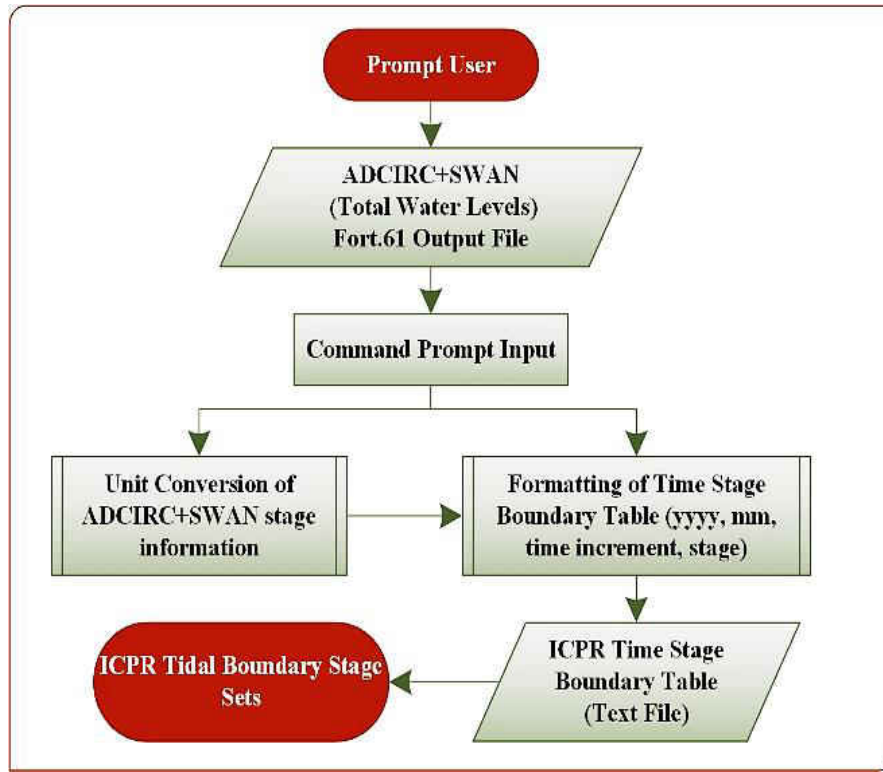
Figure 2-4: Windows-based utility for transferring ADCIRC+SWAN model total water level time series to ICPR model boundary nodes

2.3.1.2. *Future Storm Scenarios in Phase I*

To generate storm tide conditions, several scenarios were considered, which take into account landfall location, intensity, radius of maximum winds(RMW) and track. Weisberg and Zheng (2006) found that point of landfall, speed of approach and direction of approach were important factors to consider in modeling for storm surges in Tampa Bay Region. For the purposes of this study, changes in landfall location, direction of approach and storm intensity were considered. For all scenarios considered, the RMW was placed at the eyewall, assuming each storm had a well-defined eye. The range of distances for RMWs was kept between 32 and 35km (20 and 22 miles), respectively. With wind playing a greater factor in generation of storm surge and tide levels, a

relationship exists between surge height and the wind speed. Storms with stronger winds result in

larger surge heights. Category 4 storms were chosen as primary storm intensity for this study.

:

Table 2-3: Storm Scenarios & Characteristics for ADCIRC+SWAN

Track	Time Period	Intensity	Landfall Location	Direction of Approach	RMW near landfall (km)
1	October 2030	Cat. 4	Indian Rocks Beach, FL	SW-NE	35
2	October 2030	Cat. 4	Tarpon Springs, FL	S-NE	35
3	October 2030	Cat. 4	Tallahassee, FL	SE-NW	35

Figure 2-5: Storm tracks placed in GIS corresponding to Table 3 storm scenarios with Track 1(yellow), Track (red) and Track 3 (green).

Table 3 highlights storm track, landfall location, storm intensity (Saffir-Simpson Scale), RMW near landfall. Figure 5 shows the storm tracks which correspond to Table 3. The storm tracks featured drew inspiration from historical storms with varied parameters such as changes in direction of approach, wind speed, and RMW. Tracks 2 and 3 were inspired by projected storm tracks of the 1921 "Tarpon Springs Hurricane" and the 1935 "Labor Day Hurricane", respectively with some changes as mentioned previously. Track 2 relied on data from the efforts of the Hurricane Research Division of National Oceanic Atmospheric Administration (NOAA) to reexamine the National Hurricane Center's (NHC) original North Atlantic best track and intensity database (HURDAT) from 1851 to the present (Feuer et al., 2004).

2.3.1.3. Future Sea Level & Tidal Conditions in Phase I

Due to the effects of tidal constituents in the storm simulations, a time frame for analysis had to be specified particularly in determining nodal factors and equilibrium arguments for each

tidal constituent. The month of October was chosen as month of concern for storm tracks based on analysis conducted by NOAA on the climatological areas of origin and typical hurricane tracks by month. It is indicative that on-average the Tampa Bay region will most-likely experience tropical cyclone activity during the month of October with activity most-likely forming in the Caribbean Sea or Gulf of Mexico then moving north to northeastward while being carried away by an eastward-moving through (NOAA, 2015). Future projections of sea levels were necessary to define sea surface height in the ADCIRC+SWAN model for the year 2030. NOAA sea level rise projections (Tampa Bay Climate Science Advisory Panel, 2015) were utilized as reference for defining future sea levels for across the ADCIRC+SWAN model domain. A sea level rise of 0.1 m was added to the model domain.

2.3.1.4. *Future Rainfall*

With respect to future precipitation, a SCS Type II -24-hour distribution for a 50-year return period was assumed for rainfall associated from the future storm scenarios. The cumulative total rainfall derived for a SCS Type II-24-hour storm for a 50-year return period corresponds to 27.9 cm (11 in). This assumption was derived from previous work conducted by Tootle et al. (2005) in determining the magnitude and return period of rainfall associated with a Category 3 hurricane and a Category 4 hurricane which made landfall in Florida in 2004.

2.3.2. Coupled ADCIRC+SWAN Model (Phase I)

The coupled ADCIRC and SWAN model was utilized for generation of storm tide conditions. ADCIRC is a finite element model developed for simulating hydrodynamic circulations along shelves and coasts (Luettich et al.,1992; Westerlink et al.,1994) that can be run as a two-dimensional depth integrated (2DDI) model or as a three-dimensional model. SWAN is

a wind-generated wave model (Booij et al., 1999; Ris et al., 1999) that computes random, short-crested wind-generated waves in coastal regions near-shore. ADCIRC solves the shallow water equations (SWEs) using the Generalized Wave Continuity Equation (GWCE) (Eq.1) and vertically-integrated momentum equations (Eq. 4 and 5) to solve for water levels and currents, respectively. The ADCIRC model employs the continuous-Galerkin finite-element method to discretize on unstructured meshes.

$$\frac{\partial^2 \zeta}{\partial t^2} + \tau_0 \frac{\partial \zeta}{\partial t} + S_p \frac{\partial \overline{J_\lambda}}{\partial \lambda} + \frac{\partial \overrightarrow{J_\phi}}{\partial \varphi} - S_p UH \frac{\partial \tau_0}{\partial \lambda} - VH \frac{\partial \tau_0}{\partial \varphi} = 0 \qquad (2\text{-}1)$$

where:

$$\overline{J_\lambda} = -S_p Q_\lambda \frac{\partial U}{\partial \lambda} - Q_\varphi \frac{\partial U}{\partial \varphi} + f Q_\varphi - \frac{g}{2} S_p \frac{\partial \zeta^2}{\partial \lambda} - g S_p H \frac{\partial}{\partial \lambda} \left[\frac{P_s}{g \rho_0} - \alpha \eta \right]$$

$$+ \frac{\tau_{s\lambda,winds} + \tau_{s\lambda,waves} - \tau_{b\lambda}}{\rho_0} + (M_\lambda - D_\lambda) + U \frac{\partial \zeta}{\partial t} + \tau_0 Q_\lambda - g S_p H \frac{\partial \zeta}{\partial \lambda} \qquad (2\text{-}2)$$

and

$$\overline{J_\varphi} = -S_p Q_\lambda \frac{\partial U}{\partial \lambda} - Q_\varphi \frac{\partial U}{\partial \varphi} - f Q_\lambda - \frac{g}{2} S_p \frac{\partial \zeta^2}{\partial \varphi} - g H \frac{\partial}{\partial \lambda} \left[\frac{P_s}{g \rho_0} - \alpha \eta \right]$$

$$+ \frac{\tau_{s\varphi,winds} + \tau_{s\varphi,waves} - \tau_{b\varphi}}{\rho_0} + (M_\varphi - D_\varphi) + V \frac{\partial \zeta}{\partial t} + \tau_0 Q_\varphi - g H \frac{\partial \zeta}{\partial \varphi} \qquad (2\text{-}3)$$

The currents U and V are obtained from vertically-integrated momentum equations:

$$\frac{\partial U}{\partial t} + S_p U \frac{\partial U}{\partial \lambda} + V \frac{\partial U}{\partial \varphi} - fV = -g S_p \frac{\partial}{\partial \lambda} \left[\zeta + \frac{P_s}{g \rho_0} - \alpha \eta \right] + \frac{\tau_{s\lambda,winds} + \tau_{s\lambda,waves} - \tau_{b\lambda}}{\rho_0 H} + \frac{M_\lambda - D_\lambda}{H}$$

$$(2\text{-}4)$$

and

$$\frac{\partial V}{\partial t} + S_p U \frac{\partial V}{\partial \lambda} + V \frac{\partial V}{\partial \varphi} + fU = -g \frac{\partial}{\partial \varphi}\left[\zeta + \frac{P_s}{g\rho_0} - \alpha\eta\right]$$

$$+ \frac{\tau_{s\varphi,winds} + \tau_{s\varphi,waves} - \tau_{b\varphi}}{\rho_0 H} + \frac{M_\varphi - D_\varphi}{H} \qquad (2\text{-}5)$$

where $H = \zeta + h$ is the total water depth (m); ζ is the deviation of the water surface from the mean

(m); h is the bathymetric depth (m); $S_p = \cos\phi_0 / \cos\phi_\lambda$ is the spherical coordinate conversion

factor (unitless); U and V are depth-integrated currents in the x and y-directions, respectively;

$Q_x = UH$ and $Q_y = VH$ are fluxes per unit width (m²s⁻¹); f is the Coriolis parameter; g is the

gravitational acceleration ($\mathrm{m\,s^{-2}}$); P_s is the atmospheric pressure at the surface ($\mathrm{N\,m^{-2}}$); ρ_0 is the

reference density of water (kg m⁻³); η is the Newtonian equilibrium tidal potential and α is the

effective earth elasticity factor; $\tau_s, winds$ and $\tau_s, waves$ are surface stresses due to winds and waves,

respectively ($\mathrm{N\,m^{-2}}$); τ_b is the bottom stress ($\mathrm{N\,m^{-2}}$); M are lateral stress gradients ($\mathrm{N\,m^{-2}}$ per

m); D are momentum dispersion terms ($\mathrm{N\,m^{-2}}$ per m); and τ_0 is a numerical parameter that

optimizes the phase propagation properties (unitless) (Dietrich et al., 2012).

SWAN utilizes a Gauss-Seidel sweeping algorithm to propagate the wave action density while

relying on the action balance equation (Eq. 6):

$$\frac{\partial N}{\partial t} + \frac{\partial}{\partial \lambda}\left[\left(c_\lambda + U\right)N\right] + \cos^{-1}\varphi \frac{\partial}{\partial \varphi}\left[\left(c_\varphi + V\right)N\cos\varphi\right] + \frac{\partial}{\partial \theta}[c_\theta N] + \frac{\partial}{\partial \sigma}[c_\sigma N] = \frac{S_{tot}}{\sigma}$$

$$(2\text{-}6)$$

where (c_λ, c_φ) is the group velocity in geographic space (λ, φ); (U, V) is the ambient current; c_θ

and c_σ are the propagation velocities in the spectral space (θ, σ) with θ representing wave direction

and σ representing frequency; $N(t, \lambda, \varphi, \sigma, \theta)$ represents the wave density. The source term S_{tot}

represents wave growth by wind; action lost due to white capping, surf breaking, and bottom friction; and action exchanged between spectral components due to nonlinear effects in deep and shallow water. (Booji et al., 1999). The coupled model allows both ADCIRC and SWAN to run on the same unstructured mesh. This allows for "inter-model communication" in which ADCIRC and SWAN can pass information to each other without using interpolation methods. This also allows for the simulation of both waves (SWAN) and storm tide (ADCIRC) beginning in deep waters to shallow waters or near the coast (Dietrich et al., 2012) such that SWAN passes information to ADCIRC such as surface stresses due to waves and wave radiation stresses and ADCIRC can pass back information to SWAN such as total water levels, wind velocities and currents (Dietrich et al., 2012).

2.3.2.1.   *Wind and Pressure Model in Phase I*

Winds and atmospheric pressure fields are calculated using the parametric wind model, the Holland wind model (Holland, 1980) which is embedded in the ADCIRC model subroutine by accounting for the dynamic changes in the storm parameters along a specified track. ADCIRC requires a meteorological forcing file which contains necessary wind and pressure information at specific time frames for which ADCIRC will calculate wind speed and atmospheric pressure fields across the model domain at every time step specified by the user. The wind velocity V_g, represented as gradient wind velocity, and atmospheric pressure P are calculated at follows (adapted from Fleming et al, 2008):

$$V_g(r) = \sqrt{\left(\frac{R_w}{r}\right)^B - \exp\left[1-\left(\frac{R_w}{r}\right)^B\right]V_m^2 + \left(\frac{rf}{2}\right)^2} - \left(\frac{rf}{2}\right) \qquad (\textbf{2-7})$$

The gradient wind velocity is separated into its north and east components and multiplied by the atmospheric boundary layer adjustment factor β to obtain wind velocity at 10 m:

$$V_{northi} = V_g(r)\beta\cos\theta_i \qquad\qquad\qquad (2\text{-}8)$$

$$V_{easti} = -V_g(r)\beta\sin\theta_i \qquad\qquad\qquad (2\text{-}9)$$

The atmospheric pressure is calculated as follows:

$$P(r) = \frac{P_c + (P_n - P_c)\exp\left[-\left(\dfrac{R_w}{r}\right)^B\right]}{\rho_w g} \qquad\qquad (2\text{-}10)$$

where R_w = radius of maximum winds (m); r = distance from point of interest within model domain to center of storm (m); V_m = gradient wind velocity at radius of maximum wind = s_m / β (m s^{-1}); s_m = maximum storm wind speed at 10 m (= $s_f - \sqrt{v_{te}^2 + v_{tn}^2}$) (m s^{-1}); s_f = maximum forecast wind speed (m s^{-1}); v_{te}^2 = storm translation velocity in the east direction (m s^{-1}); v_{tn} = storm translation velocity in the north direction (m s^{-1}); β = boundary adjustment factor to convert the maximum wind speed at 10 m to the maximum velocity at the top of the atmospheric boundary layer (unitless); B = the Holland scaling parameter (= $\rho e V_m^2 / (P_n - P_c)$) (unitless); ρ = density of air assumed at constant 1.15 kg m^{-3} ( ); e = Euler's number (unitless); P_n = ambient atmospheric pressure (N m^{-2}); P_c = the storm central pressure (N m^{-2}), and g is the gravitational constant (m s^{-2}).

ADCIRC also accounts for wind drag using a default wind drag law from Garratt (1977):

$$\text{Wind Drag} = 0.001[0.75 + 0.067(\text{Wind Speed})] \tag{2-11}$$

2.3.2.2. *Model Domain & Setup in Phase I*

The ADCIRC+SWAN model run relies on four input files, namely the model grid and boundary condition file (fort.14), nodal attributes file (fort.13), a meteorological forcing file (fort.22), and the parameter and periodic boundary conditions file (fort.15). The model grid and boundary condition file defines the unstructured grid (node locations, elevations, and element connectivity) and specifies boundary conditions such as land or coastline, rivers and oceans. An unstructured grid (Figure 6) was constructed consisting of 108,812 nodes and 260,032 triangular elements using the ADCIRC module of the Surface-water Modeling System software (Aquaveo, 2016). The unstructured grid relied on coastline features defined by NOAA Electronic Navigational Charts (NOAA ENC) and NOAA Nation Geodetic Survey along with bathymetry data obtained from the NOAA National Centers for Environmental Information 3 arc-second U.S. Coastal Relief Model. The bathymetry associated with the grid is also shown in Figure 6. The spatial resolution consists of coarser spatial resolution in the open-ocean boundary (5 kilometers) while transiting to a finer spatial resolution of 1.5 meters near the inlets of the Cross Bayou Canal. In order to better consider wave propagation, which can affect tidal amplitudes, the model grid was merged with a larger but coarser grid (Luettich et al., 1994), which includes the Gulf of Mexico, the Caribbean and Atlantic Ocean, as represented in Figure 7.

(a)   (b)
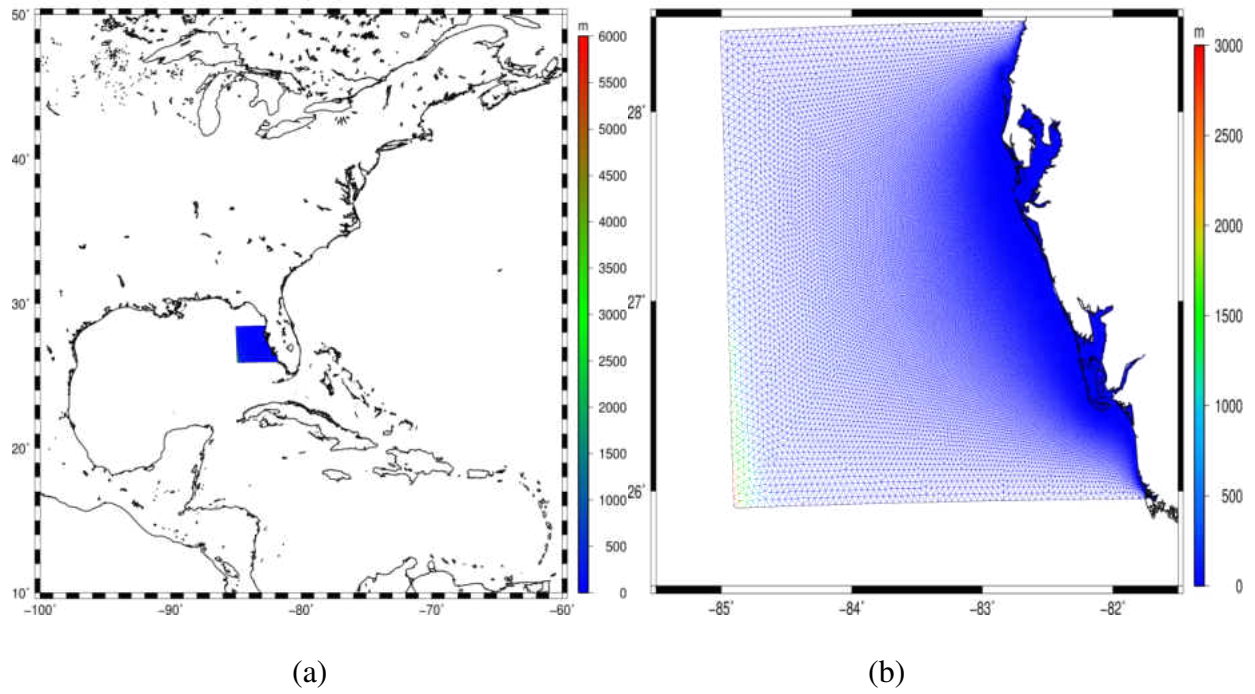
Figure 2-6:(a) Refined west Florida grid with and (b) emphasis on Tampa Bay. *Note*
Bathymetry in meters (m)
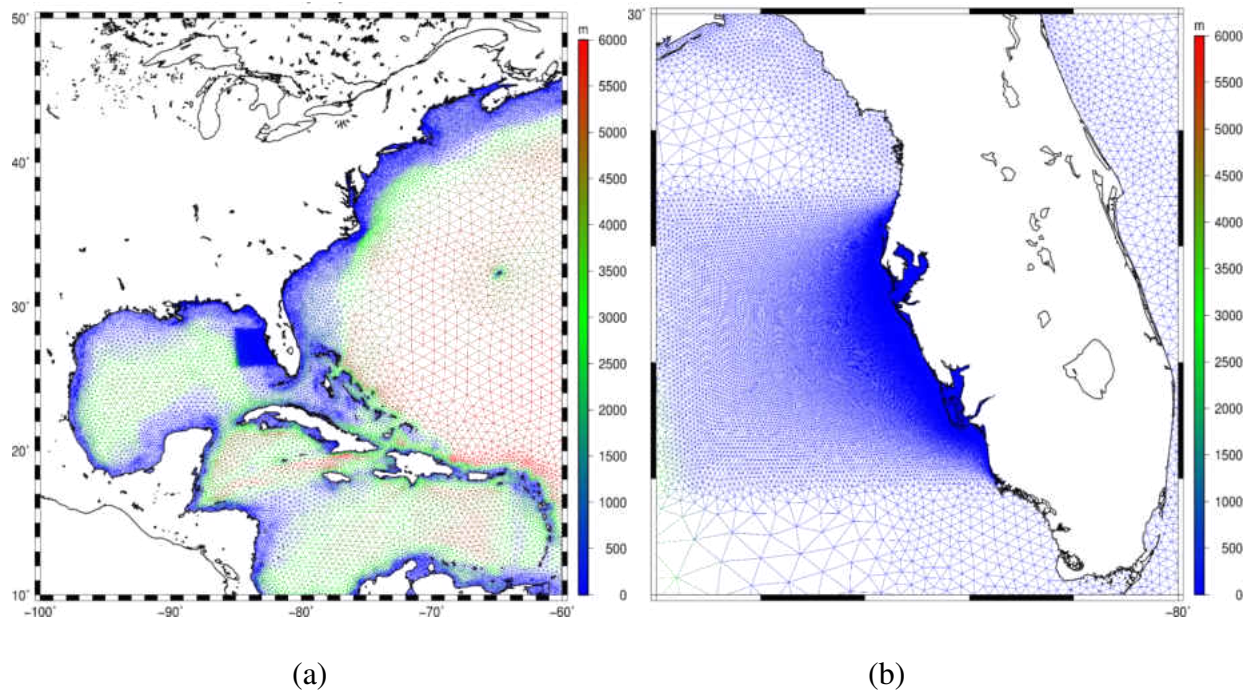
Figure 2-7: (a) "Merged" Grid using larger grid area and (b) extent of west Florida. *Note Bathymetry in meters (m)*

The nodal attributes file defines attributes for each node in the model grid. A Manning's n friction coefficient was provided in the nodal attributes file for areas of the grid that cover land along with a Manning's n coefficient for shallow water (<2.5 m). A quadratic bottom friction coefficient had to be specified for deeper waters (> 2.5 m). The Manning's n values were determined from the 2011 version of the USGS National Land Cover Database (NLCD) and interpolated onto the model grid. Local sea level data was obtained from the NOAA) and integrated as sea surface height inputs for the coupled model. The meteorological input file defines winds and pressures to be read in the model simulation for the purposes of climate forcing. The meteorological input was obtained from the NHC Hurricane Database (i.e.,

HURDAT) in the form of beat-track data. The parameter and periodic boundary conditions file specifies parameters required to run the model, as well as the inputs for the tidal forcing using Le Provost tidal database (Le Provost et al., 1998).

2.3.3. ICPR Model (Phase II)

The goal of Phase II was to generate flood hazard maps using the modeled maximum stage of combined storm tide influences and precipitation runoff in the Cross Bayou Watershed. Due to various interactions associated with an urban watershed, ICPR was constructed using a detailed model of the Cross Bayou watershed which takes into account both overland flow and groundwater flows via infiltration and water table considerations by integrating land use characteristics with inclusion of roughness coefficients, soil characteristics, digital terrain mapping along with mapping of the subsurface. Hydraulic systems are represented in the model and flows can be routed through detention ponds, pile bridges, channels, pipe networks such as storm sewer systems via nodes (specific points of interest in a study region) and links (which connect hydraulic components). In addition, ICPR includes an integrated hydrology component to model precipitation and resulting runoff which is important for modeling rainfall over the watershed from cyclonic storms.

2.3.3.1.   *Cross Bayou Watershed Model Setup in Phase II*

The ICPR model relies on several data layers (Figure 8) which accounts for both surface, such as stormwater drainage systems and overland flow, and subsurface interactions such as water table fluctuations. For the purposes of this study, the model domain consists of a flexible triangular mesh to allow for two-dimensional overland flow which intersects with soil and groundwater. The

vertices of the triangles are treated as nodes in the model and the sides of the triangles are overland flow links which allow flow across triangles. The finite volume approach is utilized in model domain setup in which control volumes are formed around the vertices and extend to the midpoints of the triangle sides and to the geometric center of the triangle (e.g., the centroid). Water is allowed to flow from one control volume to an adjacent control volume via the overland flow links or triangle sides (Streamline Technologies, 2015).
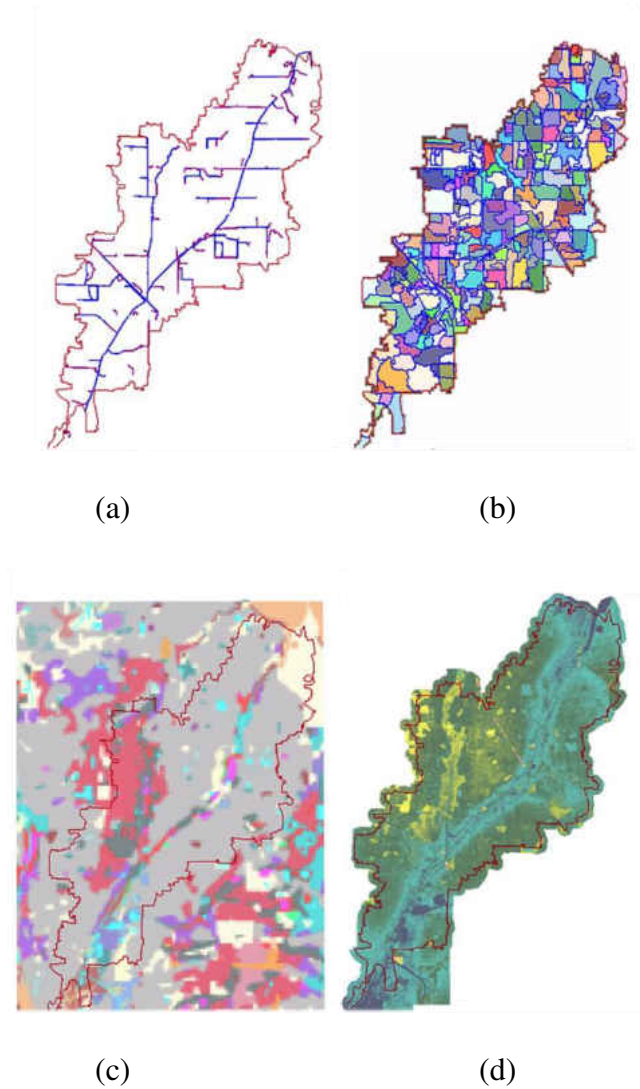
Figure 2-8: Major ICPR Data Layers: (a) water conveyance system, (b) drainage basins, (c) soil and (d) water table

ICPR uses a one-dimensional form of the momentum equation along with energy and diffusive wave options and averaged 2D ground slopes to move water between control volumes via the overland flow links. For the purpose of this study, the energy equation (Eq. 12-13) was used to calculate overland flow and flow within channels and other hydraulic systems (Eq. 14-15). The energy equation used for overland flow can be represented as follows:

$$Z_1 + \frac{V_1^2}{2g} = Z_2 + \frac{V_2^2}{2g} + h_f \qquad\qquad (\textbf{2-12})$$

Solving for Q:

$$Q = \left\{ \frac{Z_1 - Z_2}{\frac{1}{2g}\left[\frac{1}{A_2^{\,2}} - \frac{1}{A_1^{\,2}}\right] + \Delta x C_f} \right\}^{1/2} \qquad\qquad (\textbf{2-13})$$

Where

$Q = \text{flow}\left(\text{m}^3\text{s}^{-1}\right);\ Z_1 = \text{elevation}\,(\text{m})\ \text{at node1};\ Z_2 = \text{elevation}\,(\text{m})\ \text{at node2};$

$\Delta x = \text{change in length between nodes in the x}-\text{direction};\ g\ =\ \text{gravitational acceleration (m s}^{-2}\ );$

$A_1 = \text{cross sectional area}\left(\text{m}^2\right)\ \text{at node1};\ A_2 = \text{cross sectional area}\left(\text{m}^2\right)\ \text{at node2};\ C_f\ =\ \text{coefficient of friction};$

The energy equation is modified for channel and pipe flow and can be represented as follows:

$$Z_1 + \frac{\alpha_1 V_1^2}{2g} = Z_2 + \frac{\alpha_2 V_2^2}{2g} + h_f + h_{eddy} + h_{entrance} + h_{exit} + h_{bend} \qquad\qquad (\textbf{2-14})$$

Solving for Q:

$$Q = \left\{ \frac{Z_1 - Z_2}{\frac{1}{2g}\left[\left(\frac{\alpha_2}{A_2^{\,2}} - \frac{\alpha_1}{A_1^{\,2}}\right)C_{eddy}\left|\left(\frac{\alpha_2}{A_2^{\,2}} - \frac{\alpha_1}{A_1^{\,2}}\right)\right| + \left(\frac{\alpha_1 C_{entrance}}{A_1^{\,2}}\right) + \left(\frac{\alpha_2 C_{exit}}{A_2^{\,2}}\right) + \left(\frac{\alpha_{bend} C_{bend}}{A_{bend}^{\,2}}\right) + \Delta x C_f\right]} \right\}^{1/2} \qquad (\textbf{2-15})$$

where,

$Q = \text{flow} \left(\text{m}^3 \text{s}^{-1} \right)$; $Z_1 = \text{elevation} \left(\text{m} \right)$ at node1; $Z_2 = \text{elevation} \left(\text{m} \right)$ at node2;

$\Delta x = \text{change in length between nodes in the x-direction}$; $g = \text{gravitational acceleration} \left(\text{m s}^{-2} \right)$;

$A_1 = \text{cross sectional area} \left(\text{m}^2 \right)$ at node1; $A_2 = \text{cross sectional area} \left(\text{m}^2 \right)$ at node2;

$A_{bend} = \text{area of the bend} \left(\text{m}^2 \right)$; $\alpha_1 = \text{linear expansion coefficient at node 1}$;

$\alpha_2 = \text{linear expansion coefficient at node 2}$; $C_f = \text{friciton loss coefficient}$; $C_{eddy} = \text{eddy loss coefficient}$;

$C_{entrance} = \text{entrance loss coefficient}$; $C_{exit} = \text{exit loss coefficient}$; $C_{bend} = \text{bend loss coefficient}$;

Mass balance equations (Eq. 16-18) are utilized within the control volumes at each node or vertex of the triangles as follows:

$$dz = \left[\frac{\Sigma \left(Q_{in} - Q_{out} \right)}{A_{surface}} \right] dt \qquad \qquad \textbf{(2-16)}$$

Where

$dz = \text{incremental change in stage} \left(\text{m} \right)$; $dt = \text{computational time step} \left(\text{s} \right)$;

$Q_{in} = \text{total inflow rate} \left(\text{m}^3 \text{s}^{-1} \right)$; $Q_{out} = \text{total outflow rate} \left(\text{m}^3 \text{s}^{-1} \right)$;

$A_{surface} = \text{wetted surface area of control volume}$

and

$$Q_{in} = \Sigma Q_{link\ in} + \Sigma Q_{excess} + \Sigma Q_{external} + \Sigma Q_{seepage} \qquad \qquad \textbf{(2-17)}$$

$$Q_{out} = \Sigma Q_{link\ out} + \Sigma Q_{irrigation} \qquad \qquad \textbf{(2-18)}$$

where

$\Sigma Q_{link\ in} = \text{sum of all link flow rates entering the control volume} \left(\text{m}^3 \text{s}^{-1} \right)$;

$\Sigma Q_{link\ out} = \text{sum of all link flow rates leaving the control volume} \left(\text{m}^3 \text{s}^{-1} \right)$;

$\Sigma Q_{excess} = \text{sum of rainfall excess rates for all basin polygons} \left(\text{m}^3 \text{s}^{-1} \right)$;

$\Sigma\mathrm{Q}_{\mathrm{external}} = \text{sum of inflows from all external sources}\left(\mathrm{m^3s^{-1}}\right);$

$\Sigma\mathrm{Q}_{\mathrm{seepage}} = \text{sum of seepage flow from groundwater model}\left(\mathrm{m^3s^{-1}}\right);$

$\Sigma\mathrm{Q}_{\mathrm{irrigation}} = \text{sum of irrigation water pulled from surface node}\left(\mathrm{m^3s^{-1}}\right)$

With respect to ICPR, data needed include elevation data over the study region, soil data maps and land use maps, road networks, rainfall data along with stormwater and sewer system infrastructure. The above-mentioned data were provided by the Pinellas County government and Streamline Technologies (Streamline Technologies Inc., 2015). The Natural Resources Conservation Service (NRCS) digital soil survey was utilized to develop the initial/un-calibrated Green-Ampt soil parameters for the vadose zone and the surficial/unconfined aquifer within the watershed. A 1.5m x 1.5m (5ft x 5ft) ground digital elevation model (DEM) was utilized for defining the ground surface of the watershed. Since the DEM lacked accuracy below the water surface and groundwater considerations were necessary for analysis, an "engineered" surface was created that projected the bottom elevation of known water bodies to well below sea level to prevent artificial drying of the water body. For the purposes of the groundwater component of the hydrodynamic stormwater and hydrologic model, DEMs were also created for the initial water table elevation (based on wet season conditions as defined in the NRCS soil survey) and the top of the confining layer for the Intermediate Aquifer System. The initial water surface DEM was based on the NRCS depth to water table information. The confining layer top elevation was obtained from a 390 m x 390 m DEM based on contours generated using both automated and manual methods from the Florida Geological Survey (Streamline Technologies Inc., 2015).

Next Generation Radar (NEXRAD) rainfall data were obtained from the Southwest Florida Water Management District (SWFWMD) and distributed over twenty-three 2 km x 2 km grids cells fifteen minute apart covering a period from June 6, 1995 to December 31, 2014. Daily reference evapotranspiration data were collected from the United States Geological Survey and distributed on 2 km x2 km grid tiles covering a form June 1, 1995 to December 31, 2013. No urban growth models or significant land use changes were considered for this study for future climate simulations since the majority of the Cross Bayou Watershed currently is well developed.

2.3.4.   Model Calibration and Validation (Phases I and II)

2.3.4.1.   ADCIRC+SWAN Model Calibration & Validation in Phase I

Calibration of the ADCIRC+SWAN component of the coupled model consists of calibrating parameters which effect transfer of information between both ADCIRC and SWAN. The parameters of concern are as follows: (1) Ramp Time parameter which controls the time required before full tidal and meteorological forcing is applied, (2) Wave radiation stresses time step which controls the time in which SWAN wave radiation stresses are passed to ADCIRC to compute total water levels and (3) the default bottom friction parameter which is an important parameter in coastal modeling (Table 4).

Table 2-4: Useful ADCIRC+SWAN Model Parameters for Calibration

Parameter	Description
Ramp Time	Time required before full tidal and meteorological forcing is used.

Parameter	Description
Wave Radiation Stress Time Step	Time step in which SWAN wave radiation stresses are passed to ADCIRC in total water level computation
Default Bottom Friction	While bottom friction is varied by location, such as near the coastal shelf, the default is applied elsewhere.

Model validation of the ADCIRC+SWAN relied on measuring the performance of the model in replicating conditions during a historical storm event. Tropical Storm Barry, during the year 2007, was utilized for model validation of the ADCIRC+SWAN model. Tropical Storm Barry was the second named storm of the 2007 Atlantic hurricane season and was a rapidly forming tropical cyclone which made landfall off the west coast of Florida in early June 2007. A total simulation time of 6 days (5/31/2007 until 06/03/2007) with a ramp period of 3 days (5/28/2007-05/31/2007) was applied for the model domain. Four NOAA stations, including Old Port Tampa (27.859 N / 82.552 W), St Petersburg (27.761 N / 82.626 W), Port Manatee (27.635 N / 82.563 W), and Clearwater Beach (27.978 N / 82.830 W), were utilized to compare model water levels to observed water levels.

2.3.4.2. ICPR Model Calibration & Validation in Phase II

For the purposes of ICPR model calibration and validation, fifteen-minute USGS gage data was collected at the two active gages within the Cross Bayou watershed (Figure 12). USGS gage 02308870 is located along the Pinebrook Canal at Bryan Dairy Road at Pinellas Park. The gage records rainfall, stage and flow data. The stage data is relative to a local datum for

the gage. A conversion of 0.274 m (+ 0.9-ft) was used to convert the stage elevation from the local datum to NAVD88 used in the model. The gage period of record for rainfall, stage and flow are August 6th, 1999 to present, August 5, 1995 to present, and August 1, 1999 to present, respectively. Fifteen minute NEXRAD rainfall data were obtained from the SWFWMD and distributed over twenty-three 2 km x 2 km grids cells associated covering a period from June 6, 1995 to December 31, 2014. Historical hourly tide gage data, from January 1995 to December 2014, from nearby NOAA tide stations were also used in calibration and verification of the model (Streamline Technologies, 2015).

Daily reference evapotranspiration (ET) data were collected from the United States Geological Survey (USGS) and distributed on 2 km x 2 km grid tiles covering a from June 1, 1995 to December 31, 2013. Specific to the ICPR model, crop coefficients are used to adjust reference ET to specific vegetation. A generalized crop coefficient map layer was created based on vegetation coverage. While defined crop coefficients do not include impervious areas, they are used for describing vegetation types for pervious areas. A total of 7 vegetative classes were established within the layer. The Green-Ampt method was used for infiltration and rainfall excess computations. The Green-Ampt parameters were developed based on the NRCS soil data survey and later adjusted during the calibration process. For each sub-basin, an initial abstraction parameter for impervious areas was set to 0.05 inches based on calibration of the model (Streamline Technologies, 2015). ICPR was calibrated using both a single historical storm event (June 21-30, 2012) and verified using a long-term simulation between January 1, 2007 and January 1, 2014 using USGS gage stations within the Cross Bayou Watershed. Validation results of ICPR model provided in Appendix A.

2.4. Results & Discussion

2.4.1.   Phase I Model Calibration and Validation

Final calibration of key ADCIRC-SWAN parameters was carried out based upon: 1) ramp time (3 days), 2) wave radiation stresses time step (6000 sec), and 3) default bottom friction (0.025). Figure 9 shows model validation plots during Tropical Storm Barry in June 2007. The model was allowed to "ramp up" for a period of 72 hrs to prevent unstable model oscillations during start of simulation. Overall, Table 5 summarizes the prediction accuracies based on four NOAA tide gage stations for ADCIRC+SWAN calibration and validation, and the model performs relatively well at the Clearwater Beach location. The model had some difficulty accounting for much lower water levels as compared with observed as the storm progressed. This could be due to tidal propagation issues.

42
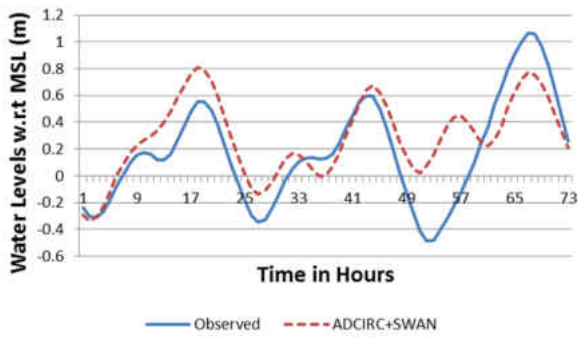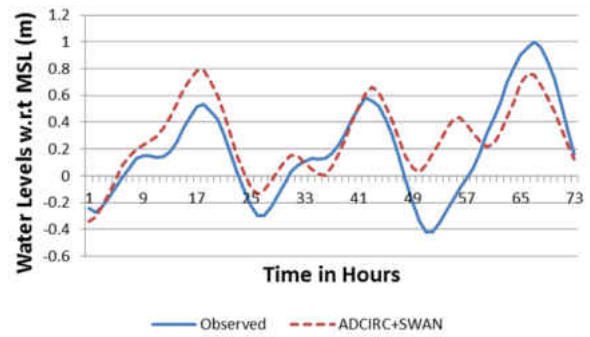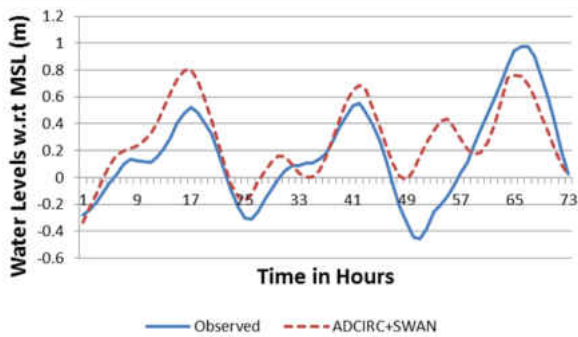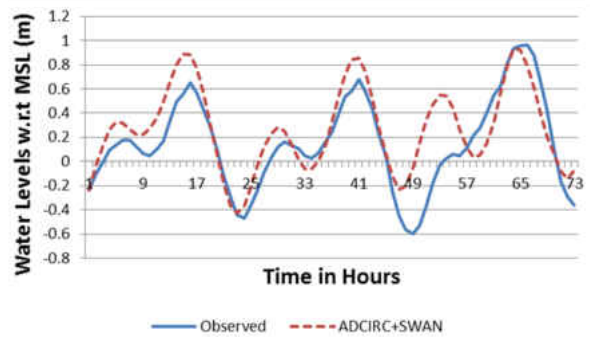
Figure 2-9: Model vs. Observed at four NOAA Station locations: (a) Old Port Tampa, (b) St Petersburg, (c) Port Manatee, and (d) Clearwater Beach during Tropical Storm Barry (5/31/2007-06/03/2007) with model ramp up period of 72 hrs (5/28/2007-5/31/2007)

Table 2-5: ADCIRC+SWAN model validation results (05/31/2007-06/03/2007)

Station Name	Latitude/Longitude	R	R^2	RMSE (m)
Old Port Tampa	27.859 N / 82.552 W	0.77	0.60	0.226
St Petersburg	27.761 N / 82.626 W	0.786	0.617	0.237
Port Manatee	27.635 N / 82.563 W	0.771	0.595	0.244
Clearwater Beach	27.978 N / 82.830 W	0.882	0.777	0.246

2.4.2. Phase I Future Storm Scenarios in 2030

To ease the illustration, we paired Figure 10 of Track 1 across model domain and Figure 11 for approaching the Tampa Bay during landfall. By the same token, Figures 12 and 13 as well as Figures 14 and 15 are paired for Tracks 2 and 3, respectively. Track 2 results in the highest storm tide levels within the Tampa Bay region as evident in Figure 18. Landfall location is particularly important when comparing Track 2 to Track 1. Since storm tide levels are significantly higher for Track 2 as opposed to Track 1, it makes landfall of Track 1 several kilometers north of Track 2 landfall location. Direction of wind field pattern was also a factor in overall storm tide levels with Track 3, approaching from the south, resulting in lower overall storm tide levels throughout the Tampa Bay region.
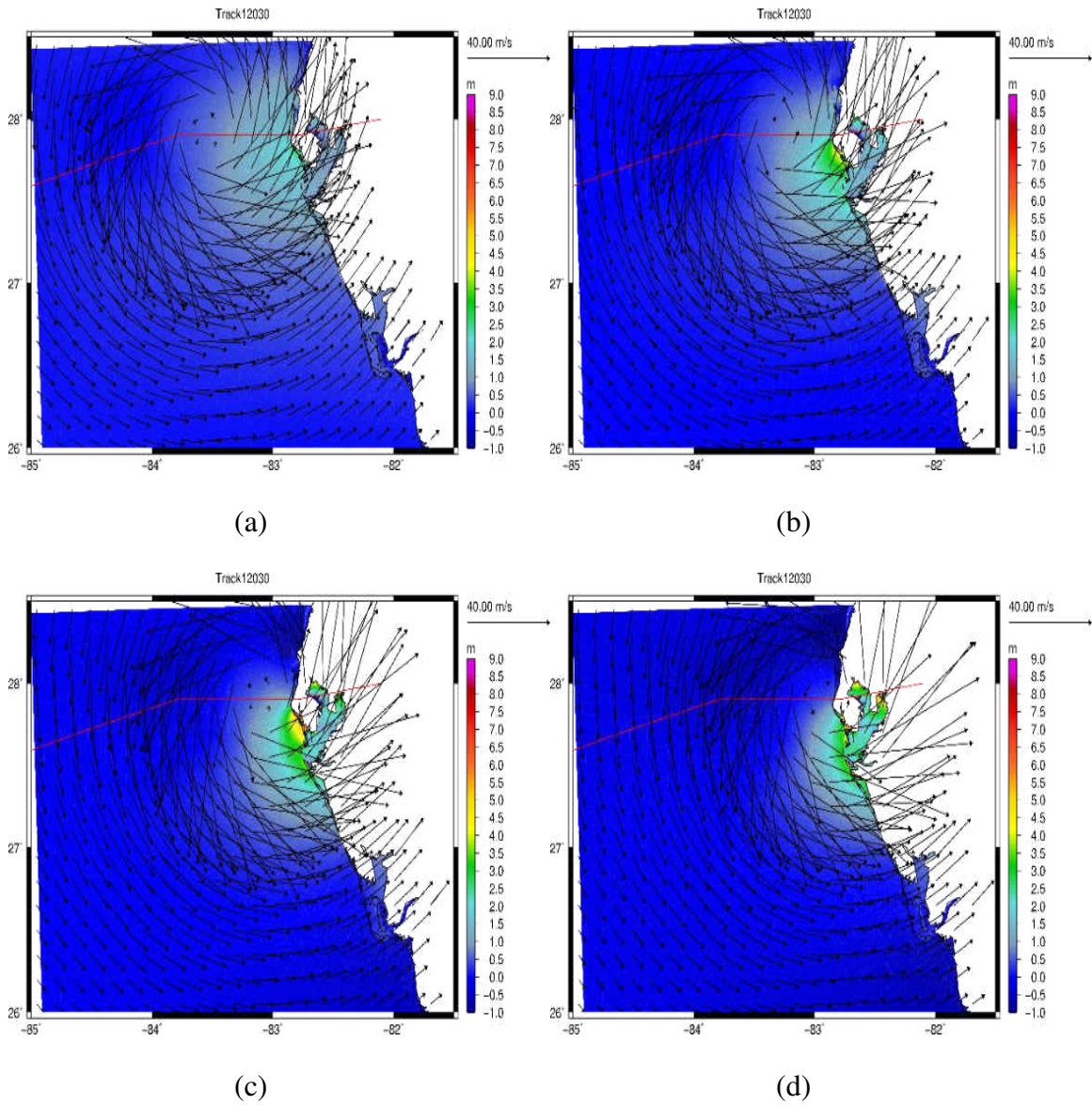
Figure 2-10: Track 1 approaching Tampa Bay (a) with outer bands within the bay (b) increased winds within the bay (c) eye wall approaching with radius of maximum winds and (d) with eyewall over Tampa Bay.
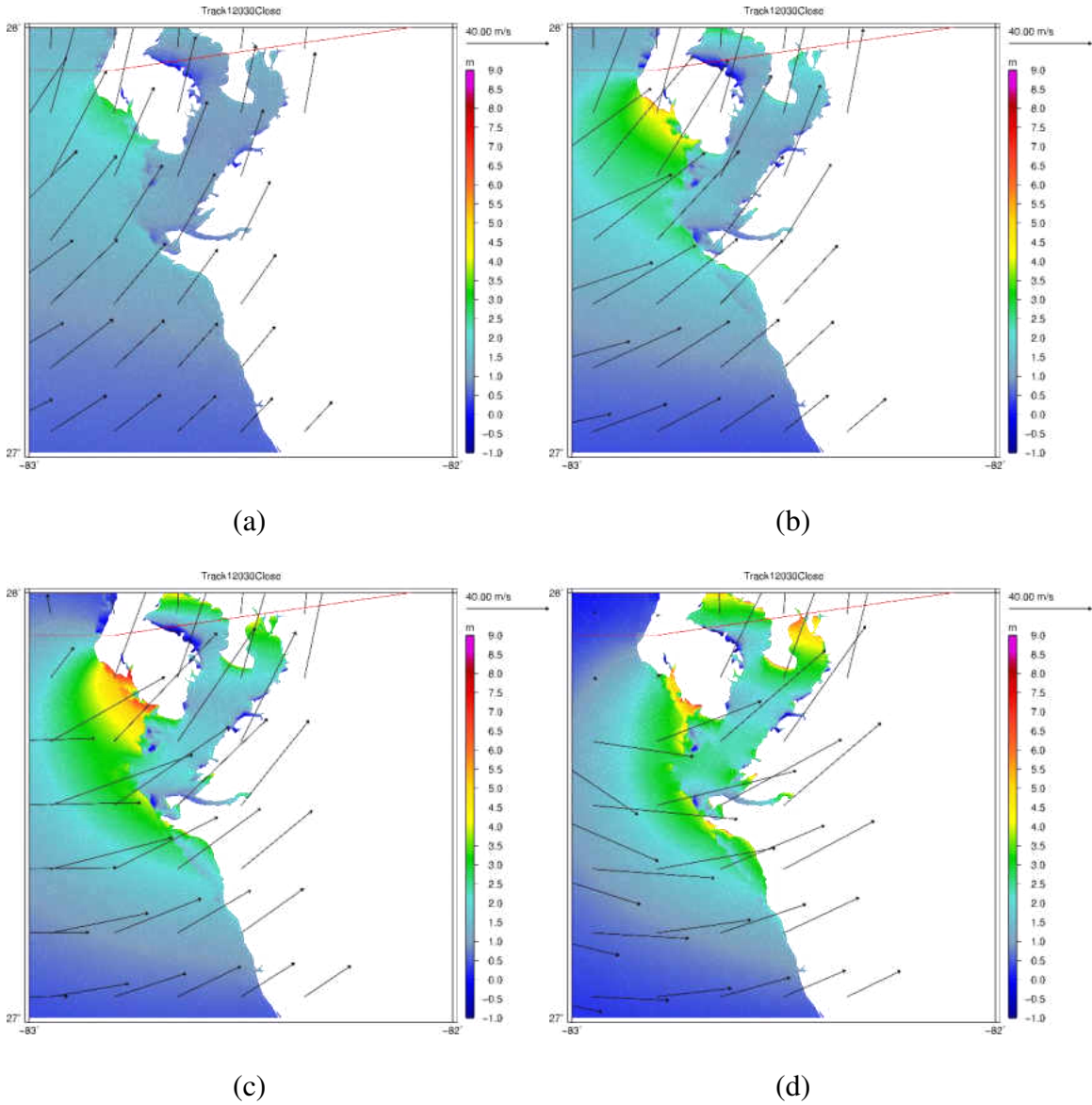
Figure 2-11: Wind fields of Track 1 and storm tide approaching Tampa Bay (a) with outer bands within the bay (b) increased winds within the bay (c) eye wall approaching with radius of maximum winds and (d) with eyewall over Tampa Bay.
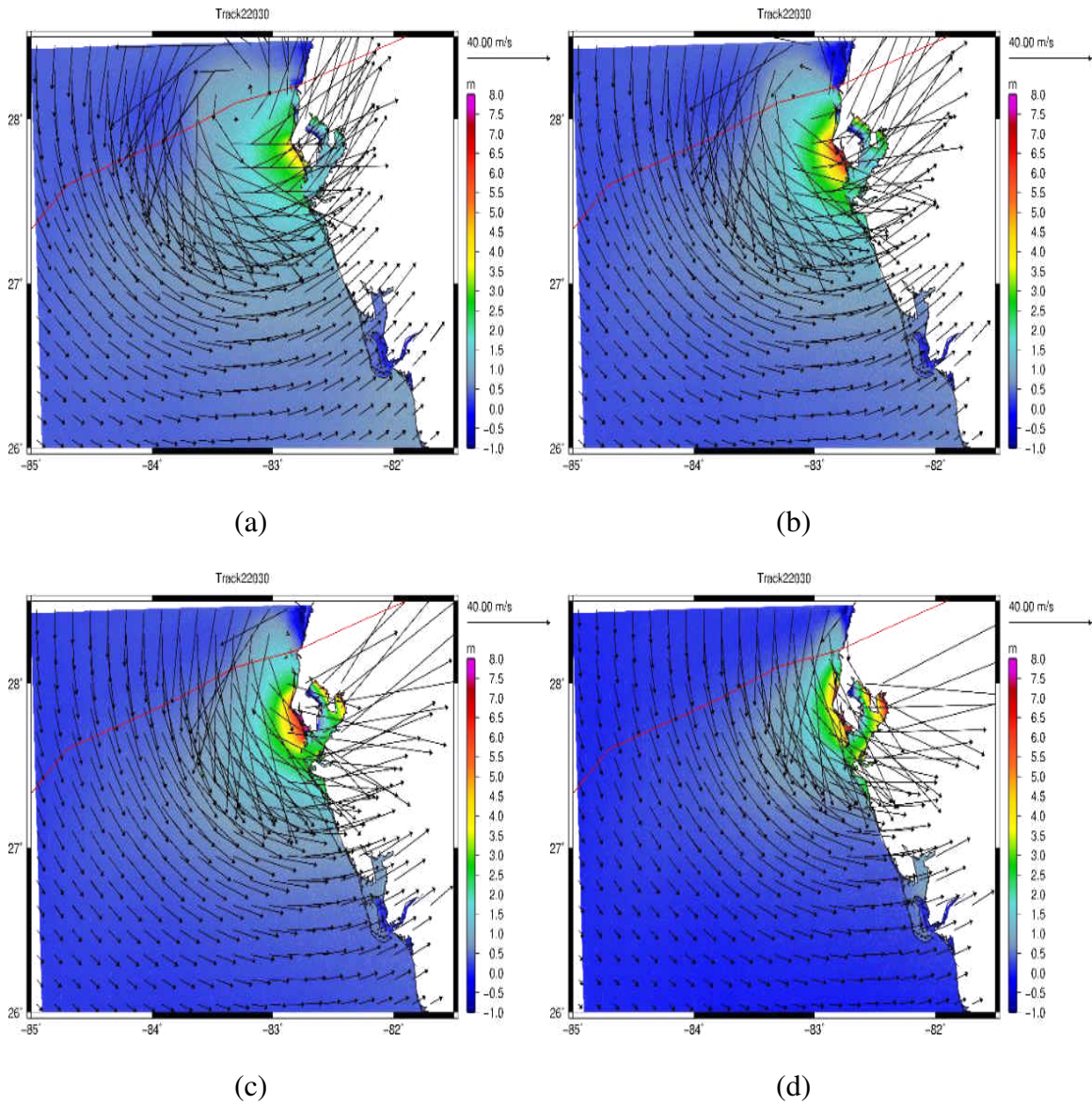
Figure 2-12: Track 2 approaching Tampa Bay (a) with outer bands within the bay (b) increased winds within the bay (c) eye wall approaching with radius of maximum winds and (d) with eyewall over Tampa Bay.

(a)

(b)

(c)

(d)
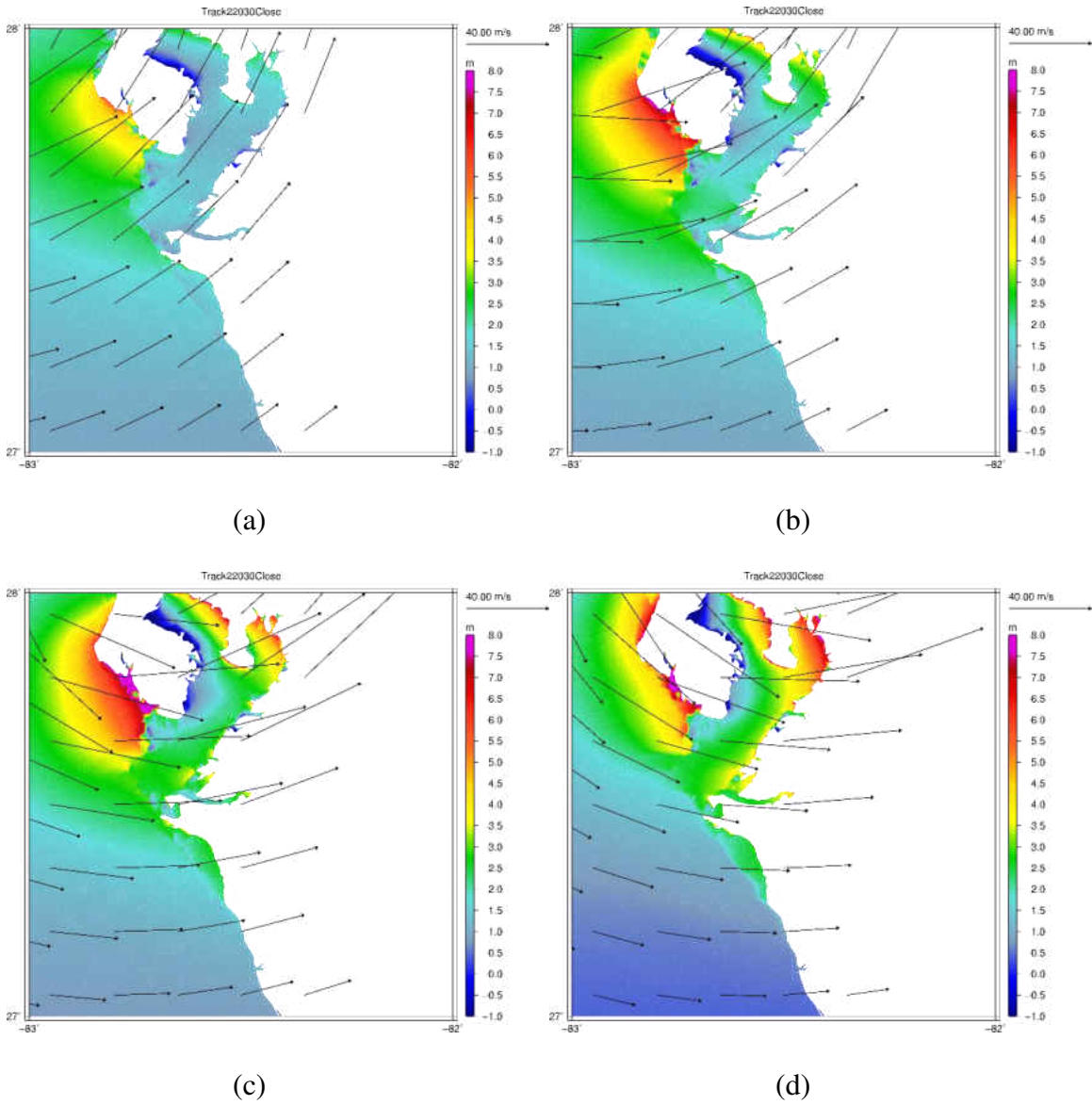
Figure 2-13: Wind fields of Track 2 and storm tide approaching Tampa Bay (a) with outer bands within the bay (b) increased winds within the bay (c) eye wall approaching with radius of maximum winds and (d) with eyewall over Tampa Bay.

(a)   (b)

(c)   (d)
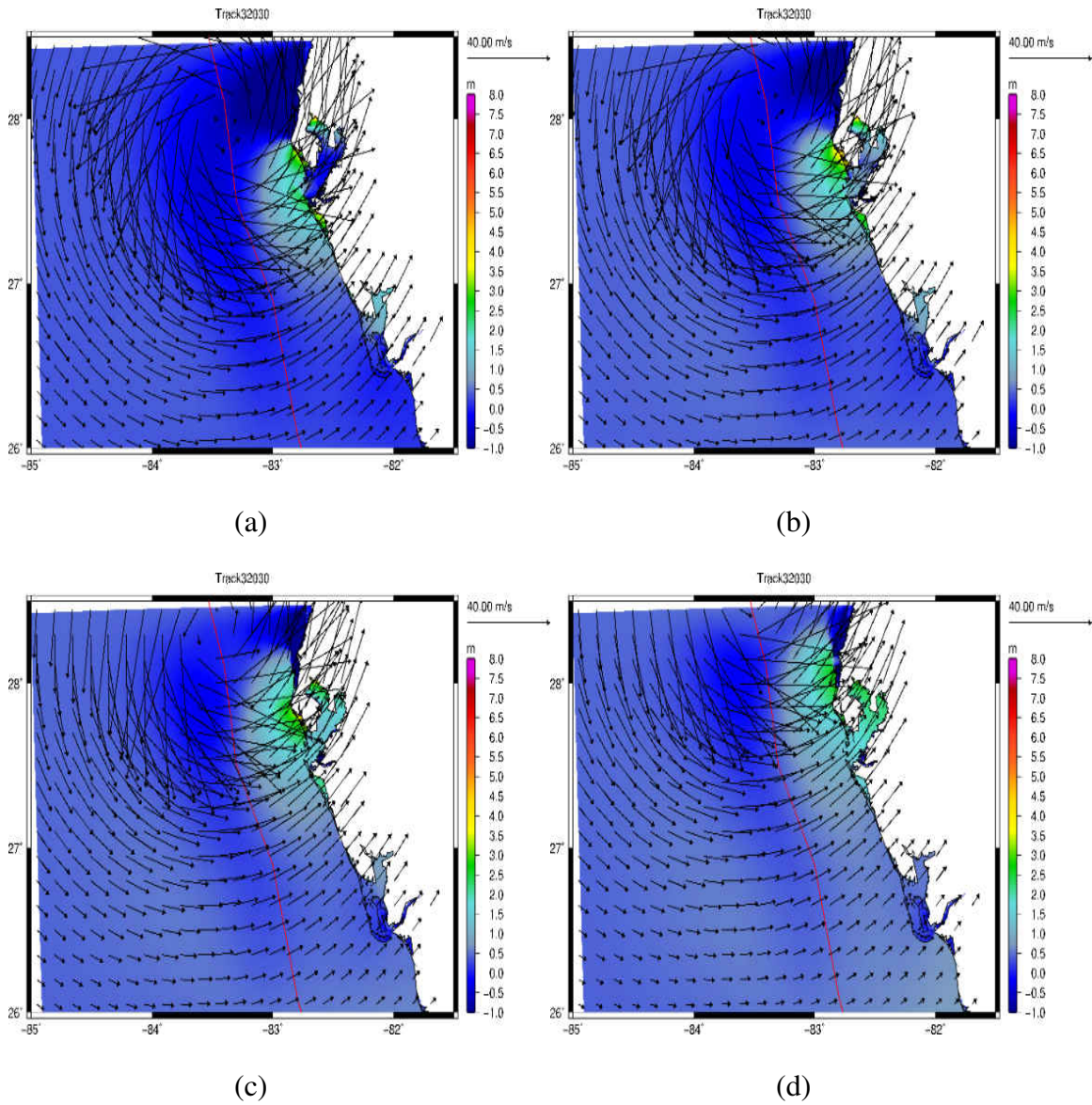
Figure 2-14:Track 3 approaching Tampa Bay from the south (a) with eyewall approaching the bay (b) eye wall passing the Tampa Bay coast (c) outer winds passing over the bay and (d) hurricane passing further north.
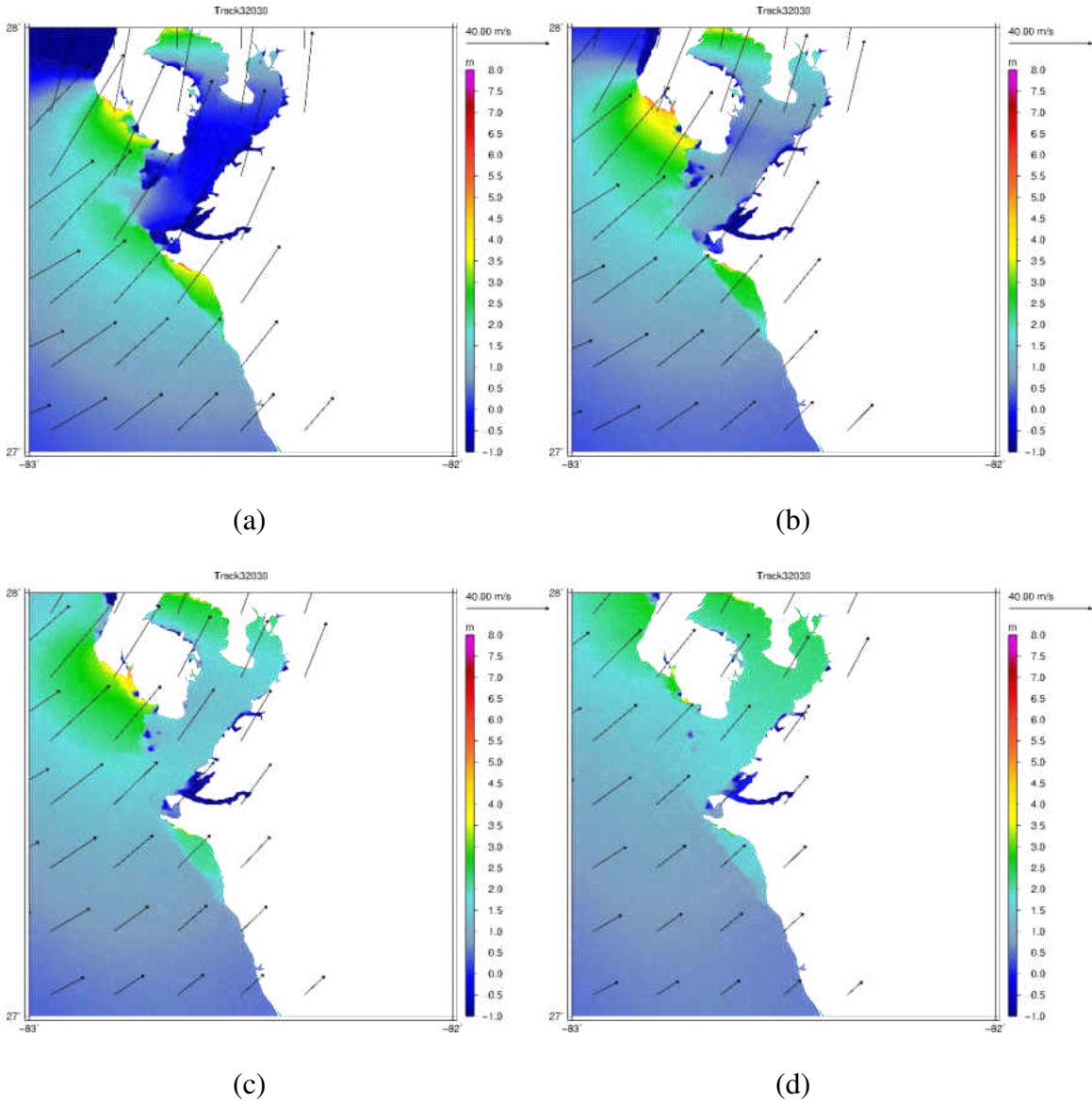
Figure 2-15: Wind fields of Track 3 with storm tide approaching Tampa Bay from the south (a) with eyewall approaching the bay (b) eye wall passing the Tampa Bay coast (c) outer winds passing over the bay and (d) hurricane passing further north.

Similar to the findings from Weisberg and Zheng (2006), the direction of pathways of hurricane track and landfall locations in this study played a significant role in total water levels such as the situation when considering Figures 16 and 17. The southwestern inlet to the Cross Bayou Canal experience the highest total water levels due to its proximity to the radius of maximum winds for each storm scenario considered. Total water levels were suppressed at the northeastern inlet of the Cross Bayou Canal for much of Tracks 1 and 2 due to the fact that the approaching hurricane tracks pushed water eastward toward Tampa and the northeastern Tampa Bay boundaries. Track 3 results in more water being pushed toward the north and northwestern Tampa Bay boundaries resulting in a slightly higher total water levels initially until end of simulation. Overall, Track 2 resulted in the highest total water levels for the southwestern inlet while Track1 resulted in the highest total water levels for the northeastern inlet. The ADCIRC-SWAN water levels were converted from local mean sea level to NAVD 88 using a constant value of +0.163 meters (NOAA Office of Coast Survey, 2017).
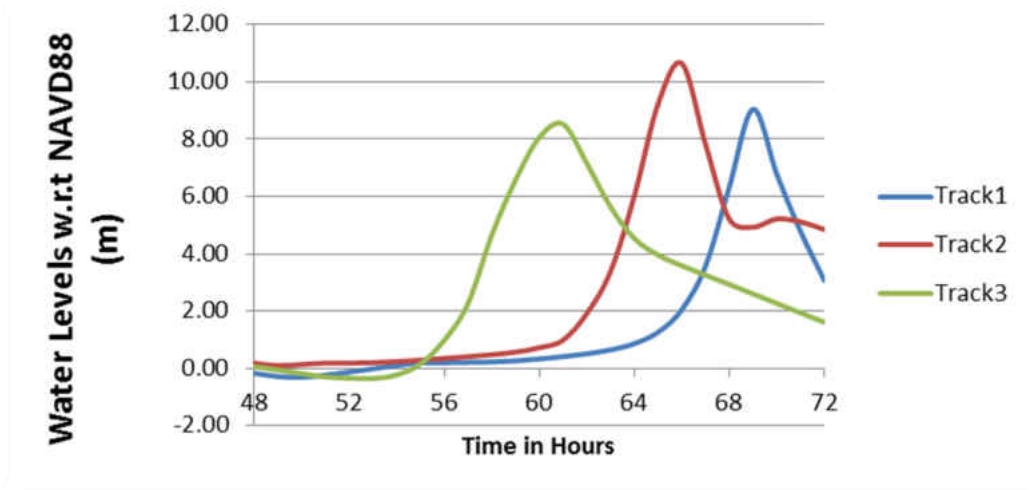
(a)
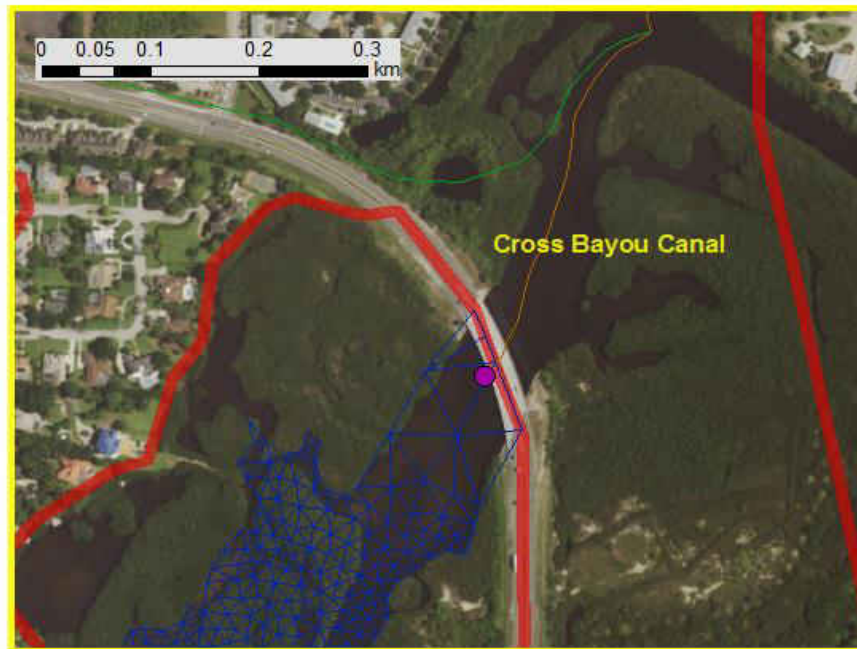
(b)

Figure 2-16: The impact of hurricane tracks on water level with respect to the southwestern side of the Cross Bayou canal. (a) Time series of total water levels (storm surge+ tides+ waves) for southwestern inlet of Cross Bayou Canal for each future storm scenario (2030) during landfall (b) Location of southwestern inlet of Cross Bayou Canal
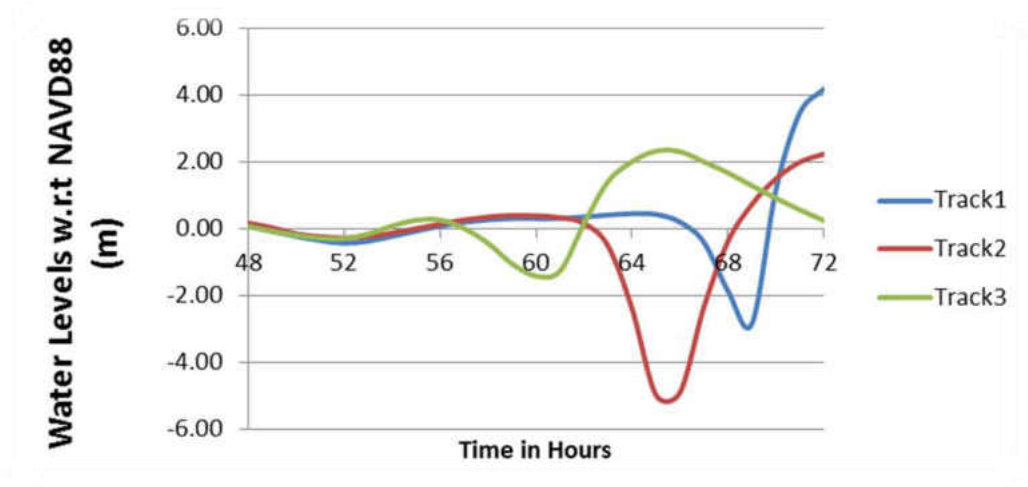
(a)
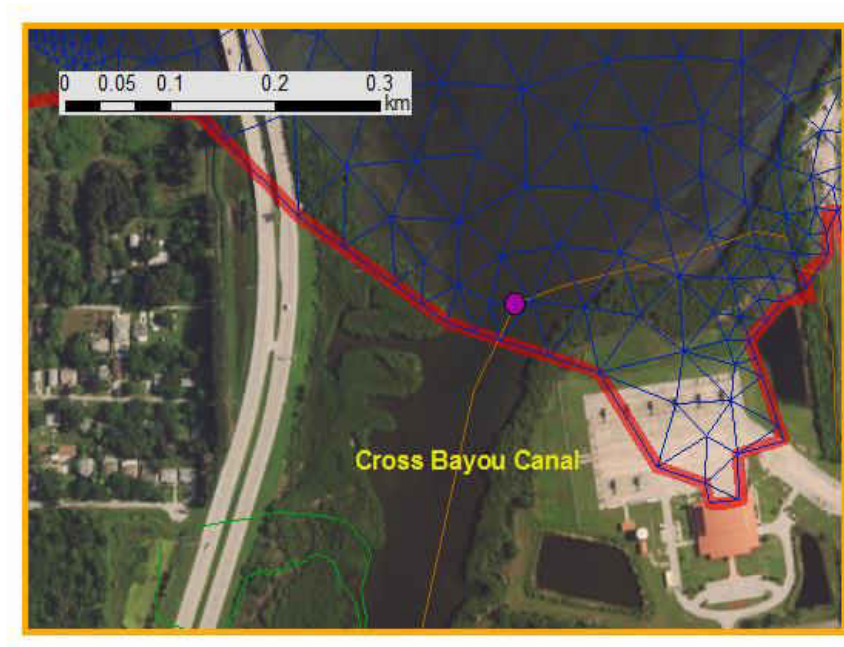
(b)

Figure 2-17: The impact of hurricane tracks on water level with respect to the nottheats side of the Cross Bayou canal. (a) Time series of total water levels (storm surge+ tides+ waves) for northeastern inlet of Cross Bayou Canal for each future storm scenario (2030) during landfall. (b) Location of northeastern inlet of Cross Bayou Canal

2.4.3. Inundation Maps

As indicated in Figures 18, 19 and 20, the southwestern inlet of the Cross Bayou Canal and subsequently the surrounding low-lying areas consistently faced the most inundation as opposed to the northeastern inlet areas of the Cross Bayou Canal. This inundation occurred primarily on the southwestern inlet of the Cross Bayou Canal since it was direct contact with the RMW as each hurricane approached. At slightly higher elevations with respect to the Cross Bayou Canal, such as areas to the northwestern region of the watershed, it is evident that rainfall runoff contributed to flooding in those areas as opposed to storm tide levels. The vulnerability of a particular area can change with respect to a specific type of hazard considered. In the case of tropical cyclones, RMW, landfall location and direction of approach can have an effect on which areas will become more exposed to inundation than others.
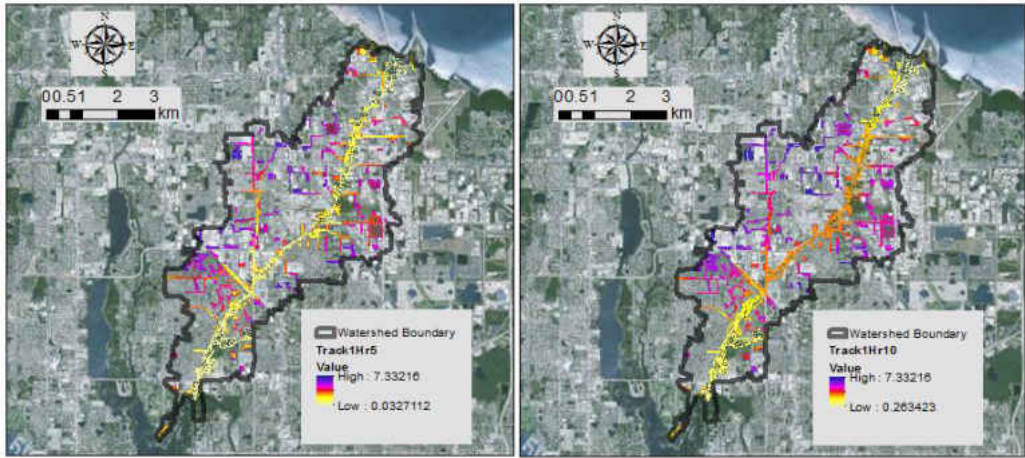
(a)   (b)
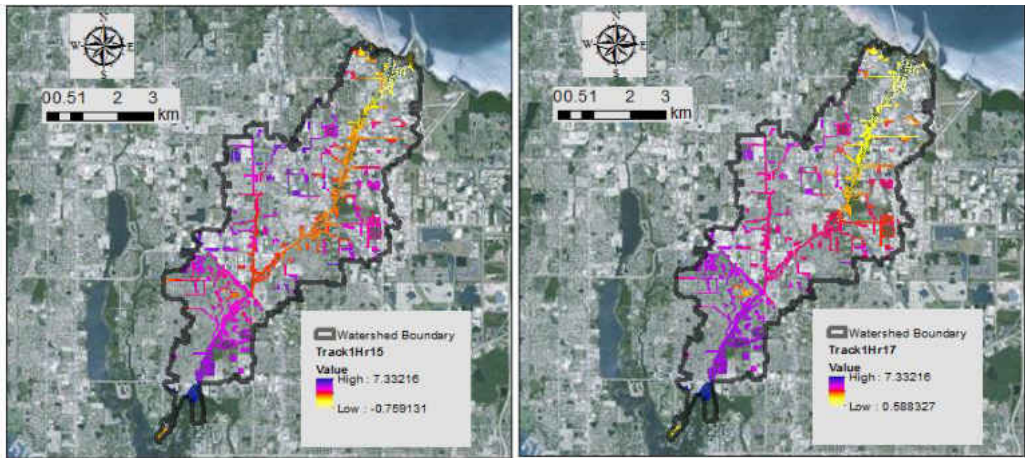
(c)   (d)

Figure 2-18: Flood Hazard maps for combined storm tide condition (Track 1) and SCS Type II 24 hr rainfall event with water depth in meters with respect to NAVD88 datum during (a)Hour 5, (b) Hour 10, (c) Hour 15 and max flooding at (d) Hour 17.
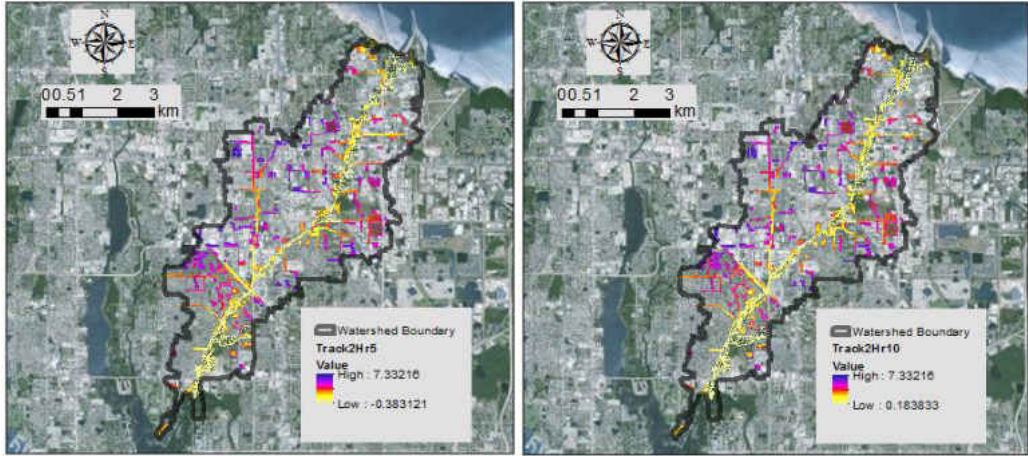
(a)   (b)
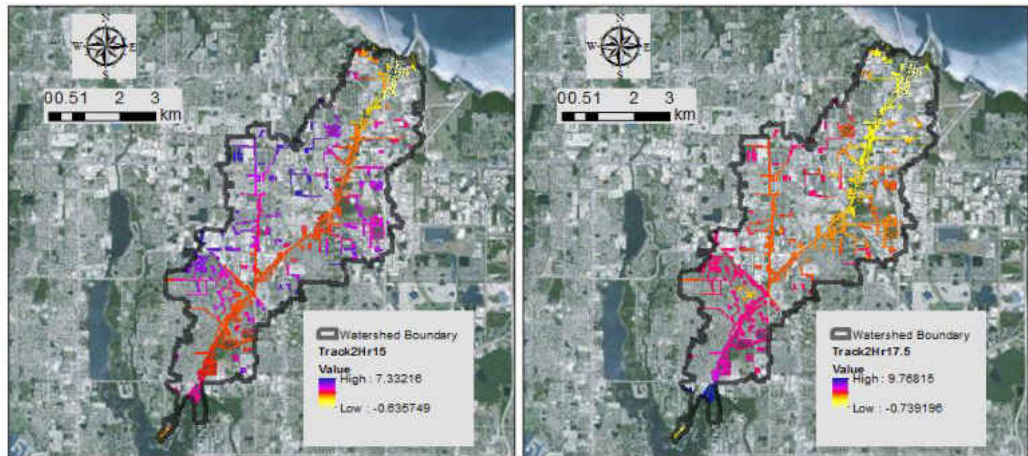
(c)   (d)

Figure 2-19: Flood Hazard maps for combined storm tide condition (Track 1) and SCS Type II 24 hr rainfall event with water depth in meters with respect to NAVD88 datum during (a)Hour 5, (b) Hour 10, (c) Hour 15 and max flooding at (d) Hour 17.5.
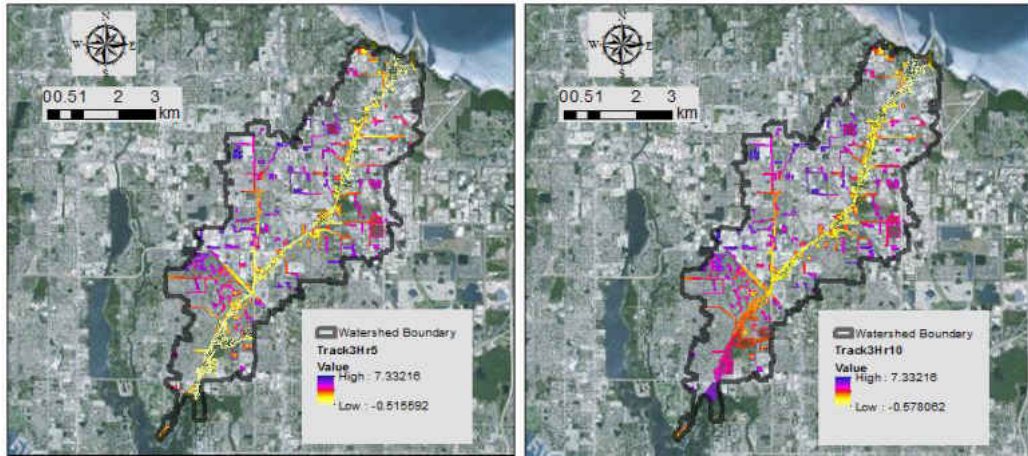
(a)

(b)
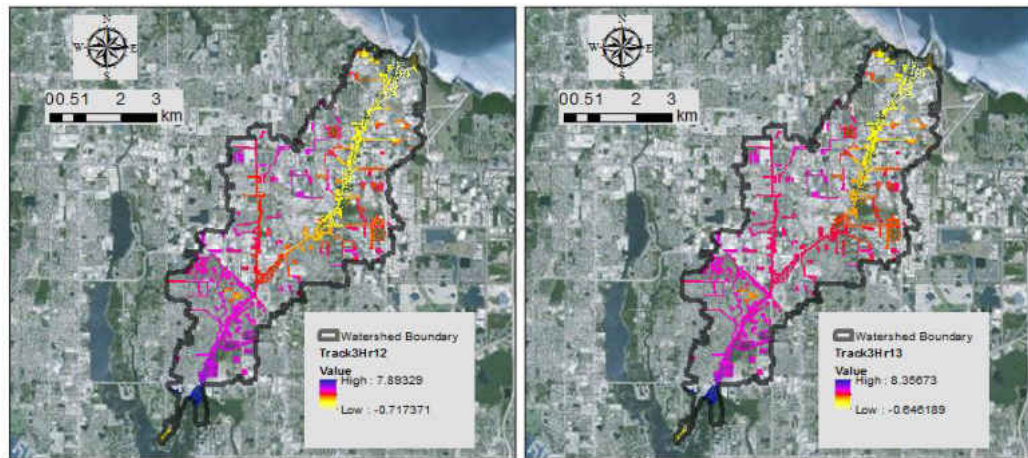
(c)

(d)

Figure 2-20: Flood Hazard maps for combined storm tide condition (Track 1) and SCS Type II 24 hr rainfall event with water depth in meters with respect to NAVD88 datum during (a)Hour 5, (b) Hour 10, (c) Hour 12 and max flooding at (d) Hour 13

2.5. <u>Conclusion</u>

Overall, this chapter highlights the need for creating a more holistic view of potential interactions coastal flood inundation assessment of coastal natural hazards, such as hurricanes, storm tides and rainfall, with the man-made environment such as stormwater drainage networks in a coastal watershed. Mapping of potential flood areas and extents, particularly at a localized level, requires complex modeling systems, since one model alone typically cannot cover the complex nature of hydraulic and hydrological interactions of coastal flooding. These interactions include generating storm tide conditions from meteorological forcings, routing storm tide conditions hydraulically through conveyance systems within a coastal urban watershed while capturing important hydrological factors and interactions between them such as rainfall runoff and groundwater table fluctuations. What is important is how changes in hazard characteristics can impact the extent of flooding resulting in the necessity of multiple flood assessments based upon hazards considered.

Depending on the nature of the study, it could require integration and/or coupling of several computational models to do so which will be a good future work of this study for continuous improvement. For modeling complex systems, what is also concerned about are the levels of uncertainty to be tackled. There exists uncertainty in modeling output which is derived from uncertainty in data used to build the model. The uncertainty in data is observational uncertainty (e.g., incomplete and noisy observational data, systematic biases, etc.) whereas the uncertainty in modeling output is model structure uncertainty (e.g., in the specification of model processes and internal relations). Lastly there are uncertainties in model parameters and states (e.g., initial and boundary conditions). Current practices of uncertainty analysis, especially in these cases of model

integration or coupling, are limited to data assimilation or model-data synthesis per se. Future work may be directed to conduct model-data fusion to further reduce the systematic uncertainties.

2.6. <u>References</u>

Aquaveo, LLC, 2016: Surface-Water Modeling System, Version 12.1, Reference Manual & Tutorials, Provo, Utah.

Bedient, P. B., Hoblit, B. C., Gladwell, D. C., and Vieux, B. E., 2000. NexRAD radar for flood prediction in Houston. *Journal of Hydrologic Engineering*, 5(3), 269-277.

Brunner, P. and Simmons, C. T., 2012. HydroGeoSphere: A Fully Integrated, Physically Based Hydrological Model. *Groundwater*, 50(2), 170-176.

Booij, N., Ris, R.C., and Holthuijsen, L.H., 1999: A third-generation wavemodel for coastal regions, Part 1: Model description and validation. *J. Geophys. Res*.: Oceans 104(C4), 7649e7666. http://dx.doi.org/10.1029/98JC02622.

Canuti, P., Casagli, N., Catani, F., and Falorni, G., 2002. Modeling of the Guagua Pichincha Volcano (Ecuador) Lahars. *Physics and Chemistry of the Earth*, 27(36), 1587–1599.

Cheng, H.-P., J.-R. C. Cheng, R. M. Hunter, and H.-C. Lin, 2010: Demonstration of a coupled watershed-nearshore model. ERDC TN-SWWRP-10-XX. Vicksburg, MS: U.S. Army Engineer Research and Development Center. Assessed July 2016 [Available online at https://swwrp.usace.army.mil/]

Condon, A. J and Sheng, Y.P., 2012: Evaluation of coastal inundation hazard for present and future climates, *Nat Hazards* 62, 345–373.

Deltares Systems, 2014. SobekSuite [Avilable online at

    http://www.deltaressystems.com/hydro/product/108282/sobek-suite]

Dietrich, J. C., Tanaka, S., Westerink, J.J., Dawson, C.N., Luettich Jr., R.A., Zijlema, M.,

    Holthuijsen, L.H., Smith, J.M., Westerink, L.G., and Westerlink, H.J., 2011: Performance

    of the unstructured-mesh, SWAN+ADCIRC model in computing hurricane waves and

    surge, *J. Sci. Comput.*, 52, 468–497, doi:10.1007/s10915-011-9555-6

Downer, C. W. and Ogden, F. L., 2004. GSSHA: A model for simulating diverse streamflow

    generating processes. *Journal of Hydrological Engineering*, 9(3), 161-174.

Feuer, S.E., Landsea, C.W., Woolcock, L., and Berkeley, J., 2004: *The reanalysis of Atlantic*

    basin tropical cyclones from the 1920's: A re-examination of three catastrophic

    hurricanes that impacted Florida. Preprints of the 26th Conference on Hurricanes and

    Tropical Meteorology, American Meteorological Society, Miami Beach, FL.

Hervouet, J. M., 2007. Hydrodynamics of Free Surface Flows Modelling with the Finite Element

    Method. doi: Wiley. 978-0-470-03558-0

Hübl, J. and Steinwendtner, H., 2001. Two-dimensional simulation of two viscous debris flows

    in Austria. *Physics and Chemistry of the Earth*, 26 (9), 639–644.

Huang, Y., Weisberg, R.H., and Zheng, L.Y., 2010: Coupling of surge and waves for an Ivan-

    like hurricane impacting the Tampa Bay, Florida region. *Journal of Geophysical*

    Research, 115**,** doi:10.1029/2009JC006090.

IPCC, 2014: Summary for Policymakers. In: Climate Change 2014: Impacts, Adaptation, and

    Vulnerability. Part A: Global and Sectoral Aspects. Contribution of Working Group II to

    the Fifth Assessment Report of the Intergovernmental Panel on Climate Change [Field,

C.B., V.R. Barros, D.J. Dokken, K.J. Mach, M.D. Mastrandrea, T.E. Bilir, M. Chatterjee, K.L. Ebi, Y.O. Estrada, R.C. Genova, B. Girma, E.S. Kissel, A.N. Levy, S. MacCracken, P.R. Mastrandrea, and L.L. White (eds.)]. Cambridge University Press, Cambridge, United Kingdom and New York, NY, USA, pp. 1-32.

Knebl, M. R., Yang, Z. L., Hutchison, K., and Maidment, D. R., 2005. Regional scale flood modeling using NEXRAD rainfall, GIS, and HEC-HMS/RAS: a case study for the San Antonio River Basin Summer 2002 storm event. *Journal of Environmental Management*, 75, 325–336.

Le Provost, C., Lyard, F., Molines, J. M., Genco, M. L., and Rabilloud, F, 1998: "A hydro-dynamic ocean tide model improved by assimilating a satellite altimeter-derived data set,"

Journal of Geophysical Research,103, 5513-5529

Luettich, R.A., Westerink, J.J., and Scheffner, N.W., 1992. ADCIRC: An Advanced Three-dimensional Circulation Model for Shelves, Coasts and Estuaries. Report 1: Theory and Methodology of ADCIRC-2DDI and ADCIRC-3DL. Department of the US Army Corps of Engineers, Washington, D.C.

National Weather Service, 2015: 1921 Tarpon Springs Hurricane. Accessed September 2015. [Available online at http://www.srh.noaa.gov/tbw/?n=tampabay1921hurricane#]

NOAA, 2015: Tropical Cyclone Climatology. Accessed September 2015. [Available online at http://www.nhc.noaa.gov/climo/]

NOAA, 2016b: Sea Level Trends. Accessed August 2016. [Available online at https://tidesand

currents.noaa.gov/sltrends/sltrends.html]

Ris, R.C., Holthuijsen, L.H., and Booij, N., 1999: A third-generation wave model for coastal

regions, Part 2: Model description and validation. *J. Geophys. Res.*: Oceans 104(C4),

7649e7666. http://dx.doi.org/10.1029/ 1998JC900123.

Streamline Technologies, Inc.,2014: ICPR Version 4 Users Manual.

Streamline Technologies, Inc., 2015: An Integrated Surface Water-Groundwater Model of the

Cross Bayou Watershed.

Tampa Bay Regional Planning Council, 2009: The Tampa Bay Catastrophic Plan: Project

Phoenix [Available online at http://www.tbrpc.org/council_members/council

agendas/2015/ 101215/8c.pdf]

Tampa Bay Climate Science Advisory Panel, 2015: Recommended Projection of Sea Level Rise

in the Tampa Bay Region [Available online at

http://www.tbrpc.org/council_members/council

agendas/2015/101215/8c.pdf]

CHAPTER 3: MULTI-SCALE MODELING SYSTEM FOR RESILIENCE ASSESSMENT OF GREEN-GREY DRAINAGE INFRASTRUCTURES UNDER CLIMATE CHANGE AND SEA LEVEL RISE IMPACT

Chapter 3 includes work accepted for publication under the following reference:

Joyce, J., Chang, N. B., Harji, R., Ruppert, T., and Imen, S., 2017: Developing a multi-scale

modeling system for resilience assessment of green-grey drainage infrastructures under

climate change and sea level rise impact. Environmental Modelling and Software, 90: 1-

26.

3.1. Introduction

Resilience, when applied to infrastructure systems, implies the ability of such infrastructure

systems (including their interconnected ecosystems and social systems) to absorb disturbance and

recover after a disturbance (Omer, 2013). In considering the resilience of networked infrastructure

systems, Omer (2013) argued that the resilient response of a system results in reduced vulnerability

and greater adaptive capacity or reduced susceptibility and greater ability to continue functionality

under adverse conditions.

These concepts of vulnerability and adaptive capacity of a system depend on the level of

disturbance. DeBruijn (2004) highlighted that the magnitude of disturbance absorbed by a

system depends on its reaction. As such, when applied to a stormwater drainage system, the

magnitude of disturbance can be represented as the storm event intensity and duration, with the

system reaction as peak outflow. Because a smaller (larger) reaction results in larger (smaller)

infiltration and capture, a stormwater drainage system would ideally reduce its reaction (i.e.,

peak inflow/outflow) via increased infiltration and capture of stormwater by the environment.

One example is Low Impact Development (LID), in which planning and structural controls can contribute to resiliency in flood management via adaptive capacity. LID, promoted in recent years as an alternative to traditional stormwater drainage systems, utilizes decentralized multifunctional site designs and incorporates on-site stormwater management practices rather than conventional stormwater management approaches that divert flow toward centralized facilities. At the local scale, the use of LID as an adaptation measure can increase onsite storage of runoff. Onsite storage has additional benefits that increase resiliency, such as reducing and delaying the runoff peak discharge (Roseen et al., 2012).

As reported by DeBruijn (2004), quantifying the response of an infrastructure system to disturbances can provide tangible information about the resilience of a system over time under a posed hazard. Birgani *et al.* (2013) analyzed the physical and technical characteristics of resilience in sustainable urban stormwater management and, in quantifying resilience, argued that capturing the disturbance and the time of recovery were required. In determining the amount of disturbance captured, Birgani *et al.* (2013) expanded on DeBruijn's (2004) assessment by highlighting that when a system is disturbed, the system reacts. When considering the Birgani *et al.* (2013) and the DeBruijn (2004) studies, the response of a stormwater drainage system to a disturbance such as a storm event can be determined by peak outflow and/or stage within a cross-sectional area of a drainage pipe. Peak outflow can be obtained from outflow hydrographs at points of interest. An additional metrics can be obtained by accounting for the time required for the drainage network to "recover" from a disturbance such as a storm event.

To apply the concepts of drainage infrastructure resilience to a real-world case study of flood assessment, the Cross Bayou Watershed, located within Pinellas County near Tampa Bay

in west-central Florida, was chosen as a specific example. The Cross Bayou Watershed has been historically sensitive to flooding from hazards such as runoff from rainfall and high tide events, and over the years, storm events and subsequent flooding have damaged the drainage infrastructure, particularly undersized conveyance systems found throughout the watershed. Drainage infrastructure is increasingly vulnerable with age and urban development, and therefore its adaptive capacity is also reduced when considering future storm events and future hazards such as sea level rise. With increasing vulnerability and decreasing adaptive capacity of the drainage infrastructure over its design life, communities dependent on this infrastructure will also face increased vulnerability and decreased adaptive capacity.

3.1.1. Chapter Objective

The objective of this chapter is to develop a multi-scale modeling platform that would help coastal areas, such as the Cross Bayou Watershed in Pinellas County, Florida, assess drainage infrastructure resilience to coastal flood hazards that pose threats to the watershed, now and in the future year 2030. From this chapter, several important questions were addressed. First, will increases in flooding stress and episodic disturbances of climate variability and sea-level rise favor regime shifts of traditional storm sewer systems toward choosing more low impact development (LID) controls and flood proofing technologies? Second, how will urban storm sewer infrastructure, LID controls, and/or flood proofing technologies alter the hydrologic response of the watershed during different types of storm events? Last, will these regime shifts toward more LID technologies increase resilience of the drainage infrastructure, and what methods or criteria can be implemented to measure the resilience of the drainage system?

3.2. <u>Study Area</u>

       The Cross Bayou Watershed of Pinellas County (Figure 1), Florida, was selected as a case study because of its vulnerability to coastal flooding and Pinellas County's efforts to implement improved stormwater management to increase the area's adaptive capacity to future hazards. The Cross Bayou watershed encompasses approximately 31 km² (7,697 acres), primarily comprising high-density residential, industrial, and commercial areas.

       An important feature of the watershed is a 16.9 km (10.5-mile) long constructed tidal canal, the Cross Bayou Canal (Figure 1), which dissects the watershed and connects both Tampa Bay and Boca Ciega Bay on its northeastern and southwestern ends, respectively. The Cross Bayou Canal also intersects the Pinebrook Canal to the southwest (Figure 1). Water within the canal can flow in either direction, depending on tidal conditions. This feature, while useful for overall watershed drainage, is potentially hazardous to surrounding communities such as the Mariners Cove residential community (Figure 2) during high tide events, particularly considering the ongoing threat of sea level rise (NOAA, 2016) near the Tampa Bay region.
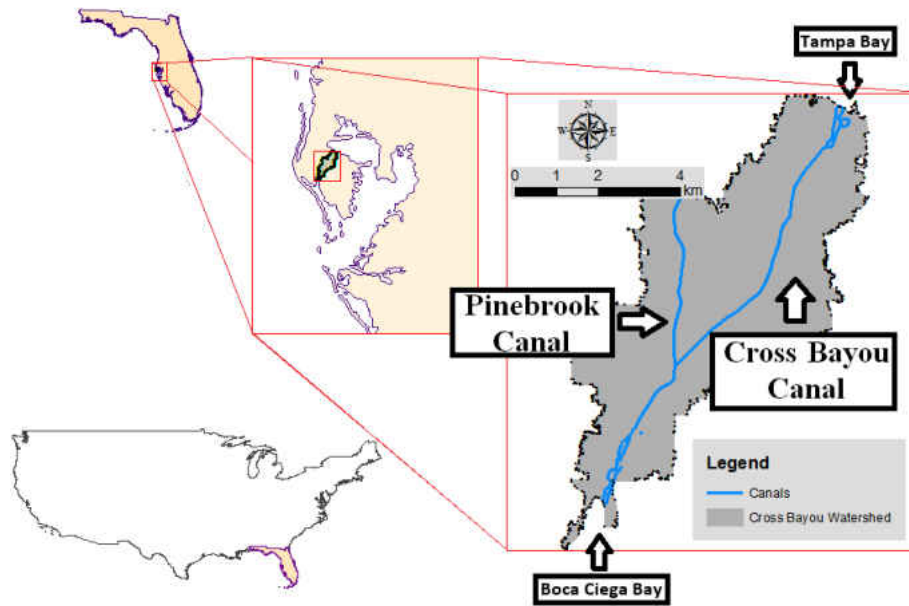
Figure 3-1: Extent of Cross Bayou Watershed

Some areas in the watershed are consistently more vulnerable and have a decreased adaptive capacity to flooding. The High Point and Mariners Cove residential communities (Figure 2) are known for significant flooding from storm events. Flooding in the Mariners Cove community is primarily caused by heavy rains and overflow of the adjacent Cross Bayou canal. Both communities have documented inadequate or inefficient drainage infrastructure due the age and size of existing drainage systems, which cannot handle runoff from increasing urban development. The Mariners Cove community, in particular, is much closer to the Cross Bayou canal. Areas most vulnerable to hazards also represent those most sociologically vulnerable; both Mariners Cove and High Point communities are predominately low-income areas. The vulnerability and adaptive capacity of these communities are much higher and lower, respectively.
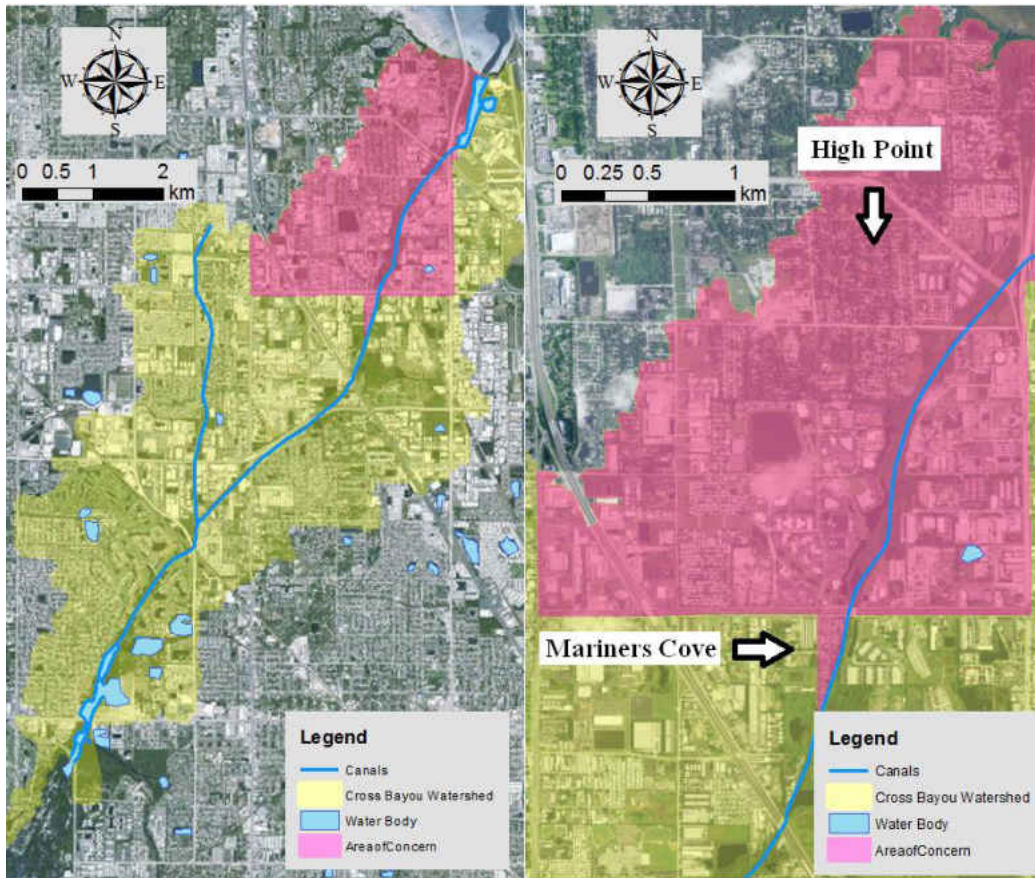
Figure 3-2: Area of Concern defines historically vulnerable areas such as the High Point and Mariners Cove residential areas.

3.3. Methodology

The methods outlined in this chapter center around the concept of infrastructure resilience for a coastal urban watershed (Figure 3) using an informatics-based multi-scale modeling approach. Quantitative resilience metrics were established to quantify engineering infrastructure resilience of the stormwater drainage system within the Cross Bayou watershed under existing and future conditions. To determine the resiliency of the stormwater management system due to flood hazards such as rainfall runoff, high tide, and sea level rise for the future year 2030, a detailed and

68

comprehensive framework is needed, particularly for the complex hydrologic and hydraulic interactions that exist within the Cross Bayou watershed. With the consideration of LID technologies for flood control, this framework contains a multi-scale modeling platform (Figure 4) that includes a comprehensive hydrodynamic and hydrologic stormwater model, called the Interconnected Channel and Pond Routing Model v.4 (ICPR4) (Streamline Technologies, 2015), in conjunction with informatics methods for effectively presenting resilience-based information and data to stakeholders.
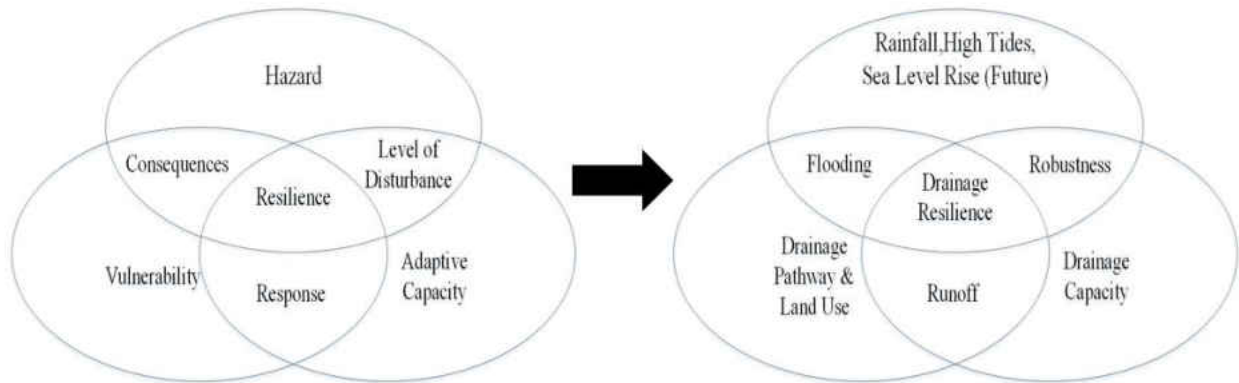
Figure 3-3: Methodology framework for drainage resilience
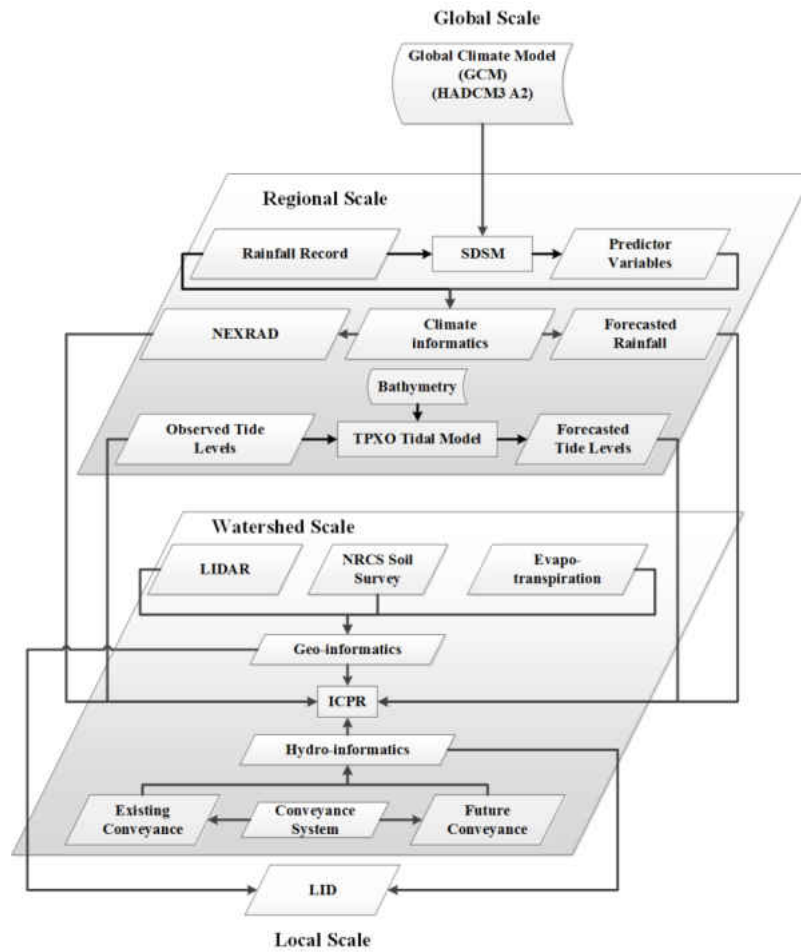
Figure 3-4:Data flow diagram highlighting a multi-scale, informatics approach to the modeling framework

3.3.1. LID Type, Sizing, Siting & Design Criteria

Determining sizing and siting options of LID within the watershed depends on not only characteristics such as elevation, slope, soil type, and land cover, but also the existing drainage network and areas of high runoff potential. The existing stormwater drainage network and points of outfall into the Cross Bayou Canal (Figure 5) can affect vulnerable areas such as Mariners Cove. In this case, the sizing and siting of LID is chosen to (1) reduce runoff collected at major conveyance systems in High Point to offer greater resilience and (2) reduce discharge of runoff

into the Cross Bayou Canal from both High Point and adjacent areas surrounding the Pinellas County Jail complex. This is linked to reduce contribution of flooding from runoff and its interaction with high tides within the canal, which could affect downstream communities such as Mariners Cove adjacent to the canal. High Point is characterized by high-density residential areas, institutional areas, and commercial sites, and the area surrounding the Pinellas County Jail complex is characterized by institutional and commercial areas, each with a considerable percentage of imperviousness (some greater than 50%).

The type of LID considered depends on the climate and environmental constraints, if any. The nature of storm events found throughout Florida changes depending on season. During the wet season, between June and October, convective rainfall dominates, whereas during the dry season, between November and May, frontal rain dominates (Ali et al., 2000). Convective rainfall results in many short-duration events with rapidly changing intensity that produce greater peak discharges, whereas frontal rain results in moderate to heavy rainfall over a longer duration that produces greater runoff volume (FHWA, 1984). These differences highlight the need for a range of LID types from swales to detention ponds. With respect to environmental constraints, particularly for the High Point area, space and high groundwater tables are limiting factors.
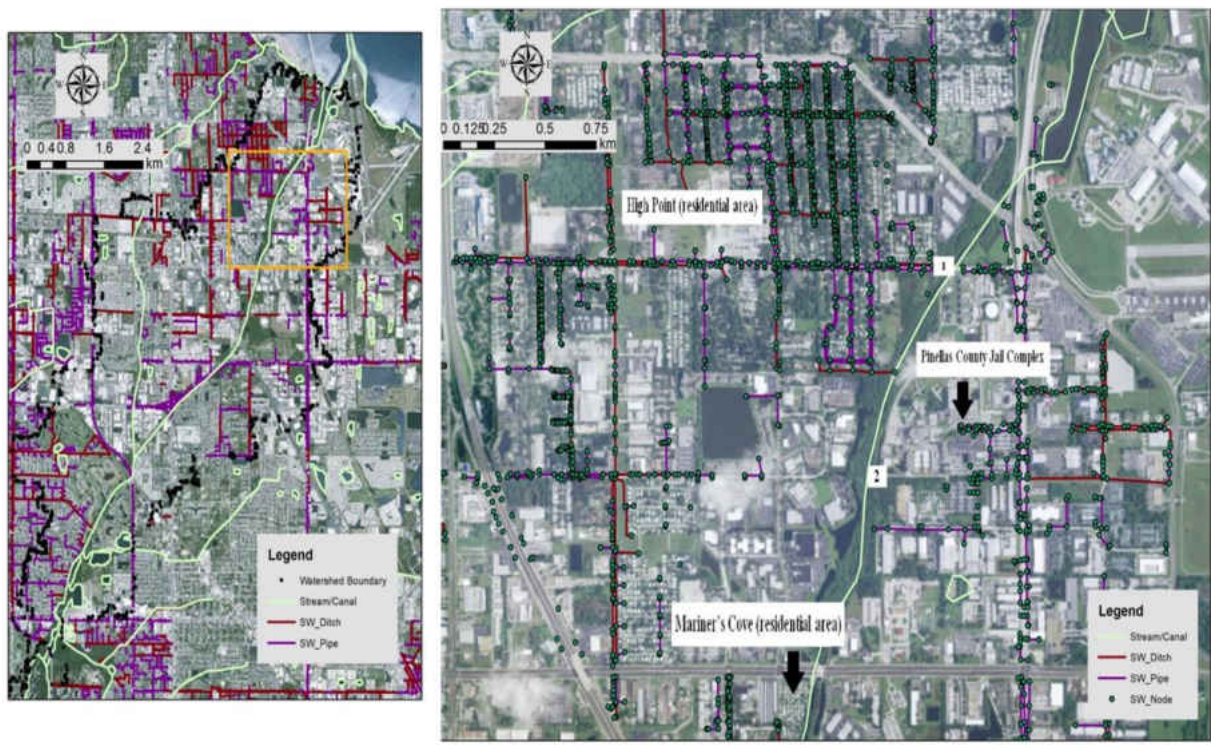
Figure 3-5: Current drainage network and key points of outfall (1&2).

3.3.2. LID Scenarios

Locations for LID implementation were proposed (Figure 6), along with LID

implementation options (Appendix B) sought for placement at areas within this study. Although

the combination of appropriate sizing of LID within these sites near High Points is vast, an

important parameter such as percent imperviousness can be useful for determining the

appropriate portfolios of LID to be implemented. Percent imperviousness is a useful parameter in

this regard and can be expressed as the total coverage by impervious surfaces to the total land

area considered. Percent imperviousness (Table 1) was determined from delineated sub-basins

around all major drainage conveyances and existing detention systems (Jones Edmunds and

Associates, Inc., 2013).
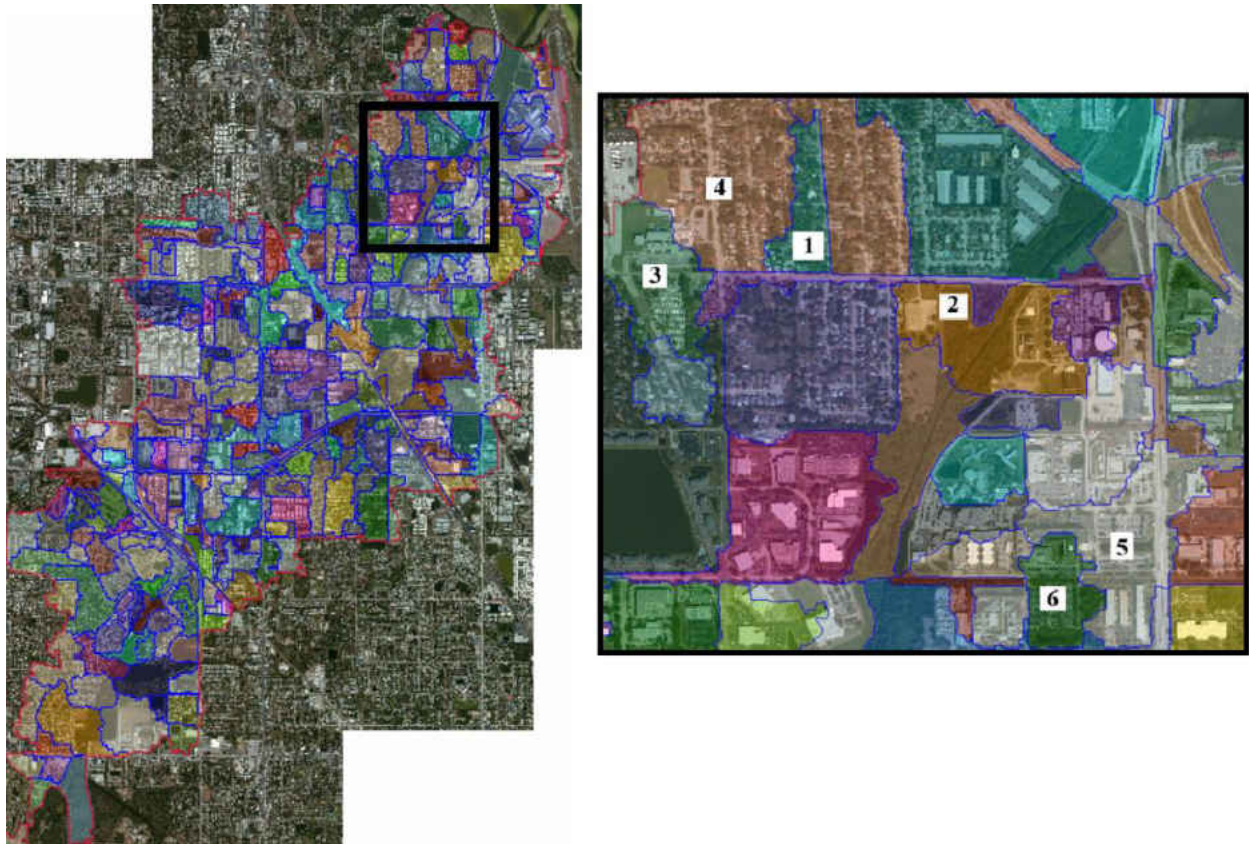
Figure 3-6: Sub-basins within Cross Bayou Watershed for future LID implementation.
Each color distinguishes each sub-basin

Table 3-1: Percent Imperviousness & Perviousness for sub-basins in Figure 8

Basin No.	Basin Size(acres)	Basin Size (m^2)	Pre-LID % Impervious	Pre-LID % Pervious
1	9.4	38,032	48.7	51.3
2	18.0	72,788	0.0	100.0
3	19.9	80,515	55.4	44.6
4	49.8	201,531	55.5	44.5
5	33.3	134,732	74.5	25.5

Basin No.	Basin Size(acres)	Basin Size (m^2)	Pre-LID % Impervious	Pre-LID % Pervious
6	13.2	53,407	76.1	23.9

Several LID scenarios were explored to reduce the percent imperviousness and increase the percent perviousness (i.e., infiltration) (Table 2), assuming that any combination of LIDs for a particular sub-basin has a total area that corresponds with a particular percent pervious. In other words, a 25% impervious reduction in Basin 1 corresponds with a 25% increase in perviousness as a replacement if that particular LID option is implemented. Based on the density of urban space in each sub-basin and soil characteristics, however, the most suitable combination of LIDs can be determined (i.e., Column 5, Table 2).

Table 3-2: Scenarios for Imperviousness Reduction in the proposed LID Portfolio

Basin No.	Existing % imperviousness	25% reduction in imperviousness (Scenario 1)	50% reduction in imperviousness (Scenario 2)	Proposed LID
1	48.7	36.6	24.4	Swales
2	0.0	0.0	0.0	Retention Pond
3	55.4	41.5	27.7	Green Roof,

Basin No.	Existing % imperviousness	25% reduction in imperviousness (Scenario 1)	50% reduction in imperviousness (Scenario 2)	Proposed LID
				Swales, Pervious Pavement
4	55.5	41.6	27.8	Green Roof, Swales, Pervious Pavement
5	74.5	55.9	37.3	Green Roof, Swales, Pervious Pavement
6	76.1	57.0	38.0	Pervious Pavement

3.3.3. Storm Scenarios

Design for stormwater management typically relies on a design storm with an associated magnitude or intensity, duration, and frequency. To reduce flooding potential via incorporation of LID, the likely magnitude, frequency, and duration of rainfall for the Cross Bayou watershed must be determined, typically via statistical techniques based on historic rainfall records such as frequency analysis. Frequency analysis involves relating the magnitude of events to their frequency of occurrence or return period via probability distribution based on the design storm(s) utilized for LID and/or best management practice (BMP) implementation by various agencies across varying levels of governance (national, state, district and county) (Table 3).

Table 3-3: LID Design Storm Approach across Varying Levels of Governance

Level of Governance	Agency/Governing Body	Design Storm for Stormwater Management	Specific to LID/BMP?	Reference
National	Environmental Protection Agency (EPA)	2-, 10- and 100-yr storms	Yes	Clar et. al (2004)
	Regional Frequency Analysis using L-moments	1-yr, 2-yr, 5-yr, 10-yr, 25-yr, 50-yr, 100-yr, 200-yr, 500-yr and 1000-yr		NOAA (2013) Hosking and Wallis (1997)

Level of Governance	Agency/Governing Body	Design Storm for Stormwater Management	Specific to LID/BMP?	Reference
		15-minute, 30-minute, 1*, 2*, 3*, 6*, 12*, 1**, 2-**, 3**, 4**, 7**, 10**, 20**, 30**, 45** and 60**		.
State	Florida Department of Environmental Protection (FDEP)	3-yr 1-hr storm	Yes	Florida Department of Environmental Protection (2014)
District	Southwest Florida Water Management District (SWFWMD)	25-yr event in an open basin or the 100-yr event in a closed basin	Yes	SWFWMD (2013)
County	Pinellas County	100-yr, 24-hr	Yes	Pinellas County (2016)

Note: (*) represents hour and (**) represents days

Currently, the design, permitting, construction, and operation of stormwater management systems in Florida are governed by laws and regulations of the State of Florida, regional water management districts, and local governments. Local governments such as Pinellas County are the primary source for design storm considerations for LID implementation in the Cross Bayou watershed because it falls within county boundaries. In addition, Pinellas County also presents the largest of possible design storms with respect to stormwater management. Although magnitude is important in the design storm, duration is equally important. Qin et al. (2013) determined effects of LID on urban flooding at the urban drainage system scale under varying rainfall characteristics such as return period and duration. This analysis is useful because of the nature of rainfall in general and specifically for Florida, given the dominant rainfall types, convective and frontal. These convective and frontal events can be obtained from sub-daily hyetographs (Hernandez, 2001).

In addition, standardized rainfall distribution curves or rainfall mass curves can be created from hyetographs and used to represent the cumulative fraction of rainfall for a given duration and return period. These mass curves have been applied within watershed stormwater management design and are documented in the literature [Huff (1967, 1990) and by the Soil Conservation Service (1973)]. Mass rainfall curves can be developed specifically for convective and frontal storm scenarios, from both the historical period and the year 2030 in 15-min hyetographs, under a given return period and duration. Rainfall distributions of convective and frontal storm events at the sub-hourly scale can reveal much needed information about their potential runoff characteristics, respectively, particularly important for determining the

effectiveness of reduced imperviousness via LID implementation across various sub-basins (Figure 6).

Table 3-4: Developing Rainfall Distributions for Convective and Frontal Storms Under Given Return Period and Duration

Step	Historical Period	Future Period
1	Develop daily hyetograph(s) for a given historical period	Develop daily hyetograph(s) for a future period of concern
2	Determine required design storm magnitude for a given duration [i.e. (N)-yr (X)-hr storm]	Determine required design storm magnitude for a given duration [i.e. (N)-yr (X)-hr storm]
3	Plot design storm magnitude on the daily hyetograph for period of concern and determine the top daily storms near design storm magnitude	Plot design storm magnitude on the daily hyetograph for period of concern and determine the top daily storms near design storm magnitude
4	Separate top daily storm(s)	Separate top daily storm(s)
5	Determine top storm(s) 15-min rainfall patterns using historical record or disaggregation methods	Determine top storm(s) 15-min rainfall patterns using disaggregation methods
6	Determine convective and/or frontal patterns from top storm(s) 15-min hyetographs	Determine convective and/or frontal patterns from top storm(s) 15-min hyetographs

3.3.4. Historical Storm Scenarios

Two known rainfall gauges (USGS 275021082450500 and NOAA/NWS/ GHCND:
USW00012873) exist within the Cross Bayou watershed; however, both gauges have varying
periods of record. NOAA/NWS/GHCND: USW00012873 station provides the longest period of
record (1998–present). The daily time scale presents challenges related to classifying convective
and frontal rain events for analysis that require fine temporal resolution, 15 minutes or less.
Alternatively, 15-minute NEXRAD rainfall data were obtained from the Southwest Florida
Water Management District (SWFWMD) with a 2 km x 2 km resolution (Figure 7). The
NEXRAD rainfall data period of record is from June 1995 to present.
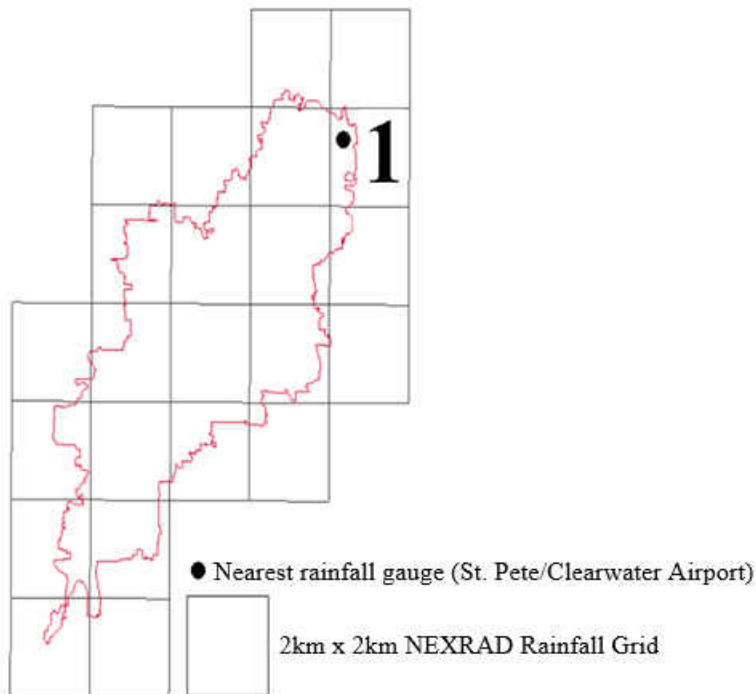
**Figure 3-7: 2 km x 2 km SWFWMD NEXRAD rainfall grid cells over the watershed with
the location of a daily rain gauge.**

From the historic and future rainfall predictions (Table 3), the first step consisted of developing daily hyetograph from the nearest rainfall gauge, the NOAA/NWS/GHCND: USW00012873 station near the St. Petersburg/Clearwater Airport. The second step was to determine the required design storm magnitude for a given duration. Because the Cross Bayou Watershed lies within Pinellas County boundaries, the Pinellas County stormwater manual was referenced to determine the design storm. Within the manual, a 25-yr, 24-hr storm (203–228 mm) was appropriate for open basins or drainage basins with discharge to a tidal waterbody, in this case the Cross Bayou Canal. The third and fourth steps plotted the design storm magnitude on the daily hyetograph from the rain gauge station and separated top daily storm(s), respectively (Figure 8).
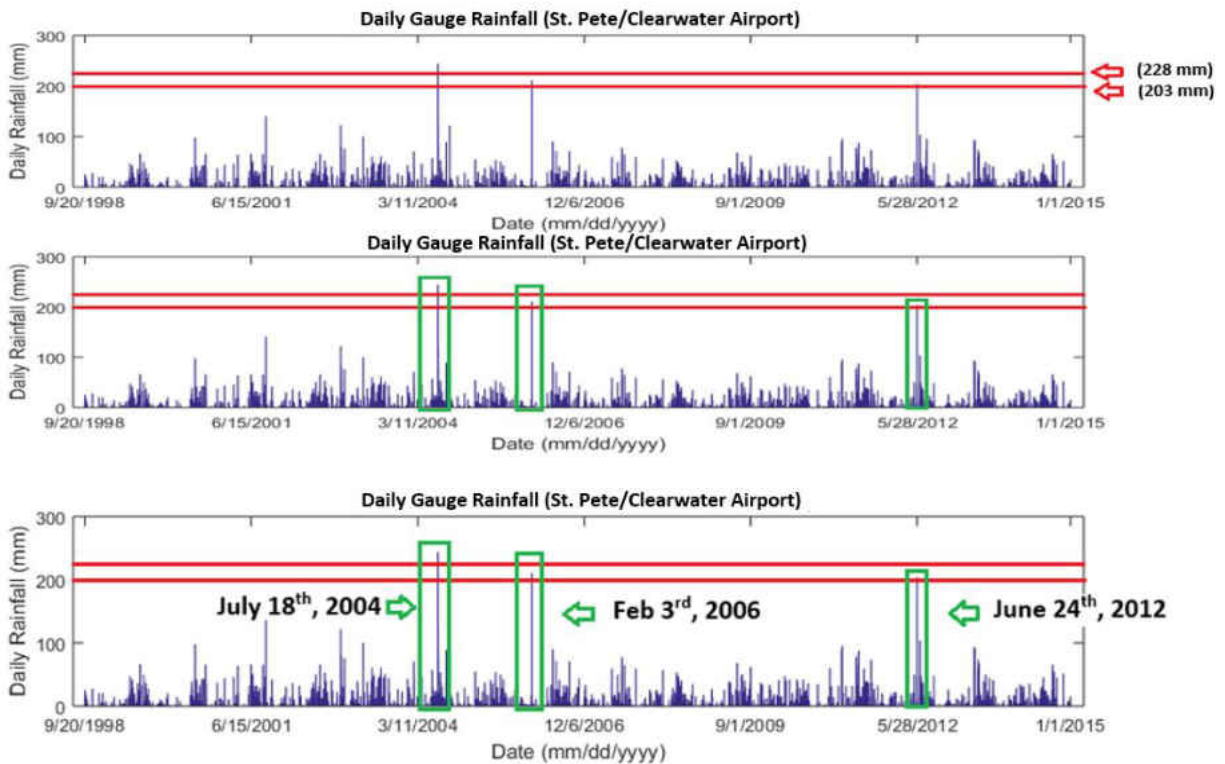
Figure 3-8: Separating top storm(s) within a given design storm magnitude range

The fifth step consisted of developing sub-hourly hyetographs, such as 15-min temporal resolution, for the top daily storms determined in steps three and four. For this study, 15-min rainfall was obtained from the SWFWMD NEXRAD rainfall grid for each top daily storm (Figure 9). Discrepancy was noted for the July 18, 2004, storm between the daily rain gauge and the NEXRAD grid. The 15-min NEXRAD hyetograph intensity for the July 18, 2004 storm was less than expected as compared to the daily rainfall gauge possibly indicating that the July 18 event was a highly localized convective storm with varying intensity throughout the 2 km x 2 km grid area. For this study, the July 18, 2004, event was omitted from further analysis while the remaining storms were kept for consideration.
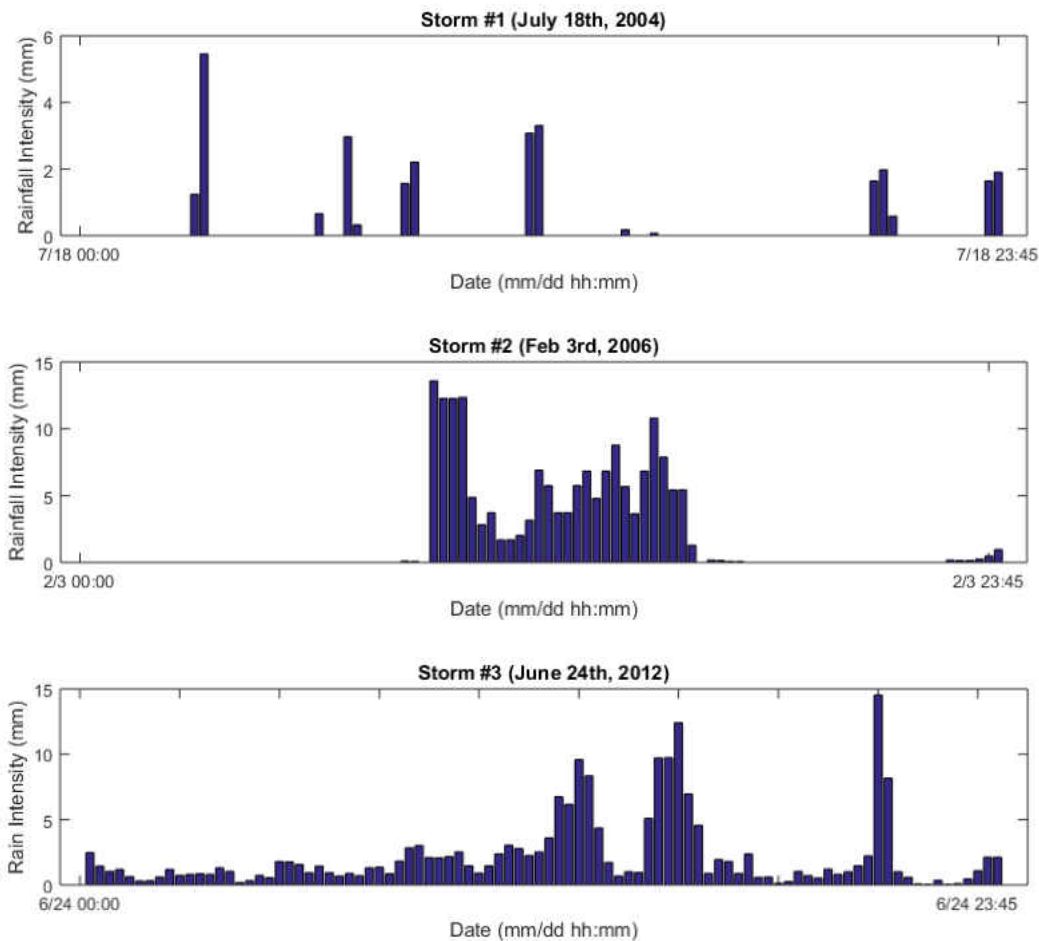
Figure 3-9:Fifteen minute hyetographs of top daily storms determined from Figure 10. Note: Storm #1 was not used in analysis due to discrepancy in radar and gauge measurements

The sixth step consisted of information from step five (Figure 9) to determine convective and frontal rainfall characteristics. With the exception of the storm on July 18, 2004, the storm on June 24, 2012, indicated a much larger variability within periods of short duration and a slightly higher intensity (Figure 9), indicating a highly convective storm nature. The storm on February 3, 2006, although indicative of maximum intensity close to that of the storm on June 24, 2012, did not exhibit large variability within a short duration. Although the storm on

83

February 3, 2006, began with higher intensity, the storm intensity decreased and remained

between 5 and 10 mm throughout midday. From this information, this particular storm may

indicate a frontal pattern. From step six, rainfall distribution curves (Figure 10) can be developed

for both the top convective and frontal storms (with the exception of the July 18, 2004, storm).

These curves define the historical storm scenarios used to determine the effectiveness of reduced

surface imperviousness via LID implementation under the historical period only.
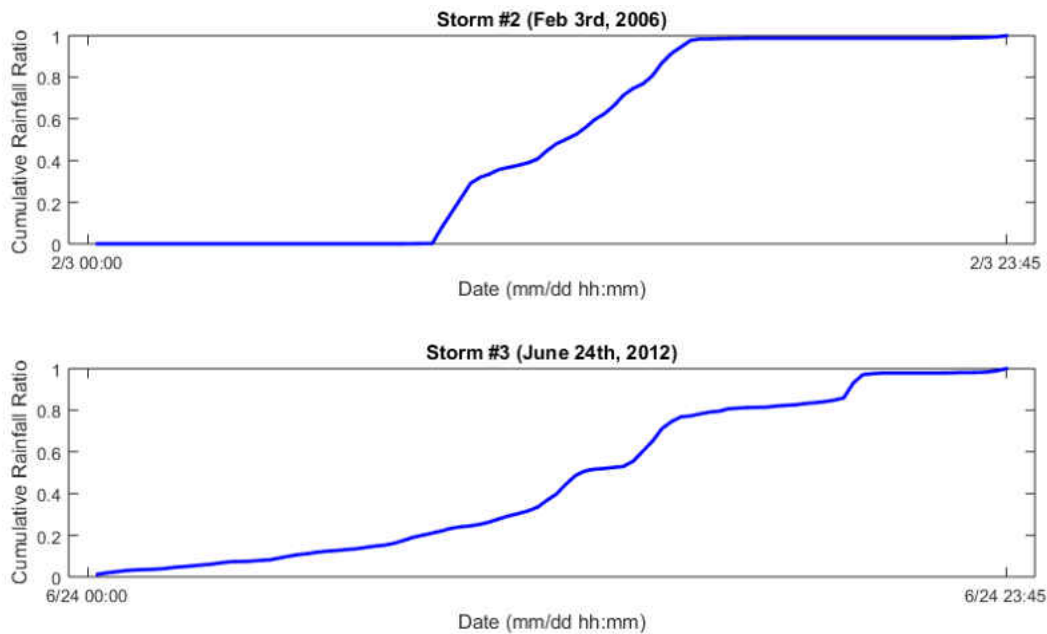
Figure 3-10:Cumulative Rainfall Curves for Top Convective (bottom) and Frontal Storms (top) from Historical Period

3.3.5. Future Storm Scenarios (Year 2030)

Future 15-min rainfall hyetographs were created using daily observed rainfall, statistical

climate modeling, and rainfall disaggregation methods. The Statistical Downscaling Model

(SDSM) (Wilby et. al, 2002) is useful in this regard and was applied to determine statistical

relationships, based on multiple linear regression techniques, between large-scale climate

variables and local climate. These relationships were developed using observed weather data and the Global Climate Model (GCM) derived atmospheric predictors to obtain local climate information for some future time period, the year 2030 for this study. Daily observed climate data (predictands) are required inputs for SDSM, with the predictand of importance being daily rainfall. Because multiple linear regression is used within SDSM, users typically would need observed data as close to normal distribution as possible. Because daily rainfall is typically positively skewed, a transformation of the data was required to obtain a near-normal distribution, achieved using the log transformation of observed rainfall data.

In addition to daily climate input, another important component of SDSM is predictor variables used to describe state of the climate for a particular period of analysis. Selecting the best predictors is a trial and error process to remove the least significant predictors until the remaining predictors are statistically significant, establishing a clear relationship between climate predictor variables and predictands, such as rainfall. Predictor variables utilized in SDSM for this study were derived from the Hadley Centre Coupled Model, version 3(HADCM3) GCM A2 scenario of the Intergovernmental Panel on Climate Change Fourth Assessment Report (IPCC, 2007). All atmospheric predictor variables were re-gridded to a standard coordinate system (2.5º latitude × 3.75º longitude) used in HADCM3 covering 1961 to 2099 (Appendix C). Validation of SDSM focused on how SDSM can capture mean monthly rainfall compared with observed. Although it is important for SDSM to capture the mean monthly rainfall during validation, it is equally important for SDSM to capture monthly variance within the validation period. The ability of SDSM to capture the monthly variance within the validation period is

important for this study because of the need to capture variation in rainfall patterns as opposed to only mean rainfall (Appendix C).

Because input and output data were on a daily scale in SDSM, disaggregation methods were needed to provide estimates of future rainfall on a sub-hourly scale or 15-min increments. Given a wide variety of disaggregation methods available for disaggregating rainfall [Koutsoyiannis, 2003; Wey, 2007; Zhang et al., 2008] across various temporal resolutions, a more recent method, the method of fragments, has been a useful in particular case studies [Pui et al., 2012; Westra et al., 2012]. The method of fragments (Equation 1) relies on a set of fragments, which are a fraction of the temporal resolution desired for disaggregation.

$$F_i = \frac{X_i}{\sum_{i=1}^{n} X_i} \qquad\qquad (\textbf{3-1})$$

Where,

F_i is the fragment at disaggregated time scale;

X_i represents the data at the disaggregated time scale.

The computed fragments become factors multiplied by generated data of the temporal resolution to be disaggregated (Equation 2).

$$X_i{}' = F_i * I \qquad\qquad (\textbf{3-2})$$

Where,

$X_i{}'$ represent the data at the disaggregated time scale;

I represent the generated data at the temporal resolution to be disaggregated;

F_i represent the fragment at disaggregated time scale.

For this study, the computed fragments are at the disaggregated time scale of 15-min, and the data being disaggregated is the daily rainfall from SDSM for the year 2030. The series of 15-min data used to compute the 15-min fragments were determined by comparing the 15-min rainfall hyetographs within the watershed boundary with 15-min rainfall hyetographs outside the watershed boundary that sum to near the 25-yr, 24-hr design storm magnitude (203–228 mm). The goal is to observe changes in sub-daily rainfall patterns with respect to watershed boundary distance. The distribution of 15-min rainfall for the February 3, 2006 (Figures 11 and 12) and June 24, 2012 (Figures 13 and 14) rainfall events were determined for two different locations.
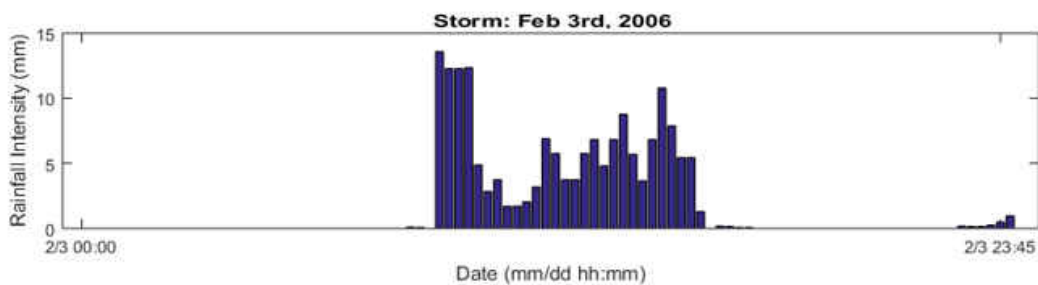
Figure 3-11:Fifteen minute hyetographs for February 3rd, 2006 storm (frontal event) within the watershed boundary [Will be denoted hereafter as frontal rainfall pattern #1]
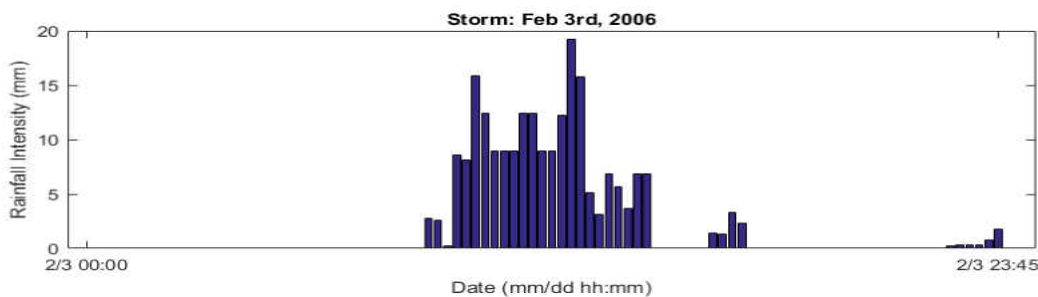
Figure 3-12:Fifteen minute hyetographs for February 3rd, 2006 storm (frontal event) approx. 4km from nearest watershed boundary. [Will be denoted hereafter as frontal rainfall pattern #2

87
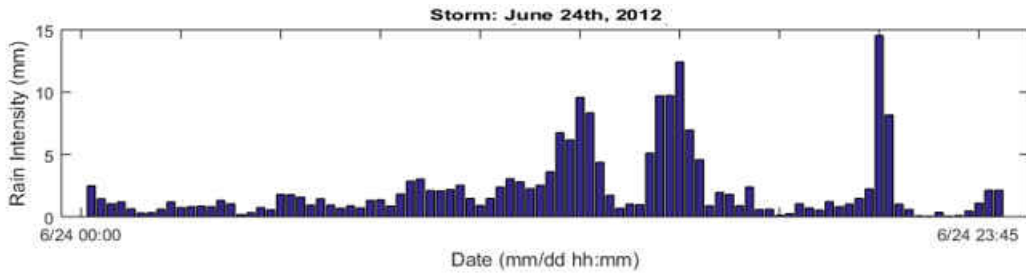
Figure 3-13:Fifteen minute hyetographs for June 24th, 2012 storm (convective event) within the watershed boundary. [Will be denoted hereafter as convective rainfall pattern #1]
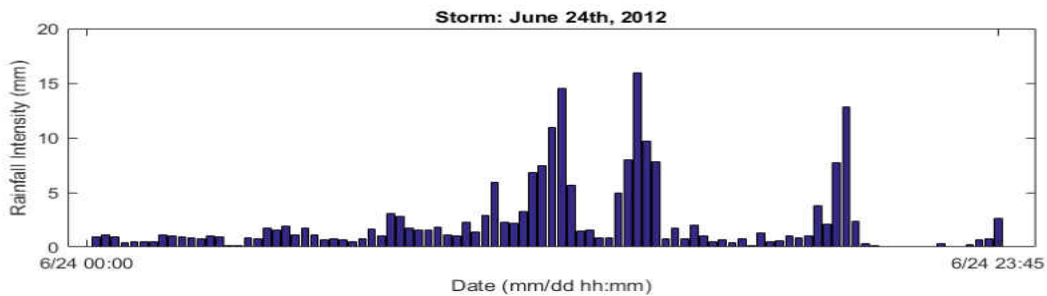
Figure 3-14:Fifteen minute hyetographs for June 24th, 2012 storm (convective event) approx. 4km from nearest watershed boundary. [Will be denoted hereafter as convective rainfall pattern #2]

Similarly, for the historical period storm analysis, the first step for future storm scenarios is to obtain a daily hyetograph for year 2030 to determine storm(s) within the design storm magnitude range. A daily hyetograph for 2030 was produced using SDSM under the HADCM3 global climate model A2 scenario, highlighting the three best series of a 20-member SDSM ensemble (Figure 15).
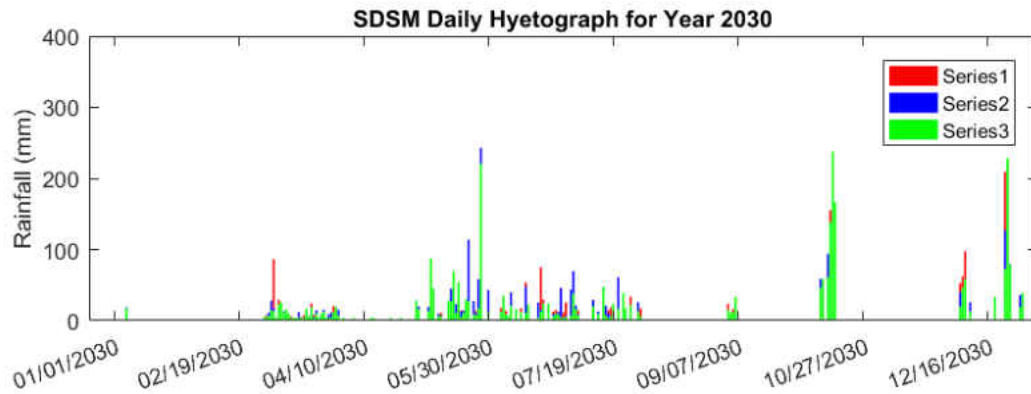
Figure 3-15: Daily SDSM rainfall hyetograph for the year 2030 for three-time series

The second step is to determine the required range of design storm magnitude for a 25-yr, 24hr storm that is the same as for the historical period storm scenarios. The third and fourth steps are to plot the design storm magnitude on the daily hyetograph from the rain gauge station and separate top daily storm(s), respectively (Figure 16). Series 3 was chosen because more than one top storm could be used. Because of significant bias for December in the SDSM validation, December storms were not considered.
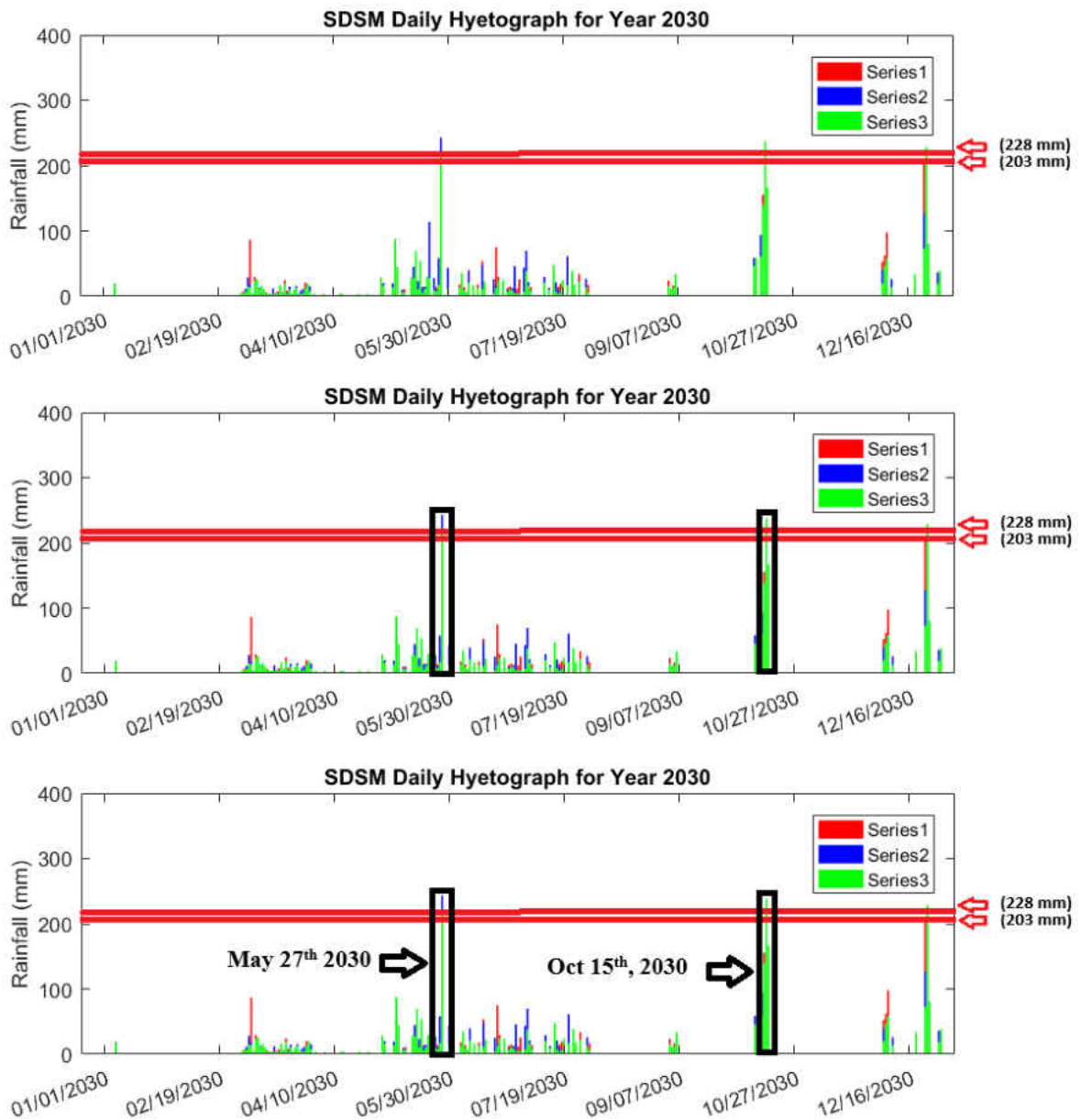
Figure 3-16: Separating top storm(s) within a given design storm magnitude range across three SDSM daily time series for the year 2030

From Figure 16, the May 27, 2030 storm is classified as a frontal storm while the October

15, 2030, is classified as a convective storm event since frontal events typically dominate from

90

November to May whereas convective events dominate from June to October (Ali et al., 2000).

The fifth step consists of developing sub-hourly hyetographs at 15-min temporal resolution, similar to historical period storm scenarios, for the top daily storms determined in steps three and four. In contrast to the fifth step for historical period storm scenarios, this step requires rainfall disaggregation of daily SDSM rainfall, accomplished using the method of fragments as previously discussed. The development of 15-min resolution fragments of the daily May 2030 frontal storm use the hyetographs from Figures 11 and 12 whereas the daily October 2030 convective storm uses hyetographs from Figures 13 and 14 to develop similar 15-min fragments.

3.3.6. Sea Level Rise (SLR)

Estimating future tide levels in the Cross Bayou tidal canal required selecting a daily time series with the highest tide levels and determining the relative sea level change for 2030 with respect to the year with the highest recorded tide levels. The intermediate-high scenario of NOAA sea level rise projections, noting a projected warming of the ocean and ice sheet loss globally, was used to determine the relative sea level change (Tampa Bay Climate Science Advisory Panel, 2015).

3.3.7. Quantitative Metrics

Inflow rate reduction was a key quantitative metric in this study for characterizing effectiveness of LID implemented in reducing runoff in relation to existing conditions. Inflow rate reduction was determined using the following expression for both historical and future convective storm scenarios:

$$\frac{\text{Existing Inflow Rate} - \text{LID Scenario Inflow Rate}}{\text{Existing Inflow Rate}} \times \mathbf{100}\% \qquad\qquad (\mathbf{3\text{-}3})$$

where,

Existing Inflow Rate = Inflow at a specific location based on existing infrastructure;

LID Scenario Inflow Rate = Inflow at a specific location under LID scenario(s) (1 & 2).

Inflow rate reduction was determined at five locations (Figure 17) during both the historical period

and future period. Inflow rates were determined using a comprehensive hydrological and hydraulic

model, the ICPR software.
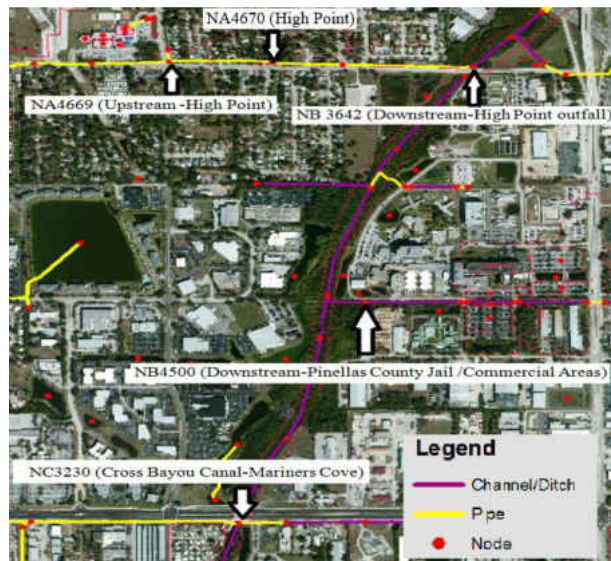
Figure 3-17: ICPR drainage outfalls for analysis

Note:

1. Node NA4669-Runoff collected at major conveyance point in High Point

2. Node NA4670-Runoff collected at major conveyance point in High Point

3. Node NC3642-Runoff into the Cross Bayou Canal from High Point conveyance

   systems

4. Node NB4500-Runoff from areas surrounding the Pinellas County Jail complex

5. Node NC3230-Combined tidal flows and discharge to Cross Bayou Canal near

   Mariners Cove

3.3.8. ICPR4 Model

The ICPR4 model is a comprehensive hydrodynamic stormwater and hydrologic model that incorporates hydroinformatics and geoinformatics along with input for climate data and processing. ICPR was utilized to construct a detailed model of the Cross Bayou watershed, which includes an integrated surface and groundwater interface. ICPR integrates terrain data, hydrologic data, hydraulic data, and climate data via a layering and data management system (Figure 18).

To determine the resiliency of the green-grey stormwater drainage system with respect to both current and future hazards, extensive data collection and processing of the stormwater drainage network was required. Urban hydroinformatics applies the concept of hydroinformatics (Abbott, 1991) to urban water management, which includes urban water systems such as stormwater networks. Its application has addressed needs for managing flow of water in the urban environment. With the use of detailed, physically based models, there is an increasing need for models to utilize and manage extensive, spatially referenced databases. In highlighting the role of urban hydroinformatics in urban flood management, Price and Vojinovic (2008) reported one of the most important factors in success of modeling analyses: the ability of a model to acquire data to improve information and understanding about described physical processes.

A survey of significant hydraulic conveyance features in the watershed, including channels, culverts, drop inlets (rise culverts), overland weirs, and structural weirs, was provided by an analysis conducted in the Cross Bayou Watershed Management Plan for Pinellas County (Jones Edmunds and Associates, Inc., 2013). These conveyance features were collected, organized, and managed within the ICPR4 model for further processing and utilization. From this information, a model of the existing drainage was constructed, focusing on major conveyance features and

outfalls. More complex drainage systems found in the watershed were incorporated in time of concentration, or time it takes for runoff to travel from the most hydraulically distant point in the watershed to an outlet point, using the National Resources Conservation Service (NRCS) method for small urban watersheds (Natural Resources Conservation Service, 1986).
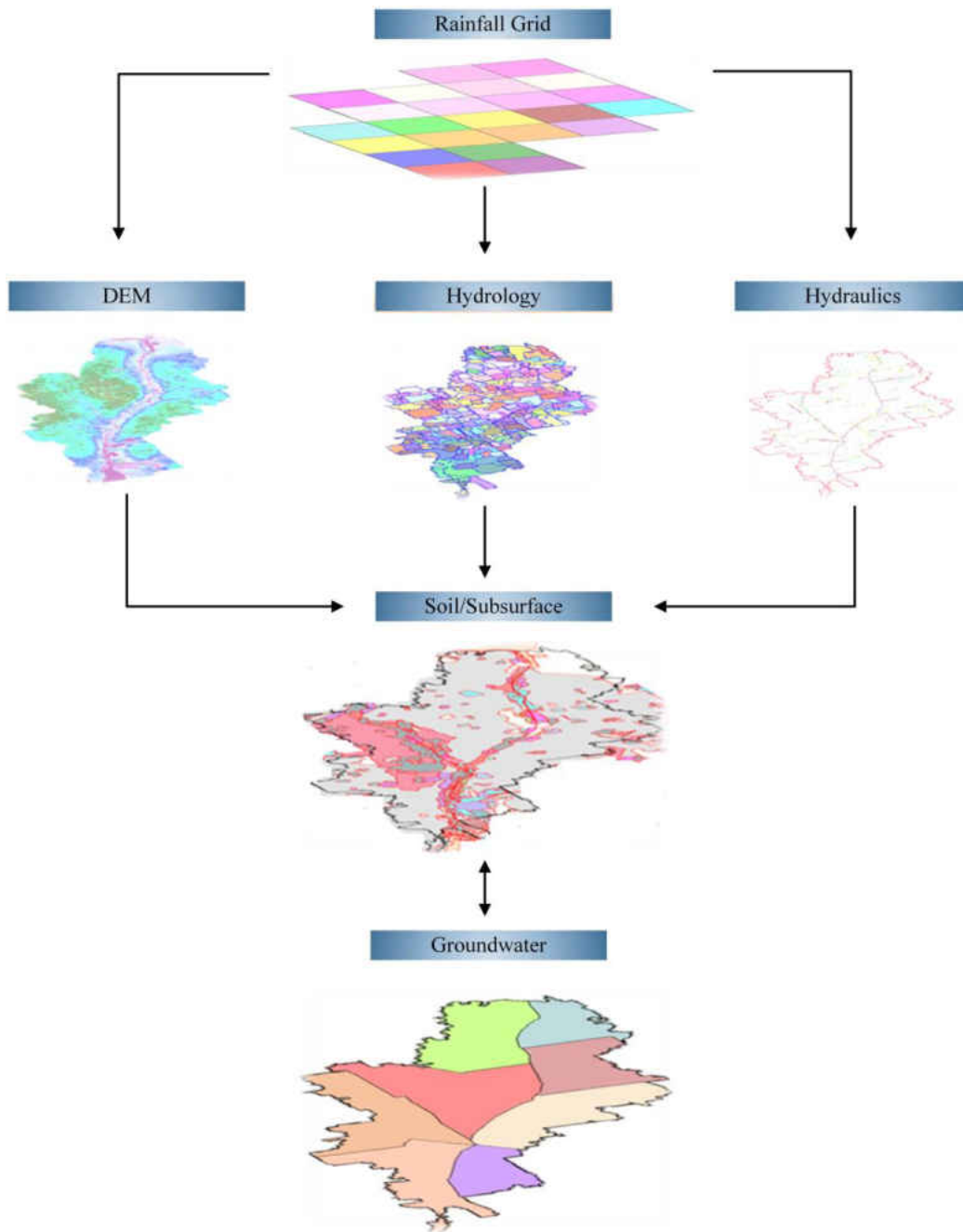
Figure 3-18:Flow of information between primary ICPR data layers

The hydrology of the Cross Bayou ICPR4 model consists of traditional basins (mapped and manual as specified in ICPR). The mapped basins are georeferenced polygons that integrate traditional hydrology (i.e., NRCS unit hydrographs with times of concentration) allowing

95

interaction with groundwater via recharge. Manual basins are basins in the ICPR model that do not interact with the groundwater. Green-Ampt infiltration was considered for each sub-basin based on the soil characteristics from the NRCS soil survey (Appendix D). Mapped basins were developed from preliminary sub-basin (catchment) delineations for the Cross Bayou watershed in accordance with the SWFWMD guidelines and specifications. The total number of sub-basins in the watershed was limited to approximately 300. Sub-basins were delineated around all major drainage conveyances and significant detention systems and at other locations as required to supply adequate definition to the model (Jones Edmunds and Associates, Inc., 2013).

Green-Ampt parameters were assumed using a typical soil class (Appendix D) for the area with no recharge to the surficial aquifer beneath the area of concern. Two manual basins were included in the Cross Bayou model to estimate offsite flow contributions into the watershed from St. Joes Creek and Pinellas Park Ditch. Times of concentration for these two basins were approximated based on the longest flow path with an assumed travel time of 0.305 $\mathrm{m\,s^{-1}}$ (1 $\mathrm{ft\,s^{-1}}$). Because these basins are highly developed or urbanized, the impervious area was assumed to be 65%, with 45% directly connected to impervious area.

In the hydraulic component of the model, major drainage conveyances deemed as part of the grey drainage infrastructure were placed in the model ICPR using a one-dimensional (1D) form of the momentum equation along with energy and diffusive wave options and averaged 2D ground slopes to move water between control volumes via the overland flow links. For this study, the 2D momentum equation was used to calculate overland flow, and the 1D energy equation was used to calculate flow within channels and other hydraulic systems such as the storm sewer system. ICPR4 was applied for the Cross Bayou watershed study and was well calibrated and validated based on

a series of storm events with the aid of two USGS gauge stations (Appendix A). The energy equation used for hydraulics can be represented as follows:

$$Z_1 + \frac{V_1^2}{2g} = Z_2 + \frac{V_2^2}{2g} + h_f$$

(**3-4**)

Solving for Q:

$$Q = \left\{ \frac{Z_1 - Z_2}{\frac{1}{2g}\left[\frac{1}{A_2^2} - \frac{1}{A_1^2}\right] + \Delta x C_f} \right\}^{1/2}$$

(**3-5**)

where

$Q = \text{flow} \left(\text{m}^3\text{s}^{-1}\right);\ Z_1 = \text{elevation} \left(\text{m}\right) \text{ at node1; } Z_2 = \text{elevation} \left(\text{m}\right) \text{ at node2;}$

$\Delta x = \text{change in length between nodes in the x} - \text{direction; } g\ =\ \text{gravitational acceleration (m s}^{-2}\text{);}$

$A_1 = \text{cross sectional area} \left(\text{m}^2\right) \text{ at node1; } A_2 = \text{cross sectional area} \left(\text{m}^2\right) \text{ at node2; } C_f\ =\ \text{coefficient of friction;}$

The energy equation is modified for channel and pipe flow and can be represented as follows:

$$Z_1 + \frac{\alpha_1 V_1^2}{2g} = Z_2 + \frac{\alpha_2 V_2^2}{2g} + h_f + h_{eddy} + h_{entrance} + h_{exit} + h_{bend}$$

(**3-6**)

Solving for Q:

$$Q = \left\{ \frac{Z_1 - Z_2}{\frac{1}{2g}\left[\left(\frac{\alpha_2}{A_2^2} - \frac{\alpha_1}{A_1^2}\right)C_{eddy}\left|\left(\frac{\alpha_2}{A_2^2} - \frac{\alpha_1}{A_1^2}\right)\right| + \left(\frac{\alpha_1 C_{entrance}}{A_1^2}\right) + \left(\frac{\alpha_2 C_{exit}}{A_2^2}\right) + \left(\frac{\alpha_{bend} C_{bend}}{A_{bend}^2}\right) + \Delta x C_f\right]} \right\}^{1/2}$$

(**3-7**)

where

$Q = \text{flow} \left(\text{m}^3\text{s}^{-1} \right);$ $Z_1 = \text{elevation} \left(\text{m} \right)$ at node 1; $Z_2 = \text{elevation} \left(\text{m} \right)$ at node 2;

$\Delta x = \text{change in length between nodes in the x} - \text{direction};$ $g = \text{gravitational acceleration (m s}^{-2}\text{)};$

$A_1 = \text{cross sectional area} \left(\text{m}^2 \right)$ at node 1; $A_2 = \text{cross sectional area} \left(\text{m}^2 \right)$ at node 2;

$A_{bend} = \text{area of the bend} \left(\text{m}^2 \right); \alpha_1 = \text{energy loss coefficient at node 1};$

$\alpha_2 = \text{energy loss coefficient at node 2};$ $C_f = \text{friciton loss coefficient}; C_{eddy} = \text{eddy loss coefficient};$

$C_{entrance} = \text{entrance loss coefficient}; C_{exit} = \text{exit loss coefficient}; C_{bend} = \text{bend loss coefficient};$

Mass balance equations are utilized within the control volumes at each node as follows:

$$dz = \left[\frac{\Sigma \left(Q_{in} - Q_{out} \right)}{A_{surface}} \right] dt \qquad\qquad (3\text{-}8)$$

where

$dz = \text{incremental change in stage} \left(\text{m} \right); dt = \text{computational time step} \left(\text{s} \right);$

$Q_{in} = \text{total inflow rate} \left(\text{m}^3\text{s}^{-1} \right); Q_{out} = \text{total outflow rate} \left(\text{m}^3\text{s}^{-1} \right);$

$A_{surface} = \text{wetted surface area of control volume}$

and

$$Q_{in} = \Sigma Q_{link\ in} + \Sigma Q_{excess} + \Sigma Q_{external} + \Sigma Q_{seepage} \qquad\qquad (3\text{-}9)$$

$$Q_{out} = \Sigma Q_{link\ out} + \Sigma Q_{irrigation} \qquad\qquad (3\text{-}10)$$

where

$\Sigma Q_{link\ in} = \text{sum of all link flow rates entering the control volume} \left(\text{m}^3\text{s}^{-1} \right);$

$\Sigma Q_{link\ out} = \text{sum of all link flow rates leaving the control volume} \left(\text{m}^3\text{s}^{-1} \right);$

$\Sigma Q_{excess} = \text{sum of rainfall excess rates for all basin polygons} \left(\text{m}^3\text{s}^{-1} \right);$

$\sum Q_{external} = $ sum of inflows from all external sources $\left(m^3 s^{-1} \right)$;

$\sum Q_{seepage} = $ sum of seepage flow from groundwater model $\left(m^3 s^{-1} \right)$;

$\sum Q_{irrigation} = $ sum of irrigation water pulled from surface node $\left(m^3 s^{-1} \right)$

A 2D overland flow region was created to allow the groundwater components to interact with surface water components through an overland flow region in the model. This interaction occurred below the specified sub-basins and within pond and channel control volumes as specified in the model. Eight groundwater regions were created within the ICPR4 model. Groundwater region boundaries were defined by channel features that were typically inundated. As water infiltrates the ground surface, a known head condition was placed at the corresponding groundwater nodes, derived from water surface elevations in the surface model component of the model.

3.3.8.1.   ICPR Model Calibration & Validation

For model calibration and verification, 15-minute USGS gauge data were collected at the two active gauges within the Cross Bayou watershed (Appendix D). USGS gauge 02308870 is located along the Pinebrook Canal at Bryan Dairy Road in Pinellas Park. The gauge records rainfall and stage and flow data. The second USGS gauge 02308861 is located along Cross Bayou at Cedar Brook Drive in Pinellas Park. This gauge only records stage data. The stage data are relative to a local datum for the gauge. A conversion of 0.274 m (+ 0.9 ft) was used to convert the stage elevation from the local datum to NAVD88. The gauge period of record for rainfall, stage, and flow were August 6, 1999, to present; August 5, 1995, to present; and August 1, 1999, to present, respectively. Fifteen-minute NEXRAD rainfall data were obtained from the SWFWMD and distributed over 23 cells with 2 km x 2 km grids from June 6, 1995, to December 31, 2014.

Historical hourly tide gauge data from January 1995 to December 2014 recorded at nearby NOAA tide stations were also used in calibration and verification of the model.

Daily reference evapotranspiration (ET) data from June 1, 1995, to December 31, 2013, were collected from the United States Geological Survey and distributed on 2 km x 2 km grid tiles. Specific to the ICPR model, crop coefficients were used to adjust reference ET to specific vegetation. A generalized crop coefficient map layer was created based on vegetation coverage. Although defined crop coefficients do not include impervious areas, they were used to describe vegetation types for pervious areas. Seven vegetative classes were established within the layer. The Green-Ampt method was used for infiltration and rainfall excess computations. The Green-Ampt parameters were developed based on the NRCS digital soils data and later adjusted during the calibration process (Appendix D). For each sub-basin, an initial abstraction parameter for impervious areas was set to 0.05 inches based on calibration of the model.

ICPR was calibrated using both a single historical storm event (June 21–30, 2012) and verified using a long-term simulation between January 1, 2007, and January 1, 2014, using USGS gauging stations within the Cross Bayou Watershed. Years 2007 and 2008 were considered "warm-up" years for the continuous simulation. The model did not reach "normal" conditions until after approximately 2 simulated years, reflected in the statistical comparisons for 2007 and 2008, which were considerably lower than the following 5 years (2009–2014). Statistical comparisons during a 5-year period (2009–2014) were made using 6 statistical parameters to assess the accuracy of ICPR model stage to observed stage information (Appendix A).

3.4. <u>Results and Discussion</u>

    3.4.1.   Peak Inflow Reduction (Historical Period)

Greater peak inflow reduction was achieved for LID Scenario 2 (all locations, Table 5 and 6) because LID Scenario 2 corresponds with decreased imperviousness. With respect to NC3230, an increase in peak inflow occurred for both LID Scenario 1 and LID Scenario 2 (denoted by a negative sign), possibly due to rising groundwater tables at that specific location (within the Cross Bayou Canal), with LID Scenario 2 having the greatest increase in peak inflow compared to LID Scenario 1 for both storm types. Peak inflow reduction was much lower for NB4500 than expected, indicating other factors possibly at the subsurface.

Table 3-5: Peak Inflow Reduction for Historical Frontal Storm Event (February 3rd, 2006) + SLR

NA4669		NA4670		NC3642		NB4500		NC3230	
LID Scenario 1	LID Scenario 2	LID Scenario 1	LID Scenario 2	LID Scenario 1	LID Scenario 2	LID Scenario 1	LID Scenario 2	LID Scenario 1	LID Scenario 2
5.17%	9.69%	5.39%	10.62%	0.579%	1.161%	1.309%	2.402%	-0.095%	-0.175%

Table 3-6: Peak Inflow Reduction for Historical Convective Storm Event (June 24th, 2012) + SLR

NA4669		NA4670		NC3642		NB4500		NC3230	
LID Scenario 1	LID Scenario 2	LID Scenario 1	LID Scenario 2	LID Scenario 1	LID Scenario 2	LID Scenario 1	LID Scenario 2	LID Scenario 1	LID Scenario 2
2.65%	5.56%	4.17%	10.00%	0.32%	0.61%	1.15%	2.54%	-0.10%	-0.17%

3.4.2. Peak Inflow Reduction (Future Period-2030)

Results of peak inflow reduction for future frontal and convective storms (Tables 7 and 8) are similar to the historical frontal and convective storms (Tables 5 and 6) because of the similar defined rainfall patterns. LID Scenario 2 provides the greatest peak inflow reduction, as expected, except for location NC3230 where LID Scenario 2 causes the greatest increase in peak inflow compared to LID Scenario 1 (Table 9). The greatest peak inflow reduction occurred at Nodes NA4669 and NA4670 in Table 10. However, the greatest increase in peak inflow occurs at locations downstream (NC3642, NB4500, NC3230) of upstream locations (NA4669 and NA4670) (Table 10). Considering the storms defined in Table 7 and Table 9 fall under the same storm magnitude, they are associated with a different frontal rainfall pattern which results in the variation in peak inflow reduction values between them. Similarly, for storms defined in Table 8 and Table 10, which have the same storm magnitude, their convective rainfall patterns are different resulting in differences in peak inflow reduction. This indicates that rainfall patterns are important in this analysis.

Table 3-7: Peak Inflow Reduction for Future May 2030 Frontal Storm (Frontal Rainfall Pattern #1+ SLR)

NA4669		NA4670		NC3642		NB4500		NC3230	
LID Scenario 1	LID Scenario 2	LID Scenario 1	LID Scenario 2	LID Scenario 1	LID Scenario 2	LID Scenario 1	LID Scenario 2	LID Scenario 1	LID Scenario 2
5.17%	9.69%	5.39%	10.62%	0.579%	1.161%	1.309%	2.402%	-0.095%	-0.175%

Table 3-8: Peak Inflow Reduction for Future October 2030 Convective Storm(Convective Rainfall Pattern #1+ SLR)

NA4669		NA4670		NC3642		NB4500		NC3230	
LID Scenario 1	LID Scenario 2	LID Scenario 1	LID Scenario 2	LID Scenario 1	LID Scenario 2	LID Scenario 1	LID Scenario 2	LID Scenario 1	LID Scenario 2
2.65%	5.56%	4.17%	10.00%	0.32%	0.61%	1.15%	2.54%	-0.10%	-0.17%

Table 3-9: Peak Inflow Reduction for Future May 2030 Frontal Storm (Frontal Rainfall Pattern #2+ SLR)

NA4669		NA4670		NC3642		NB4500		NC3230	
LID Scenario 1	LID Scenario 2	LID Scenario 1	LID Scenario 2	LID Scenario 1	LID Scenario 2	LID Scenario 1	LID Scenario 2	LID Scenario 1	LID Scenario 2
3.4%	6.9%	2.60%	5.23%	0.371%	0.736%	0.590%	1.207%	-0.070%	-0.118%

Table 3-10: Peak Inflow Reduction for Future October 2030 Convective Storm (Convective Rainfall Pattern #2+ SLR)

NA4669		NA4670		NC3642		NB4500		NC3230	
LID Scenario 1	LID Scenario 2	LID Scenario 1	LID Scenario 2	LID Scenario 1	LID Scenario 2	LID Scenario 1	LID Scenario 2	LID Scenario 1	LID Scenario 2
9.02%	12.5%	11.6%	13.5%	-0.71%	-0.45%	-1.76%	-0.36%	-2.119%	-2.218%

3.4.3. Groundwater Impacts & Sea Level Rise

A separate analysis was completed to determine how (1) the impacts sea level rise and (2) increased perviousness upstream via LID implementation under sea level rise could change groundwater flow along the Cross Bayou tidal canal. Nodes NC3642 and NC3230 represent locations within the Cross Bayou canal where seepage outflow information can be obtained. For both node locations, seepage outflow information was obtained for four simulations for both the large convective (June 24, 2012, rainfall pattern) and frontal (February 3, 2006, rainfall pattern) events: (1) existing land use/infrastructure with no sea level rise, (2) existing land-use/infrastructure with sea level rise, (3) 25% impervious reduction (Scenario 1) with sea level rise, and (3) 50% impervious reduction (Scenario 2) with sea level rise.
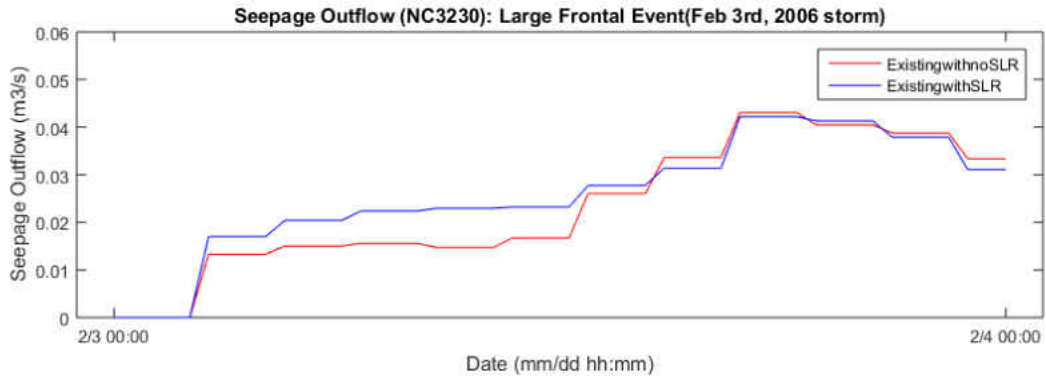
Figure 3-19: Seepage Outflow into Cross Bayou Canal at node location NC3230 under existing infrastructure conditions with no SLR and with SLR
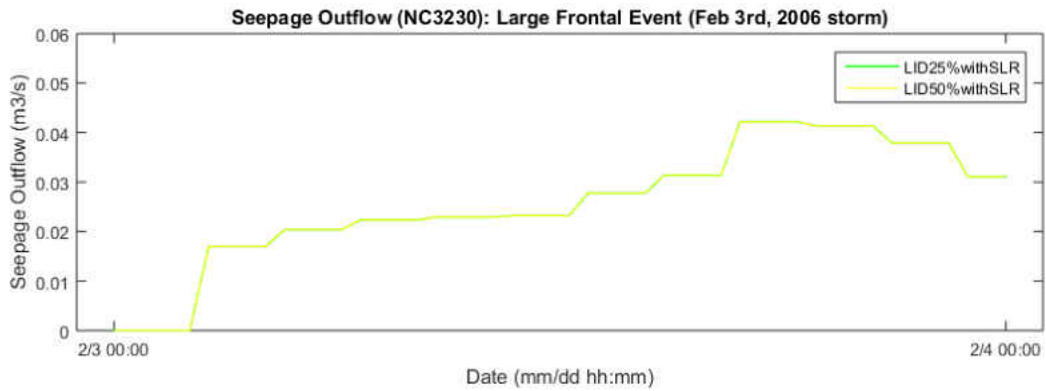
Figure 3-20: Seepage Outflow into Cross Bayou Canal at node location NC3230 under LID Scenario 1(25% impervious reduction) with SLR and NC3230 under LID Scenario 2(50% impervious reduction) with SLR
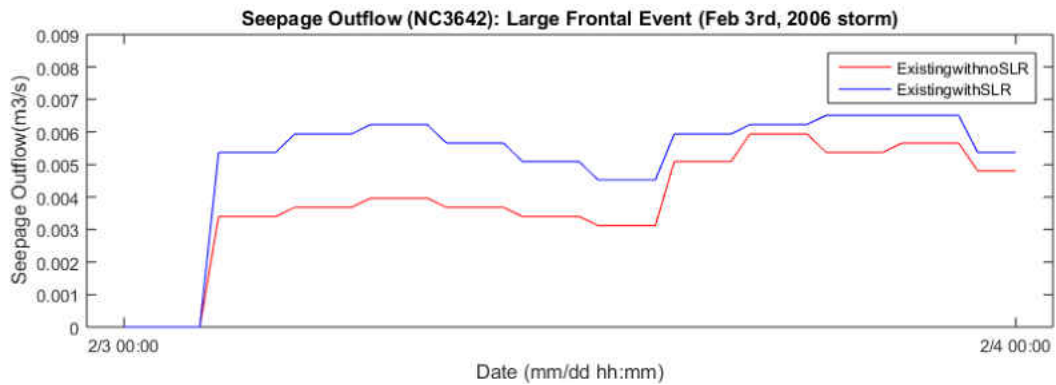
Figure 3-21: Seepage Outflow into Cross Bayou Canal at node location NC3642 under existing infrastructure conditions with no SLR and with SLR
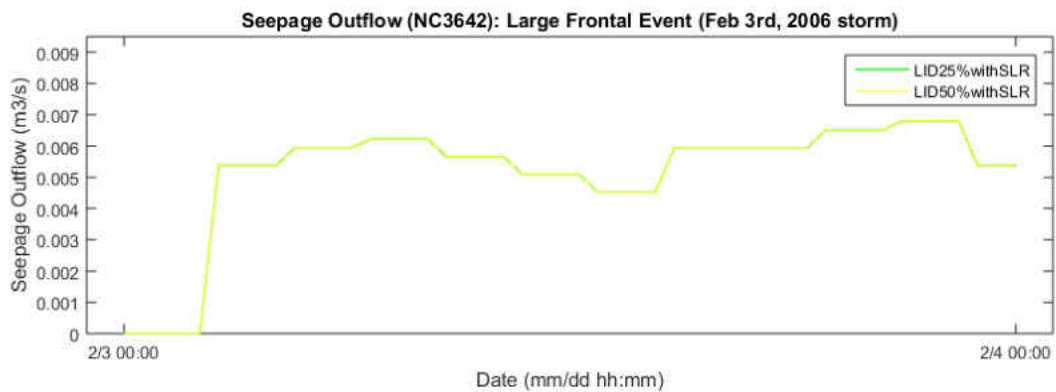
Figure 3-22: Seepage Outflow into Cross Bayou Canal at node location NC3642 under LID Scenario 1(25% impervious reduction) with SLR and NC3642 under LID Scenario 2(50% impervious reduction) with SLR
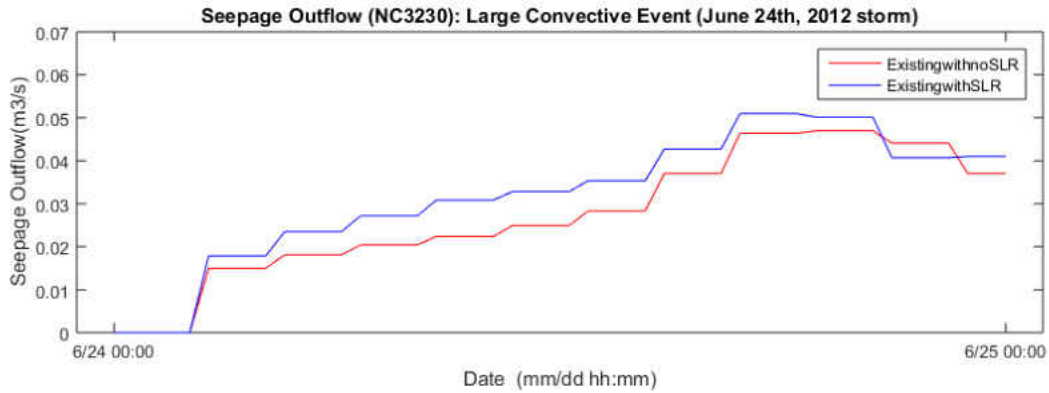
Figure 3-23: Seepage Outflow into Cross Bayou Canal at node location NC3230 under existing infrastructure conditions with no SLR and with SLR
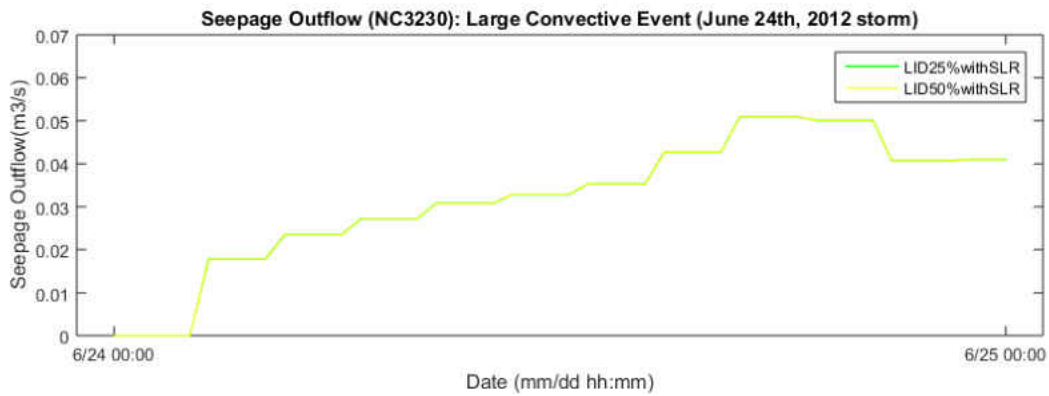
Figure 3-24: Seepage Outflow into Cross Bayou Canal at node location NC3230 under LID Scenario 1(25% impervious reduction) with SLR and NC3230 under LID Scenario 2(50% impervious reduction) with SLR
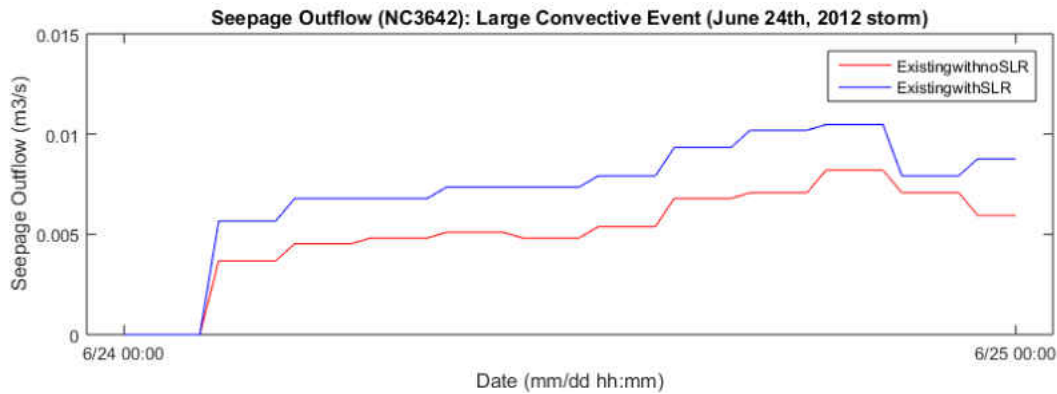
Figure 3-25: Seepage Outflow into Cross Bayou Canal at node location NC3642 under existing infrastructure conditions with no SLR and with SLR
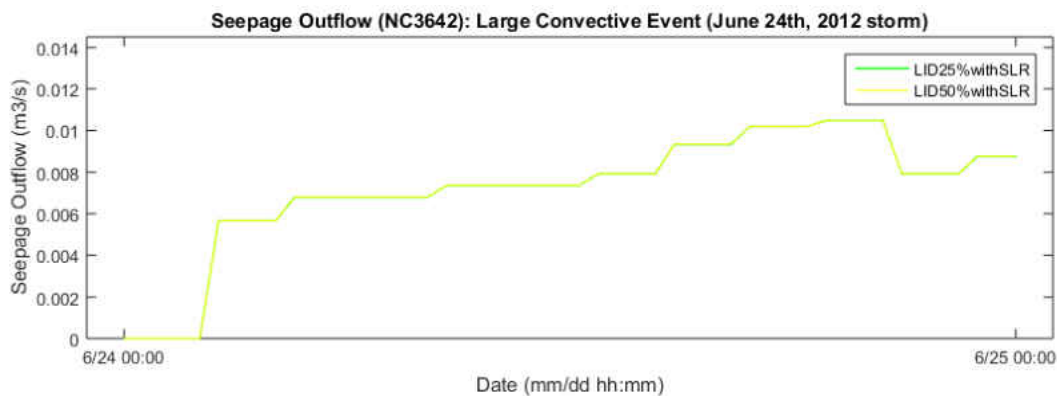
Figure 3-26: Seepage Outflow into Cross Bayou Canal at node location NC3230 under LID Scenario 1(25% impervious reduction) with SLR and NC3230 under LID Scenario 2(50% impervious reduction) with SLR

Without LID implementation (Figures 19, 21, 23 and 25), greater seepage outflow from the groundwater table into the Cross Bayou canal occurs under SLR as opposed to without SLR. Considering LID implementation only (Figures 20, 22, 24 and 26), seepage outflow from the groundwater table remained constant between LID scenarios. Overall the seepage outflow rates from the groundwater table were considerably lower for the frontal event (Figures 19, 20, 21 and 22) as opposed to seepage outflow rates during the convective event (Figures 23, 24, 25 and 26).

113

Seepage outflow from the groundwater table into the Cross Bayou Canal are reflected in peak

inflow reduction trends at node locations within the Cross Bayou Canal. For instance, at nodes

NC3230 and NC3642, lower seepage outflow for the frontal event (Figures 20 and 22) resulted

in greater peak inflow reduction (Table 5), whereas a higher seepage outflow for the convective

event resulted in lower peak inflow reduction at nodes NC3230 and NC3642 (Table 6).

3.5. <u>Conclusion</u>

As reflected in this chapter, rainfall type affects LID implementation strategies when considering rainfall runoff reduction via the peak inflow reduction metric. Variations in sub-daily rainfall patterns also affects rainfall runoff reduction regardless of whether total daily rainfall is the same. Sea level rise effects on the groundwater table also affects the ability to incorporate infiltration-based LID alternatives to reduce imperviousness. Adding infiltration-based LID alternatives to areas affected by sea level rise could result in higher groundwater tables for these areas. For these reasons, before LID implementation can be evaluated as an adaptive stormwater drainage measure, rainfall type, sub-daily rainfall patterns, and a groundwater analysis must be considered under chosen "design-storm" magnitude(s). Overall LID implementation within a watershed can alter the hydrologic response of existing grey drainage infrastructure as to offer increased peak inflow reduction across varying rainfall type and sub-daily rainfall patterns. The deployment of LID to capture runoff under various storm scenarios associated with rainfall types and patterns while accounting for subsurface processes would be beneficial when considering long-term drainage resilience.

3.6. <u>References</u>

Abbott, M.,1991: Hydroinformatics: Information technology and the aquatic environment, Avebury Technical Brookfield, USA.

Ali, A, Abtew, W, Van Horn, S, Khanal, N., 2000: Temporal and spatial characterization of rainfall over Central and South Florida. *Journal of the American Water Resources Association* 36: 833–848

Bosch, D. D., and Davis., F.M., 1999. Rainfall Variability and Spatial Patterns for the Southeast.

   Proceedings of the Fourth International Conference on Precision Agriculture: 535-545.

Birgani, Y. T., Yazdandoost, F. and Moghadam, M. 2013: Role of resilience in sustainable urban

   stormwater management. *Hydraulic Structures* 1(1): 44–53.

Chang, N., 2010: Hydrological Connections between Low-Impact Development, Watershed Best

   Management Practices, and Sustainable Development. *J. Hydrol. Eng.* 15, SPECIAL

   ISSUE: Low Impact Development, Sustainability Science, and Hydrological Cycle, 384–

   385.

Clar, M., Barfield, B. J., and O'Conner, T., 2004: Stormwater Best Management Practices

   Design Guid Volume 1-General Considerations. U.S. Environmental Protection Agency,

   Washington, DC, EPA/600/R-04/121.

De Bruijn, K. M. 2004: Resilience and flood risk management. Water Policy 6: 53-66.

Federal Highway Administration (FHWA), 1984: HEC 19-Hydrology. Accessed October 2016.

   [Available online at http://www.fhwa.dot.gov/engineering/hydraulics/library_listing.cfm?

   archived=true]

Florida Department of Environmental Protection, 2014: Chapter 62-25 Regulations of

   Stormwater Discharge. Accessed October 2016. [Available online at

   http://www.dep.state.fl.us/legal/Rules/surfacewater/62-25.pdf]

Hernandez, Tatiana X., 2001:Rainfall-runoff modeling in humid shallow water table

   environments. Graduate Theses and Dissertations. Assessed October 2016. [Available

   online at http://scholarcommons.usf.edu/etd/1537]

Huff, F.A., 1967: Time distribution of rainfall in heavy storms. *Water Resources Research*, 3(4): 1007–1019.

Huff, F.A., 1990: Time distributions of heavy rainstorms in Illinois: Champaign, Illinois. *Illinois State Water Survey*, Circular 173.

Jones Edmunds and Associates, Inc., 2013: Floodplain Analysis, Cross Bayou Watershed Management Plan. Pinellas County Board of County Commissioners and Southwest Florida Water Management District.

Laniak, G.F., Olchin, G., Goodall, J., Voinov, A., Hill, M., Glynn, P., Whelan, G., Geller, G.,Quinn, N., Blind, M., Peckham, S., Reaney, S., Gaber, N., Kennedy, R., Hughes, A., 2013: Integrated environmental modeling: A vision and roadmap for the future, *Environmental Modelling & Software*, 39:3-23.

Natural Resources Conservation Service (NRCS), 1986: "Urban Hydrology for Small Watersheds, Technical Release 55", USDA.

NOAA, 2016: Sea Level Trends. Accessed August 2016. [Available online at https://tidesand currents.noaa.gov/sltrends/sltrends.html

Omer. M., 2013: The resilience of networked infrastructure systems. *World Scientific*.

Pinellas County Planning Department, 2012: Pinellas County Comprehensive Plan. Accessed July 2015. [Available online at http://www.pinellascounty.org]

Pinellas County Planning Department, 2015: Pinellas County Stormwater Manual Jan 2015. [Available online at http://www.pinellascounty.org]

Pinellas County Planning Department, 2016: Pinellas County Stormwater Manual May 2016. [Available online at http://www.pinellascounty.org]

Price, R.K. and Vojinovic, Z., 2008: Urban flood disaster management, *Urban Water Journal*, 5:3, 259-276, DOI: 10.1080/15730620802099721

Pui,A., Sharma, A., Mehrotra, R.,Sivakumar, B., Jeremiah, E., 2012: A comparison of alternatives for daily to sub-daily rainfall disaggregation, Journal of Hydrology 138: 470-471

Qin, H-p., Li, Z-x., and Fu, G., 2013: The effects of low impact development on urban flooding under different rainfall characteristics, *Journal of Environmental Management*, 129 (15): 577-585

Rothman, D. S., Robinson, J. B., 1997: Growing Pains: A Conceptual Framework for Considering Integrated Assessments. *Environmental Monitoring and Assessment*, 46(1): 23–43

Roseen, R., T. Janeski, M. Simpson, J. Houle, J. Gunderson, & T. Ballestero. 2012: Economic and Adaptation Benefits of Low Impact Development. Conference Proceedings, 2011 Low Impact Development Symposium. Accessed Feb 2016. [Available online at www.unh.edu/unhsc/sites/unh.edu.unhsc/files/pubs_specs_info/JEE%20FTL%203-30-12.b.pdf.]

Shuster, W. D. and Rhea, L. K.., 2013: Catchment-scale hydrologic implications of parcel-level stormwater management (Ohio USA). *Journal of Hydrology* 485: 177-187.

Soil Conservation Service, 1973, A method for estimating volume and rate of runoff in small watersheds: Washington, D.C., U.S. Department of Agriculture, Soil Conservation Service, SCS–TP–149

Southwest Florida Water Management District (SWFWMD), 2013: Environmental Resource

 Permit Applicant's Handbook Volume II-Design Requirements for Stormwater

 Treatment and Management Systems Water Quality and Water Quantity. Assessed

 October 2016. [Available online at

 https://www.swfwmd.state.fl.us/files/database/site_file_sets/2479/Applicants_

 Handbook_II_-_Revised.pdf]

Streamline Technologies, Inc., 2015: An Integrated Surface Water-Groundwater Model of the

 Cross Bayou Watershed.

Tampa Bay Climate Science Advisory Panel, 2015: Recommended Projection of Sea Level Rise

 in the Tampa Bay Region [Available online at

 http://www.tbrpc.org/council_members/council agendas/2015/101215/8c.pdf]

U.S. Department of Agriculture and Natural Resources Conservation Service, 2007. National

 Engineering Handbook, title 210–VI. Part 630, Chapter 7. Washington, DC. [Available

 online at http://directives.sc.egov.usda.gov/]

Wey, K., 2007: Temporal Disaggregation of Daily Precipitation Data in a Changing Climate.

 UWSpace. http://hdl.handle.net/10012/2859

Westra S, Mehrotra, R, Sharma, A and Srikanthan, R, 2012: Continuous rainfall simulation: 1 A

 regionalized subdaily disaggregation approach, Water Resources Research, 48:W01535,

 doi:10.1029/2011WR010489

Wilby, R.L, Dawson, C.W., Barrow, E.M., 2002: SDSM—a decision support tool for the

 assessment of regional climate change impacts. *Environmental Modelling & Software*,

 17(2): 145–157.

CHAPTER 4: COUPLING INFRASTRUCTURE RESILIENCE AND FLOOD RISK ASSESSMENT FOR A COASTAL GREEN-GREY-BLUE DRAINAGE SYSTEM UNDER EXTREME WEATHER EVENTS

4.1. <u>Introduction</u>

Highlighting interdependence and multi-dimensional nature of flooding and climate processes, covers only one aspect of overall flood risk. Without considering resilience to these interdependent and multi-dimensional events, overall flood risk cannot be assessed. Quantifying flood resilience depends on interconnection of the urban space and the natural space. This interconnection can be represented by the concept of networked systems or networked infrastructure systems when considering infrastructure (Omer, 2013). With regard to flood risk and resilience, natural and man-made systems such as rivers, canals, stormwater drainage channels and pipes are seen as the first system(s) that natural flooding hazards interact with before effects are felt within surrounding systems, such as residential communities, given the level of resilience of such systems. As a result, the adaptive capacity of natural and man-made systems become important to the overall flood risk and resilience due to "cascade effect" of interconnected systems (Omer, 2013; Park et al., 2013).

A useful real-world example for consideration of both flood risk and infrastructure resilience is the Cross Bayou Watershed, located within Pinellas County near Tampa Bay region of West-Central Florida. Low lying areas within the Cross Bayou Watershed have been historically prone to flooding driven by rainfall runoff and/or high tide events. Over the years, storm events and subsequent flooding have taken a toll on the drainage infrastructure particularly for undersized conveyance systems found throughout the watershed which are not equipped to

handle increased runoff from surrounding urbanization. Tidal flooding has also impacted low-lying areas near a tidal canal which dissects the watershed connecting neighboring bays for which inadequate protection exists. Water within the canal can flow in either direction depending upon tidal conditions. Flooding occurs periodically in several low-lying communities with strong interactions between the surface water and the groundwater systems. In dealing with such a complex system, the Interconnected Pond and Channel Routing (*ICPR*) catchment model (Streamline Technologies Inc., 2015) is applied to the study region for coupling risk and resilience in support of multi-criteria flood impact assessment.

4.1.1. Chapter Objectives

The objectives of this chapter are to: (1) determine the dependence structure of potential flood hazards, (2) link flood risk and engineering resilience via implementing a risk formulation, and (3) conduct a multi-criteria flood risk and resilience assessment for decision analysis. Such efforts may lead to answer the following science questions: 1) can the copulas analysis fully support the risk analysis? 2) how to offset potential flood risk by modeling adaptive measures for increasing drainage infrastructure resilience with the aid of ICPR? 3) can the well coupled flood risk and engineering resilience lead to a better decision making via a multi-criteria flood impact assessment?

4.2. Study Area

The Cross Bayou Watershed of Pinellas County (Figure 1), Florida, was selected as a case study because of its vulnerability to coastal flooding and Pinellas County's efforts to

implement improved stormwater management to increase the area's adaptive capacity to future hazards. The Cross Bayou watershed encompasses approximately 31 km^2 (7,697 acres), primarily comprising high-density residential, industrial, and commercial areas. An important feature of the watershed is a 16.9 km (10.5-mile) long constructed tidal canal, the Cross Bayou Canal (Figure 1), which dissects the watershed and connects both Tampa Bay and Boca Ciega Bay on its northeastern and southwestern ends, respectively. The Cross Bayou Canal also intersects the Pinebrook Canal to the southwest (Figure 1). Water within the canal can flow in either direction, depending on tidal conditions. This feature, while useful for overall watershed drainage, is potentially hazardous to low-lying communities during high tide events, particularly when considering the ongoing threat of sea level rise (NOAA, 2016b) near the Tampa Bay region.

Low lying areas within the Cross Bayou Watershed have been historically prone to flooding driven by rainfall runoff and/or high tide events. Over the years, storm events and subsequent flooding have taken a toll on the drainage infrastructure particularly for undersized conveyance systems found throughout the watershed which are not equipped to handle increased runoff from surrounding urbanization. Tidal flooding has also impacted low-lying areas near a tidal canal which dissects the watershed connecting neighboring bays for which inadequate protection exists. Water within the canal can flow in either direction depending upon tidal conditions. Flooding occurs periodically in several low-lying communities with strong interactions between the surface water and the groundwater systems.

Figure 4-1: Extent of Cross Bayou Watershed

Some areas in the watershed are consistently more vulnerable and have a decreased adaptive capacity to flooding. The Mariners Cove residential community (Figure 2), in particular, is known for significant flooding from storm events. Flooding in the Mariners Cove community is primarily caused by heavy rains and high tide events of the adjacent Cross Bayou canal.

Figure 4-2: Extent of the Mariners Cove area) within Cross Bayou Watershed at high risk to flooding (Source of Satellite Imagery: Esri, DigitalGlobe, GeoEye, Earthstar Geographics, CNES/Airbus DS, USDA, USGS, AeroGRID, IGN and GIS User Community).

4.3. <u>Methodology</u>

4.3.1. Formulating Risk

Risk, in a generalized formulation, can be represented as follows:

$$\text{Risk} = \text{f(likelihood or probability of consequences occurring and consequences)} \qquad (\,4\text{-}1\,)$$

Risk as a function of likelihood of consequences and consequences is related to decision theory such that risk can be represented as an expected value as follows:

$$\text{Risk (Expected Value)} = \text{likelihood of consequences occurring} \times \text{consequences} \qquad (\,4\text{-}2\,)$$

$$\text{Likelihood or probability of consequences occurring} = \text{f(Hazard, Vulnerability)} \qquad (\,4\text{-}3\,)$$

$$\text{Consequences} = \text{f(Exposure, Resilience)} = \text{f(Hazard, Vulnerability)} \qquad (\,4\text{-}4\,)$$

The likelihood or probability of consequences occurring is a function of hazard, vulnerability and resilience. The consequences are a function of exposure, which is also a function of hazard and vulnerability. In regard to how the elements of hazard, vulnerability, resilience and exposure are related mathematically, literature can provide some guidance. In an attempt to provide a mathematical formulation of risk, the following in Table 3 can entail the essence of this issue.

Table 4-1: Variations in the risk formulation in literature

Risk Formulation	Source
$\text{Risk} = \text{Hazard} \times \text{Vulnerability}$	• Ciurean, Schroter and Glade (2013)

Risk Formulation	Source
	• UN International Strategy for Disaster Reduction (UNIDSR, 2002)
$\text{Risk} = \dfrac{\text{Hazard} \times \text{Vulnerability}}{\text{Adaptive Capacity}}$	• Food and Agriculture Organization (FAO) of the United Nations (Economic and Social Department) • World Health Organization (WHO)
$\text{Risk} = \text{Hazard} \times (\text{Exposure} \times \text{Sensitivity} \times \text{Resilience})$	• Johansen (2010)

In the aforementioned risk formulation, sensitivity is the degradation in performance, from a physical system perspective during continuous effects from hazards (Johansen, 2010). Aside from the generalized formulations presented in Table 3, mathematically, the formulations have advantages and disadvantages and will be presented on a case by case basis as below:

Case I: $\text{Risk} = \text{Hazard} \times \text{Vulnerability}$

For this case, the risk formulation is general and not specific in scope such that the application of this risk formulation assumes that hazard and vulnerability are only considered without other elements such as exposure or resilience unless defined further by the user of such formulation.

Case II: $\text{Risk} = \text{Hazard} \times (\text{Exposure} \times \text{Sensitivity} \times \text{Resilience})$

For this case, the risk formulation is expounded upon by breaking down the vulnerability term as a product of exposure, sensitivity and resilience. This formulation is less simplistic than in Case I. However this formulation can only be applied carefully depending on how the resilience term is defined

Case III: $\text{Risk} = \dfrac{\text{Hazard} \times \text{Vulnerability}}{\text{Adaptive Capacity}}$

Case III applies a quotient. Adaptive capacity is also one aspect of resilience as defined in literature such as Francis and Bekera (2014). However, the quotient term presents challenges given how adaptive capacity is defined or formulated such that adaptive capacity could be large or small. In the case of very small numbers for adaptive capacity, the risk can be considerably large. Conceptually this makes sense, however, quantitatively this presents challenges for interpretation.

4.3.2. Resilience Metric

The success of the risk formulation in Cases II and III, quantitatively, depends on how the adaptive capacity term or overall resilience term is defined. The resilience term, throughout literature, does not have a consistent form and varies given the system and assumed response.

For infrastructure or engineering systems, Yodo and Wang (2016) have outlined how resilience metrics are developed based on three categories or approaches, as summarized in Table 4.

Table 4-2: Framework for Defining Engineering/Infrastructure Resilience Metrics as Adapted from Yodo and Wang (2016)

Category/Approach	Based on theoretical resilience curves	Based on pre- and post-disruptions performances	Based on reliability and restoration
Description	Quantitative resilience metric developed from the properties of theoretical resilience curves	Quantitative resilience metrics developed from system performance before (pre-) and after (post-) disruption	Quantifies resilience from system's ability to maintain its capacity and performance during a given period of time and to restore its capacity and performance

With respect to the first category/approach from Table 2, defining a quantitative resilience metric based on theoretical resilience curves may present problems since resilience curves could non-linear in form and may not follow a defined pattern given variation in hazard or disruption. Defining quantitative resilience metric based on (1) pre- and post-disruptions performances and (2) reliability and restoration may be more useful for this study. Francis and

Bekera (2014) proposed a resilience metric that can account for both pre- and post-disruptions along with reliability and restoration in the following formulation:

$$\text{Resilience} = S_p \times \left(\frac{F_r}{F_o} \right) \times \left(\frac{F_d}{F_o} \right) \qquad (4\text{-}5)$$

where $S_p =$ speed recovery factor $= \begin{cases} \left[\left(\dfrac{t_\delta}{t_r^*} \right) e^{[-a(t_r - t_r^*)]} \right] & \text{for } t_r \geq t_r^* \\ \left(\dfrac{t_\delta}{t_r^*} \right) & \text{otherwise} \end{cases}$

$F_r =$ system recovery state

$F_o =$ original system state

$F_d =$ system state following disruption

$\left(\dfrac{F_r}{F_o} \right) =$ adaptive capacity

$\left(\dfrac{F_d}{F_o} \right) =$ absorptive capacity

$t_\delta =$ slack time or the max time during post-disruption that is accepted before recovery begins

$t_r =$ time to final recovery (i.e. new equilibrium state)

$t_r^* =$ time to complete initial recovery actions

a = decay in resilience parameter representing time to new equilibrium state

From the resilience metric aforementioned, the decay factor, a, is represented such that if the initial recovery takes longer than the slack time then the resilience metric decreases. However this metric as proposed by Francis and Bekera (2014) presented a challenge such as what value to assign the decay parameter. In addition the slack time variable is subjective depending on the system of concern and the decision-maker. Lastly when considering flooding, the variable representing the original system state, F_o would be assumed zero since the system (i.e., drainage) is at a dormant or no activity state, resulting in the ratio becoming undefined. In this specific case, a potentially useful metric should be modified as such by considering the

129

difference between the initial recovery time (i.e., initial reduction in inundation depth after maximum inundation area) and the final recovery time (i.e., no inundation or no exposure):

$$\text{Relative Change in Time of Exposure} = \frac{\mathrm{T}_f - T_i}{T_i} \qquad\qquad \textbf{(4-6)}$$

T_i = initial recovery time (time in which inundation depths are initially reduced from maximum inundation depths, i.e. max exposure)
T_f = final recovery time (time in which inundation depths are non-existent following maximum inundation depths, i.e. max exposure)

A resilience metric can be created that is the reciprocal of the relative change in time of exposure and is represented as follows:

$$\text{Resilience} = \frac{1}{\left[\dfrac{\mathrm{T}_f - T_i}{T_i}\right]} \qquad\qquad \textbf{(4-7)}$$

Visually, the resilience term can be represented by Figure 3. The goal of the resilience metric is to minimize the difference in the numerator ($\mathrm{T}_f - T_i$) such that the system in question can achieve recovery in a shorter period of time (i.e. $\mathrm{T}_f - T_i$ is small in value). Achieving shorter recovery times highlights greater resilience such that when considering concepts proposed by Francis and Bekera (2014), absorptive capacity, adaptive capacity and restorative capacity of the system are greater. The goal subsequently would be to implement a system that achieves greater absorptive, adaptive capacity and restorative capacity.
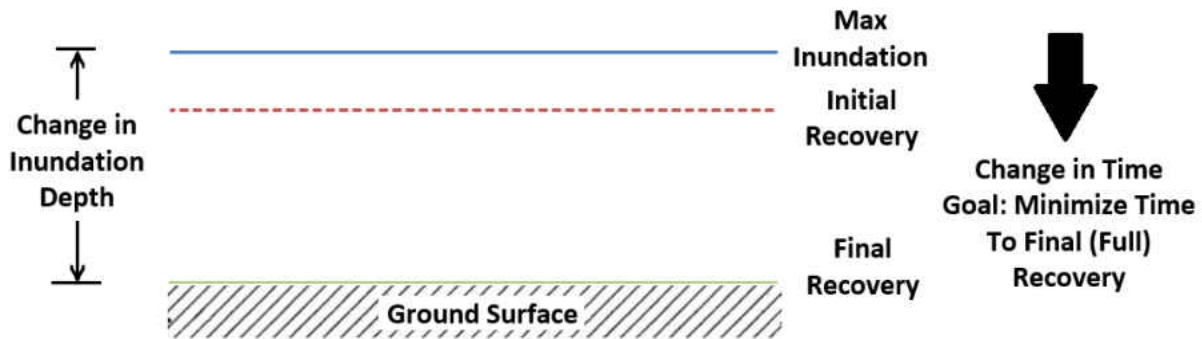
Figure 4-3: Schematic of determining the resilience metric

4.3.3. The Proposed Risk Formulation

. Given the proposed resilience metric, the Case III risk formulation is more appropriate to utilize in this study and can be represented in the following generalized formulation:

$$\text{Risk} = \frac{\text{Hazard} \times \text{Vulnerability x Exposure}}{\text{Resilience}}$$ (**4-8**)

4.3.3.1.   Hazard Component of Risk Formulation

When considering flooding in risk analysis and resilience assessment in particular, flooding can be caused by any combination of hazards. Any combination of such hazards would impact both risk and resilience. For low-lying coastal areas in particular, such as the Cross Bayou Watershed, flooding can occur for two cases: (1) with respect to storm tide and/or rainfall from a tropical storm event or (2) high tide and/or rainfall from a non-tropical storm event. Flooding does not occur in isolation and is dependent on several variables within nature. In this study, the potential interdependence of daily stage levels in the Cross Bayou Canal, daily rainfall, daily average wind speed, daily barometric pressure and moon phasing (fraction of moon illumination) (Figure 5) from observed stations (Figure 6) are sought to characterize flood hazard potential.

131

Tidal stage within the canal could be affected by factors such as the following: (1) rainfall runoff which drains into the canal from upstream areas, (2) high winds from tropical storms which can cause storm surges, (3) barometric pressure which can increase tidal stage with decreasing pressure, and (4) moon phasing such that tides can rise higher and fall lower during new and full moons (fraction of moon illumination values of 0 and 1 respectively) while rising and falling moderately during first and third-quarter moon phases (values near 0.25 and 0.75, respectively). As evident in Figure 5, weak to no correlation is present between the following: (1) tidal stage and wind direction, (2) tidal stage and barometric pressure and (3) tidal stage and fraction of moon illumination. These combinations will not be evaluated by the proposed copula analyses in this study. The year 2012 is a target year for copula analysis with associated daily rainfall and daily tidal stage at their maximums, during the year 2012, compared with the entire period compared with period of record (2002-2014) with the exception of wave height data which was not continuous for the period 2002-2014. Wave height data was used for the year 2012 only.

(a)

(b)

133

(c)

(d)

134
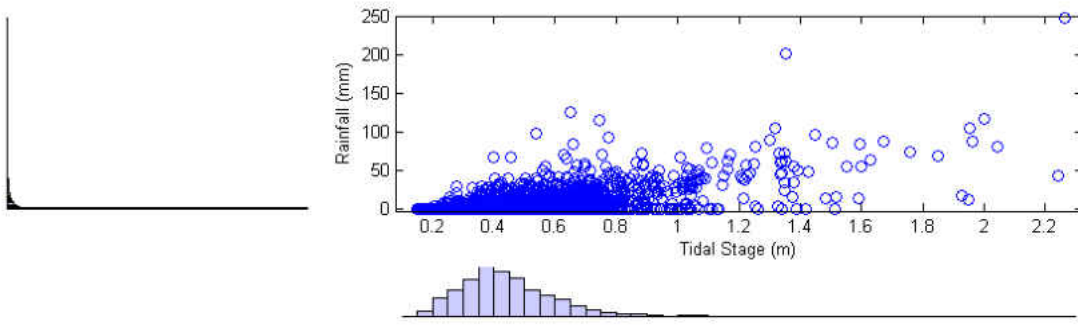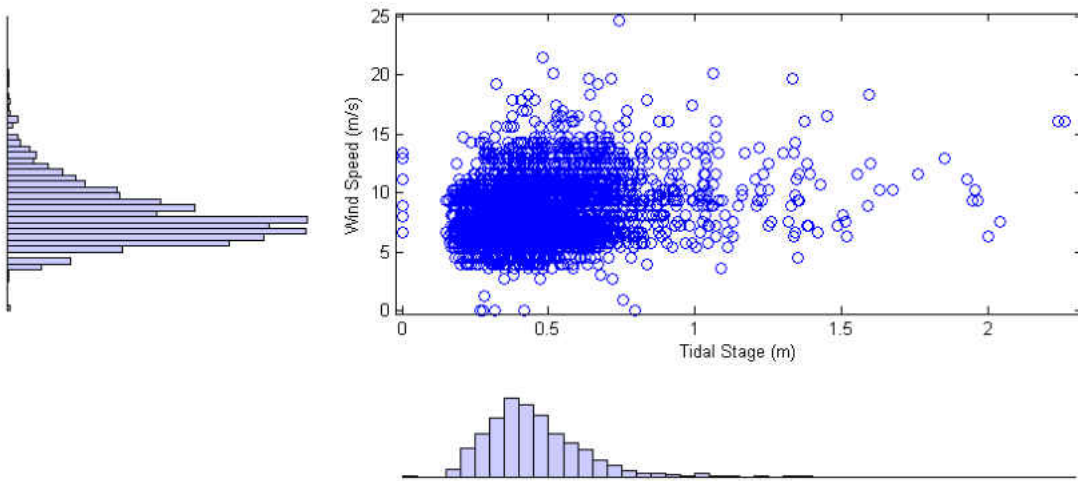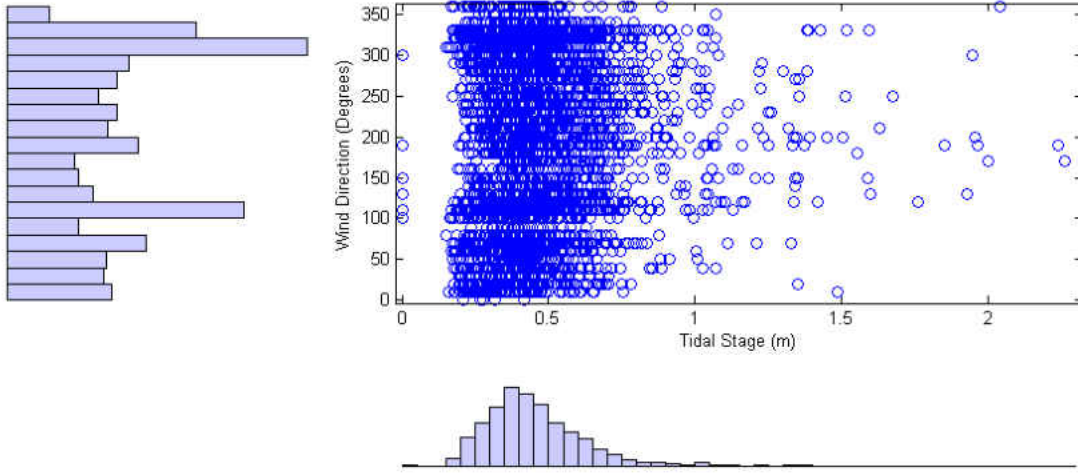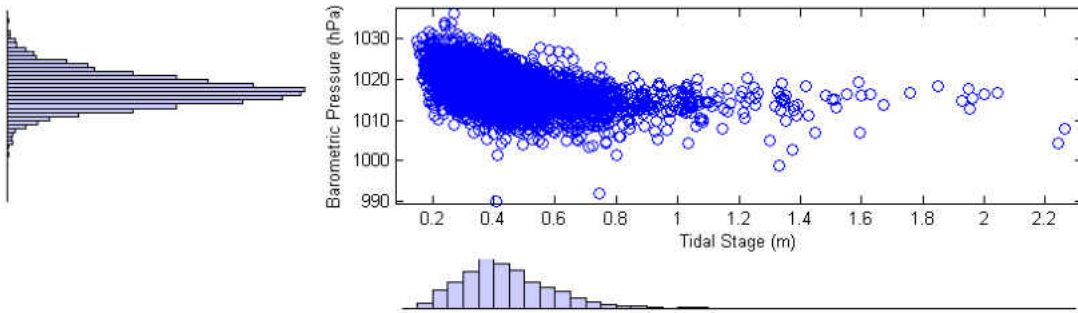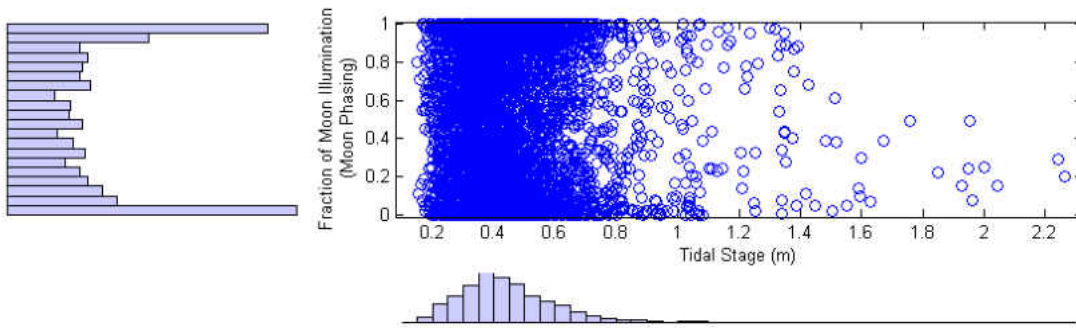
(e)
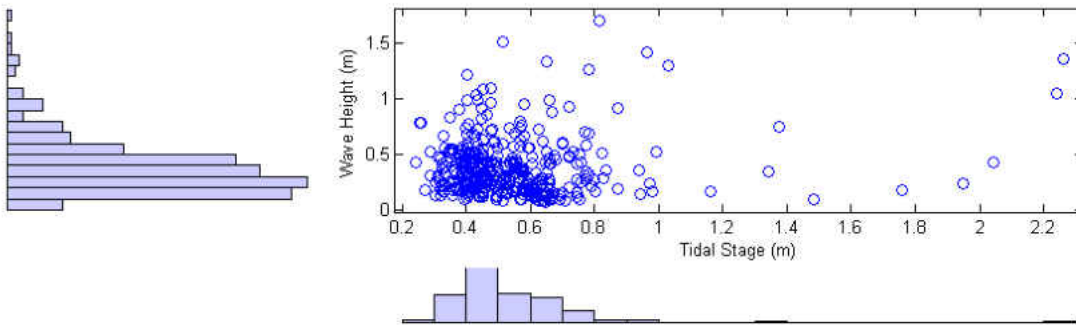
(f)

Figure 4-4: Relationship between (a) tidal stage and rainfall (2002-2014) (b) tidal stage and fastest 2-minute wind speed (2002-2014), (c) tidal stage and wind direction for fastest 2-minute wind speed(2002-2014), (d) tidal stage and barometric pressure(2002-2014), (e) tidal stage and moon phasing(2002-2014) and (f) wave height and tidal stage (Year 2012 only).

135
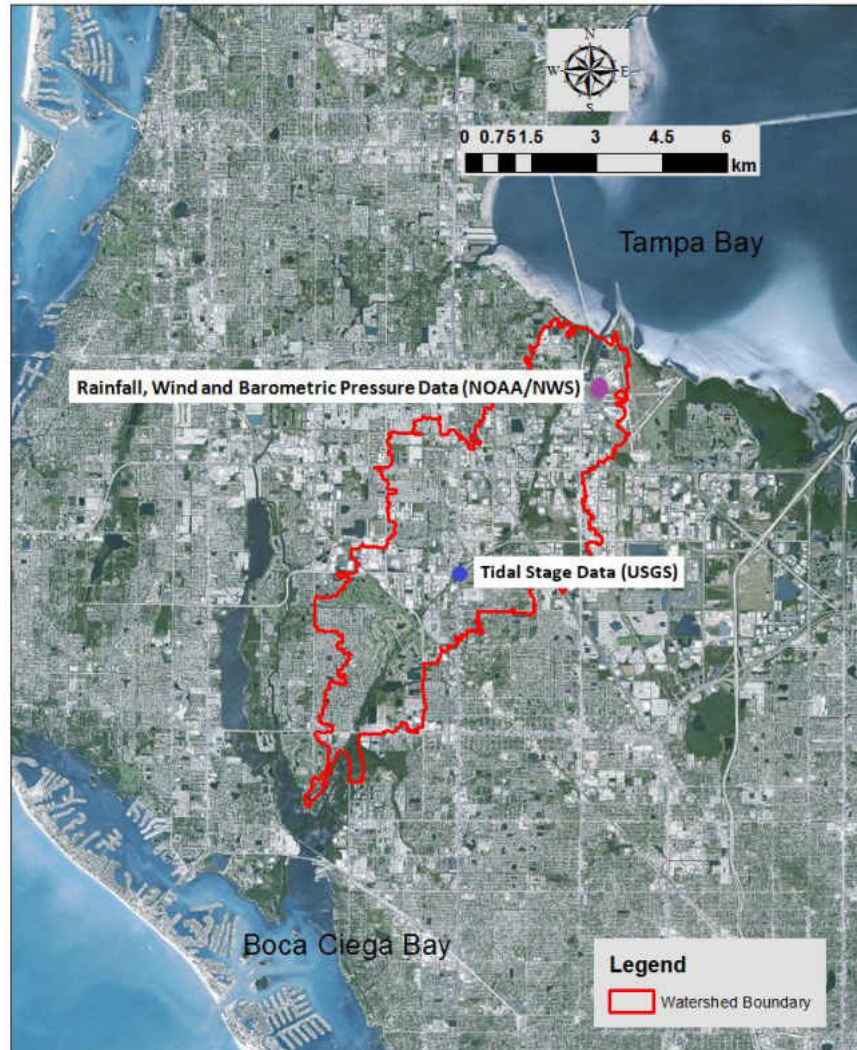
Figure 4-5: Locations of tidal stage, rainfall, wind speed and barometric pressure data for copula analysis. Note: Wave Height Data obtained from offshore buoy (27°20'29'' N 84°16'20'' W) managed by the NOAA National Data Buoy Center. Fraction of Moon Illumination data obtained from Astronomical Applications Department of the U.S. Naval Observatory. Note: NOAA is National Oceanic Atmospheric Administration, NWS is the National Weather Service and USGS is the United States Geological Survey. Source of Satellite Imagery: Esri, DigitalGlobe, GeoEye, Earthstar Geographics, CNES/Airbus DS, USDA, USGS, AeroGRID, IGN and GIS User Community

4.3.3.2. *Application of Copulas*

There exists a level of uncertainty of any combination of hazards occurring with corresponding consequence(s). Joint probability analysis is useful in this regard for determining probability of potential flooding hazards occurring simultaneously rather than in isolation. A univariate analysis alone cannot provide a complete assessment of the occurrence probability of potential flooding hazards or scenarios, particularly if they are interdependent (Chebana and Ouarda, 2011). However, with typical multivariate analyses, one condition is for the variables in question to be independent from another (Wahl et. al, 2012). A univariate analysis also lacks consideration of flooding under multivariate hazards, particularly for coastal communities, when worst case flooding can occur under combined heavy rainfall and high tide events (Xu et. al, 2014). The choice of multivariate analysis must take into the consideration that the variables in question could be interdependent, may not be under the same family of marginal distributions and are not normally distributed.

For this reason, copulas can be particularly useful. While copulas have wide applications across several disciplines such as finance and insurance, the applications of copulas, within hydrology, in particular, is important since hydrological processes are typical multidimensional in nature and indicate certain levels of interdependence (Salvadori & De Michele, 2007). Several applications of copulas in hydrology (Table 1) consisted of analyzing joint behavior of several hydrological variables during storm events while capturing important statistical dependences (De Michele and Salvadori 2003; Salvadori and De Michele 2004; Balistrocchi and Bacchi, 2011), modeling of multivariate hydrological extremes (Favre et al., 2004; Zhang et

al.,2011), rainfall frequency analysis (Zhang and Singh, 2007), flood frequency analysis (Wang et al., 2009) and hydraulic structural design for flooding (De Michele et al., 2005).

Table 4-3: Applications of Copulas for Varying Hydrology Topics

Topic of Concerns	Copula Variables	References
● Rainfall Characteristics	● Storm intensity and duration[1] ● Rainfall volume and duration[2]	● De Michele and Salvadori (2003)[1] ● Salvadori and De Michele (2004)[1] ● Balistrocchi and Bacchi, (2011)[2]
● Extremes	● Peak flows and volumes	● Favre et al. (2004)
● Rainfall Frequency Analysis	● Rainfall duration and intensity ● Rainfall depth and intensity ● Rainfall duration and depth	● Zhang and Singh (2007)
● Flood Frequency Analysis	● Peak flow (confluence)	● Wang, Chang, and Yeh (2009)
●Structural Design (Flood Risk)	● Flood peak and volume	● De Michele et al. (2005)

Particularly for inland coastal areas, copulas have been useful in analyzing coastal hazards (Table 2) with underlying hydrological and hydrodynamic processes (De Michele et al., 2007; Wahl et al., 2012; Corbella and Stretch, 2013; Xu et al., 2014; Trepanier et al.,2014).

Table 4-4: Applications of Copulas for Coastal Hazards

Hazard	Copula Variables	References
● Sea Storm	● Significant wave height, storm duration, storm direction, and storm inter-arrival time[1] ●Wave height, wave period and storm duration[2]	● De Michele et al. (2007)[1] ● Corbella and Stretch (2013)[2]
● Storm Surge	● Highest turning point, intensity and significant wave height	● Wahl et al. (2012)
● Extreme Rainfall ● Storm Tide	● Annual peak 24-hr rainfall and tide level	● Xu et al. (2014)
● Tropical Cyclones	● Storm surge height and wind speed	● Trepanier et al. (2014)

The copula has its origins from Sklar's theorem (Nelsen, 2006), which states that given a joint distribution function, H, with marginal distributions F_1 and F_2, there exists a copula function C for all real values of x and y

$$H(x, y) = C(F_1(x), F_2(y))\tag{4-9}$$

Sklar's theorem can also be applied to n-dimensions such that a distribution function H, of n-dimensions, with marginal distributions $F_1, F_2,..., F_n$ there exists a copula C of n-dimensions for all real values of x

$$H(x_1, x_1,..., x_n) = C(F_1(x), F_2(x),..., F_n(x))\tag{4-10}$$

The choice in copula is important based upon its ability to capture dependency structure of the variables considered. Archimedean copulas are used in a wide range of applications because they are easily constructed (Nelson, 2006) and are capable of capturing wide ranges of dependence.

Archimedean copulas, include the one-parameter families (Gumbel, 1960; Clayton 1978; Ali, Mikhail and Haq, 1978; Frank, 1979; Joe, 1993) and the bivariate two-parameter BB1-BB3 and BB6-BB9 families (Joe, 1997). An Archimedean copula of d-dimension(s) can be represented in the following form:

$$C(x_1,...,x_d) = \psi[\psi^{-1}(x_1)+...+\psi^{-1}(x_d)] \qquad\qquad \textbf{(4-11)}$$

where ψ is a continuous generator function that satisfies the following conditions: (1) $\psi(1) = 0$; (2) $\psi(0) = \infty$; (3) $\psi'(t) < 0$ and (4) $\psi''(t) > 0$ for all values of $t \in (0, 1]$. Widely used Archimedean copulas include the Gumbel-Hougaard, Clayton, Frank copulas. Given d-dimension(s), the Gumbel- Hougaard copula, Clayton copula, and Frank copula are represented in Table 5.

Table 4-5: Archimedean Copulas utilized in this study

Copula	$C_\theta(x_1,...,x_d)$	ψ (t)	θ
Gumbel-Hougaard	$\exp\left\{-[(-\ln F(x_1))^\theta +...+ (-\ln F(x_d))^\theta]^{1/\theta}\right\}$	$(-\ln t)^\theta$	$\theta \geq 1$
Clayton	$(F(x_1)^{-\theta}+...+F(x_d)^{-\theta}-1)^{-1/\theta}$	$\dfrac{t^{-\theta}-1}{\theta}$	$\theta \geq 0$
Frank	$-\dfrac{1}{\theta}\ln\left[1+\dfrac{(e^{-\theta F(x_1)}-1)(e^{-\theta F(x_2)}-1)...(e^{-\theta F(x_d)}-1)}{e^\theta -1}\right]$	$\dfrac{e^{-\theta t}-1}{e^{-\theta}-1}$	$\theta \neq 0$

where θ is a dependence parameter. The Frank copula allows for both positive and negative dependence while the Gumbel-Hougaard copula allows for more positive dependence and the Clayton copula allows for more negative dependence. However before the choice in copula can be made for determination of joint hazard probability, a separate methodology (Figure 7) consisting of optimization techniques must be developed.

As such, before the identification of the best-fit copula can be made, appropriate parameters must be estimated with a corresponding likelihood value. The best-fitting of the copula is best determined by parameter and likelihood estimation.

The "Maximum Likelihood Estimation" method can be utilized as a first step toward determining the best-fit Archimedean copula due to its inherent versatility for varying models and data types (Khadka, 2008). The following steps (Figure 7) are used outline the determination of maximum log-likelihood using Archimedean copula parameters.
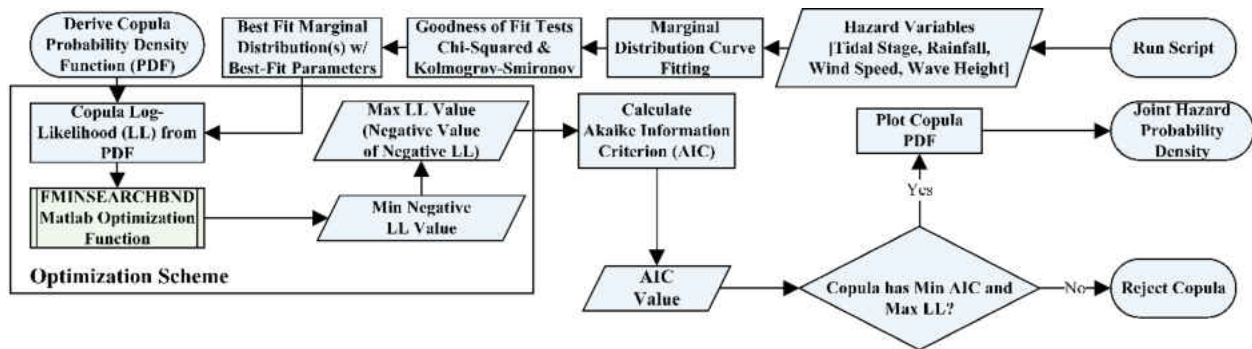
Figure 4-6: Methodology for determination of best-fit Archimedean copula

1. Given a d-dimensional copula of the form $C(x_1, ..., x_d) = \partial F(F_1^{-1}(x_1)...F_n^{-1}(x_d))$, the corresponding copula density function can be expressed as

$$c(x_1, ..., x_d) = \frac{\partial^2 C(x_1, ..., x_d)}{\partial x_1...\partial x_d} = \frac{\partial F(F_1^{-1}(x_1)...F_n^{-1}(x_d))}{\partial x_1...\partial x_d} \qquad (4\text{-}12)$$

Table 4-6: PDFs of Archimedean copulas utilized in this study

Copula	$c_\theta(x_1,...,x_d)$
Gumbel-Hougaard	$\exp\{-[(-\ln F(x_1))^\theta + ... + (-\ln F(x_d))^\theta]^{1/\theta}\}(F(x_1)...F(x_d))^{-1}\left\{\dfrac{[(-\ln F(x_1))...(-\ln F(x_d))]^{\theta-1}}{[(-\ln F(x_1))^\theta + ... + (-\ln F(x_d))^\theta]^{2-\frac{1}{\theta}}}\right\}\left\{[(-\ln F(x_1))^\theta + ... + (-\ln F(x_d))^\theta]^{\frac{1}{\theta}} + \theta - 1\right\}$
Clayton	$(F(x_1)...F(x_d))^{-\theta-1}(\theta+1)(F(x_1)^{-\theta} + ... + F(x_d)^{-\theta} - 1)^{-\frac{1}{\theta}-2}$
Frank	$\dfrac{\theta e^{-\theta(F(x_1)+...+F(x_d))}(e^{-\theta}-1)}{(e^{-\theta(F(x_1)+...+F(x_d))} - e^{-\theta F(x_1)}...-e^{-\theta F(x_d)}e^{-\theta})^2}$

2. Assuming parameters for the copula C and marginal CDFs $(F_i,...F_d)$ as θ and

$\hat{\boldsymbol{\theta}} = [\hat{\theta}_1,...,\hat{\theta}_k] = [(\alpha_1,...,\alpha_y),...(\alpha_k,...,\alpha_y)]$, respectively, with $k=1,...,d$ where d represents the

number of dimensions and y is the number of parameters for a respective marginal distribution

can be represented by the following density function

$$f(x_1,...,x_d;\theta,\hat{\boldsymbol{\theta}}) = c(F_1(x_1;\hat{\theta}_1),...,F_d(x_d;\hat{\theta}_d);\theta)\prod_{k=1}^{d} f_k(x_k;\hat{\boldsymbol{\theta}})$$

(**4-13**)

3. Define a likelihood function L: $L(\theta;x_i) = \prod_{i=1}^{n} f(x_i;\theta)$ such that the likelihood of some parameter(s)

being a certain value, given the data $x_i,...,x_n$ of n-observations, is similar to the probability of

observing the data given some parameter(s). Given the log-likelihood is $\ln L(\theta;x_i) = \sum_{i=1}^{n} \ln f(x_i;\theta)$ the

log-likelihood of Eqn. (12) can be represented as

$$\ln L(\theta,\hat{\boldsymbol{\theta}};x_1,...,x_n) = \sum_{i=1}^{n} \ln f(x_{ik},...,x_{nd};\theta,\hat{\boldsymbol{\theta}}) =$$

$$\sum_{i=1}^{n} c(F_1(x_{i1};\theta_k),...,F_d(x_{id};\theta_d);\theta) + \sum_{i=1}^{n}\sum_{k=1}^{d} \ln f_k(x_{ik};\hat{\boldsymbol{\theta}})$$

(**4-14**)

for k = 1,…,d where d = number of dimensions.

4. The negative-log likelihood can be determined by a determining the negative of Eqn. (13) as represented

$$-\ln L(\theta,\hat{\boldsymbol{\theta}};x_1,...,x_n) = -\sum_{i=1}^{n}\ln f(x_{ik},...,x_{nd};\theta,\hat{\boldsymbol{\theta}}) =$$

$$-\left[\sum_{i=1}^{n}c(F_1(x_{i1};\hat{\boldsymbol{\theta}}),...,F_d(x_{id};\theta_d);\theta) + \sum_{i=1}^{n}\sum_{k=1}^{d}\ln f_k(x_{ik};\hat{\boldsymbol{\theta}})\right]$$

(4-15)

with the goal of minimizing the negative log-likelihood which is equivalent to maximizing the log-likelihood. The negative log-likelihood is found using copula-based MATLAB algorithms adapted for Patton (2004) however with changes to include optimization functions to maximize the log-likelihood (negative of negative log likelihood).

Once the maximum log-likelihood of each copula, with an associated dependence parameter, is determined, additional criteria is needed to determine the best-fit copula for the data. The Akaike Information Criterion (AIC) (Akaike, 1974), is typically applied in selection of semiparametric and parametric copula models, however the Copula Information Criterion has been recently developed to provide criteria for copulas specifically with the drawback of increased computational cost (Jordanger and Tjostheim, 2014). As such, the AIC will be a recommended criterion for this study and is determined as follows

$$AIC = 2K - 2\ln(LL)$$

(4-16)

Where K is the number of parameters estimated and LL is the log-likelihood. Given a set of candidate models for the data, the preferred model is the one with the minimum AIC value for maximum likelihood. The AIC value reflects the goodness of fit but it also includes a penalty with each increase in the number of estimated parameters to discourage overfitting.

Vulnerability Component of Risk Formulation

The vulnerability component of the risk formulation can be qualitatively defined using several criteria (Table 5). The criteria are as follows: (1) the distance to a major water body, (2) slope, (3) elevation from a digital elevation map (DEM), (4) soil condition and (5) percent imperviousness

Table 4-7: Vulnerability Criteria

Criteria	Description	Data Source
Distance to Water body	Distance of area relative to major water body such as a river. Higher weight assigned to small distances	Pinellas County
Slope	Higher weight assigned to relatively flat areas	From DEM (Pinellas County)
Elevation	Higher weight assigned to smaller elevations	DEM (Pinellas County)
Soil Condition	Higher weight applied to poorly drained soil (soil with higher runoff potential when wet).	USDA/NRCS Web Soil Survey
Imperviousness (%)	Runoff potential based upon level of imperviousness. Higher weight assigned to areas with low % imperviousness.	National Land Cover Database 2011

4.3.3.4.   Exposure Component of Risk Formulation

The exposure component of the risk formulation is representative of the level of inundation due to the hazards considered. Tropical Storm Debby in late June 2012 was chosen as a test case for determining exposure due to its associated heavy rainfall, high tides and waves. The level of inundation is determined via a watershed model, the Interconnected Channel and Pond Routing Version 4 software (ICPRv.4). The ICPRv.4 model (Streamline Technologies Inc., 2015) is a comprehensive hydrodynamic stormwater and hydrologic model that incorporates integrates terrain data, hydrologic data, hydraulic data, and climate data via a layering and data management system. ICPRv.4 was utilized to construct a detailed model of the Cross Bayou watershed, which includes an integrated surface and groundwater interface. The ICPRv.4 software can also determine potential flood inundation via 2D overland flow algorithms.

4.3.4. Risk Components and Weighting Criteria

Given the proposed risk formulation in Equation 7, applying normalization to avoid the impact of scale is more appropriate. This can accomplished by defining weighting criteria for the components of the risk formulation (hazard, vulnerability, exposure and resilience) as follows:

1. **Risk =** Expected value of negative impact given the product of hazard, vulnerability, exposure and resilience components. Increases in hazard, vulnerability and exposure could increase risk however with minimizing the overall recovery time, represented by the resilience metric, risk can be reduced.

$$\text{Risk} = \cfrac{\left[\underbrace{\prod \text{Hazard Weight} \; x \; \prod \text{Vulnerability Weight}}_{Likelihood} \; x \; \overbrace{\text{Exposure Weight}}^{Consequences} \right]}{\text{Resilience}}$$

(4-17)

2. **Hazard**= Product of joint probabilities of combinations of variables that could contribute to flood hazard via Archimedean copula PDF plots.

3. **Vulnerability** = Product of applied weights, normalized between 0 and 1 with 1 being the highest, to a given area of concern based upon several factors such as elevation, distance to waterbodies and drainage capacity.

4. **Exposure** = Inundation depth value for an area of concern, normalized from 0 to 1.

5. **Resilience**

6. $\quad$ **Resilience**$= \cfrac{1}{\left[\cfrac{T_f - T_i}{T_i} \right]}$

$T_i =$ initial recovery time (time in which inundation depths are initially reduced from maximum inundation depths, i.e. max exposure)

$T_f =$ final recovery time (time in which inundation depths are non-existent following maximum inundation depths, i.e. max exposure)

Minimizing the difference between the initial recovery time and the final recovery time [i.e., the numerator $(T_f - T_i)$] results in reduction of risk due to faster recovery.

4.3.5. Scenarios

For comparative purposes in determining the effectiveness of the risk formulation with the resilience term, it would be necessary to evaluate the formulation under varying scenarios. These scenarios range from inclusion of no action (existing conditions) to incorporation of "adaptive measures" such as low impact development (LID), dredging and tidal walls at key locations (Figure 7). Details of such adaptive measures are presented in Table 8 Eight scenarios (Table 9) were considered with each scenario including a variation in adaptive measures, with exception of scenario 1 for which no measure is applied.
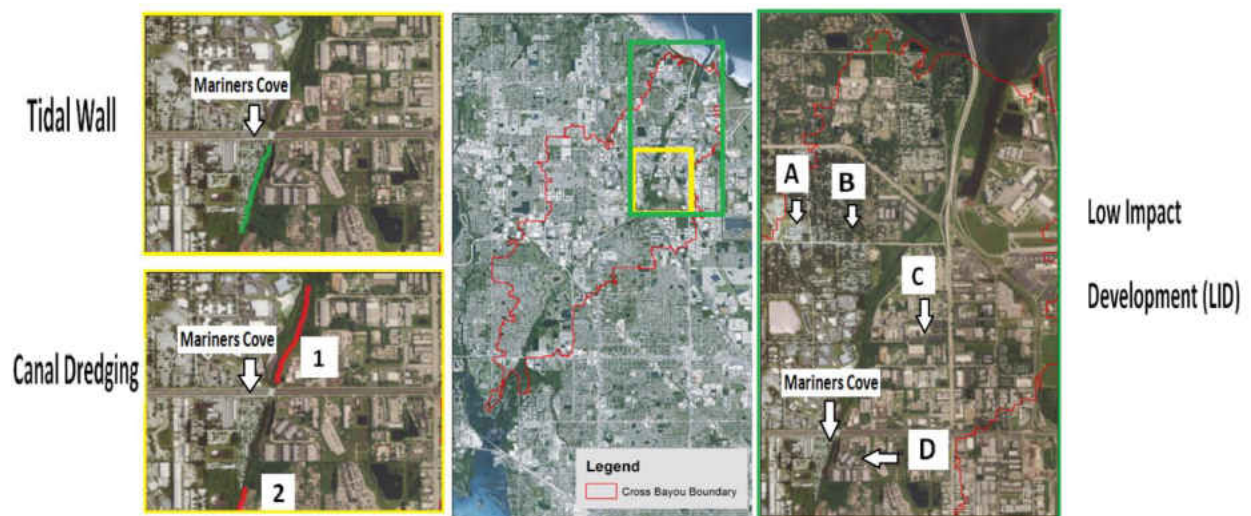
Figure 4-7: Locations of adaptive measures

Table 4-8: Description of Adaptive Measures

Measure	Description
Canal Dredging(Section 1)	Removal of sediments and material from the Cross Bayou Canal to restore capacity of canal such as depth. Increase depth by 0.61m (2 ft.).
Canal Dredging(Section 2)	Removal of sediments and material from the Cross Bayou Canal to restore capacity of canal such as depth. Increase depth by 0.61m (2 ft.).
Tidal Wall (with stormwater inlets)	Protection against high tide events. Minimum height of wall = 3.04 m (10 ft.). Divert rainfall runoff using stormwater inlets with underground pipes back to canal downstream.
Low Impact Development (LID) Sites A-D	Incorporation of natural drainage pathways to reduce

Measure	Description
	runoff by reducing imperviousness by 25%

Table 4-9: Scenarios Considered for Analysis with Inclusion of Adaptive Measures

Scenario	Adaptive Measure(s)	Type and Location of Adaptive Measure(s)
1	No Action	None
2	LID Only	Site A (Pervious Pavement) Site B (Swales) Site C (Pervious Pavement) Site D(Pervious Pavement) (Figure 9)
3	Dredging Only	Sites 1 and 2 (Figure 9)
4	Tidal wall Only	Tidal Wall with stormwater inlets (Figure 9)
5	LID & Dredging	Site A (Pervious Pavement) Site B (Swales) Site C (Pervious Pavement) Site D(Pervious Pavement) (Figure 9)

Scenario	Adaptive Measure(s)	Type and Location of Adaptive Measure(s)
		Sites 1 and 2 (Figure 9)
6	LID & Tidal wall	Site A (Pervious Pavement) Site B (Swales) Site C (Pervious Pavement) Site D(Pervious Pavement) Tidal Wall with stormwater inlets (Figure 9)
7	Dredging & Tidal wall	Tidal Wall with stormwater inlets Sites 1 and 2 (Figure 9)
8	LID, Dredging & Tidal wall	Site A (Pervious Pavement) Site B (Swales) Site C (Pervious Pavement) Site D(Pervious Pavement) (Figure 9) Sites 1 and 2 (Figure 9) Tidal Wall with stormwater inlets

4.3.6. Decision-Makers Analysis of Risk and Resilience

Decision-makers often rely on criteria and weighing possible outcomes before choosing the most beneficial plan of action. This is particularly concerning for municipalities evaluating potential measures for improving infrastructure for their constituents to rely on. This is particularly evident in areas that are prone to flooding and often rely on adequate drainage infrastructure to minimize damage such as to property. This is important from the advantage point of national policies related to flood risk and insurance. The National Flood Insurance Program (NFIP) aims to reduce the impact of flooding on private and public property by providing affordable insurance to property owners. The Community Rating System (CRS) of the NFIP is a voluntary program that encourages communities to adopt and enforce flood management practices which exceed NFIP requirements as an incentive for reducing flood insurance premiums. Recommended flood management practices under CRS include flood protection measures such as structural projects along with drainage system maintenance and improving flood risk mapping. The adaptive measures considered in the study such as LID, the tidal wall with stormwater inlets and dredging are examples of such recommended flood management practices.

With respect to decision analyses, weighting criteria can be a useful approach toward choosing a beneficial plan of action. The following five criteria are considered: (1) initial recovery time, (2) final recovery time, (3) capital investment effort, (4) areal-average risk, and (5) areal-average exposure. The initial and final recovery times have been previously defined as related to the resilience metric. The capital investment effort is the capital investment required to implement the proposed adaptive measure and is assigned a value from 0 to 3, with 0 indicating

151

no capital investment and 3 indicating large capital investment. The areal-average risk and areal-average exposure are the areal means of the risk value and exposure or inundation depth, respectively, over the entire area of concern.

4.4. <u>Results</u>

4.4.1. Joint Hazards & Copulas
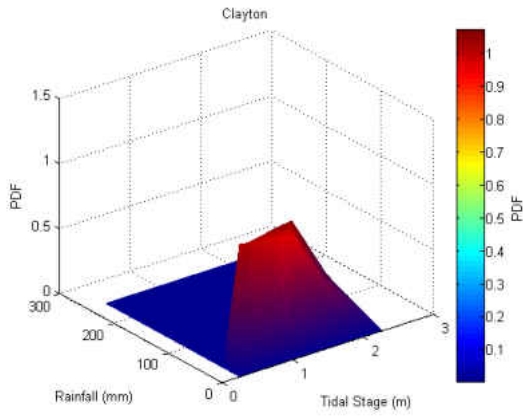
(a)
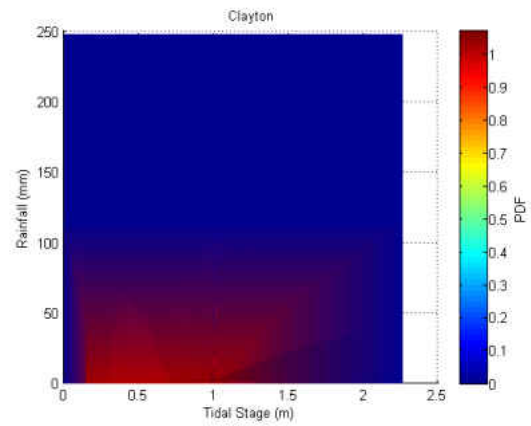
(b)
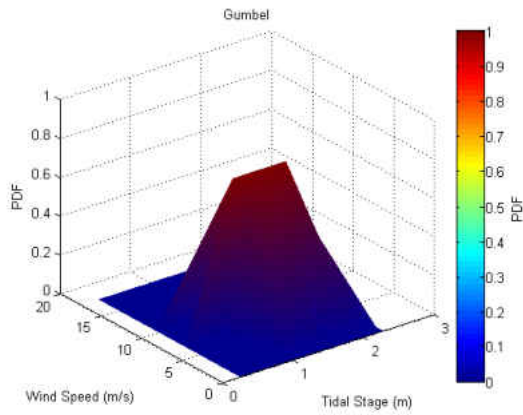
(c)
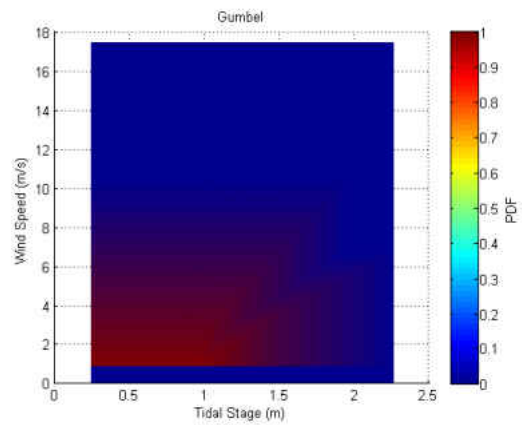
(d)
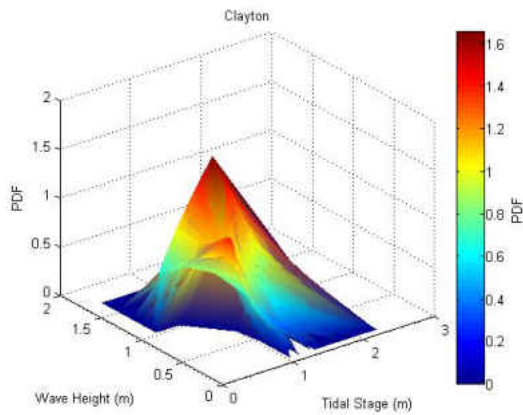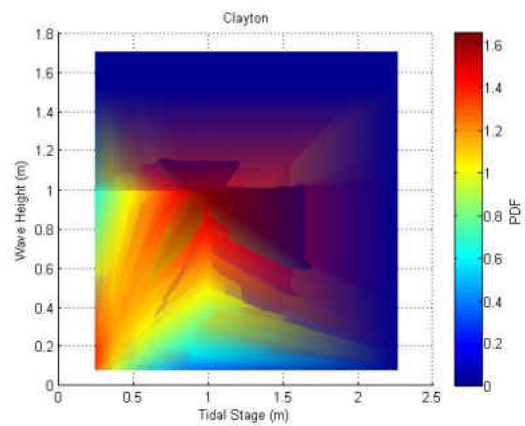
(e)   (f)

Figure 4-8:(a) Clayton PDF plot Rainfall and Tidal Stage (2002-2014) (3D view) with (b)

Rainfall and Tidal Stage (2002-2014) (top view) (c) Gumbel Wind Speed and Tidal Stage

(2002-2014) (3D view) with (d) Wind Speed and Tidal Stage (2002-2014) (top view) and (e)

Wave Height and Tidal Stage (2012) (3D view) with (f) Wave Height and Tidal Stage (2012)

(top view).

4.4.2. Vulnerability
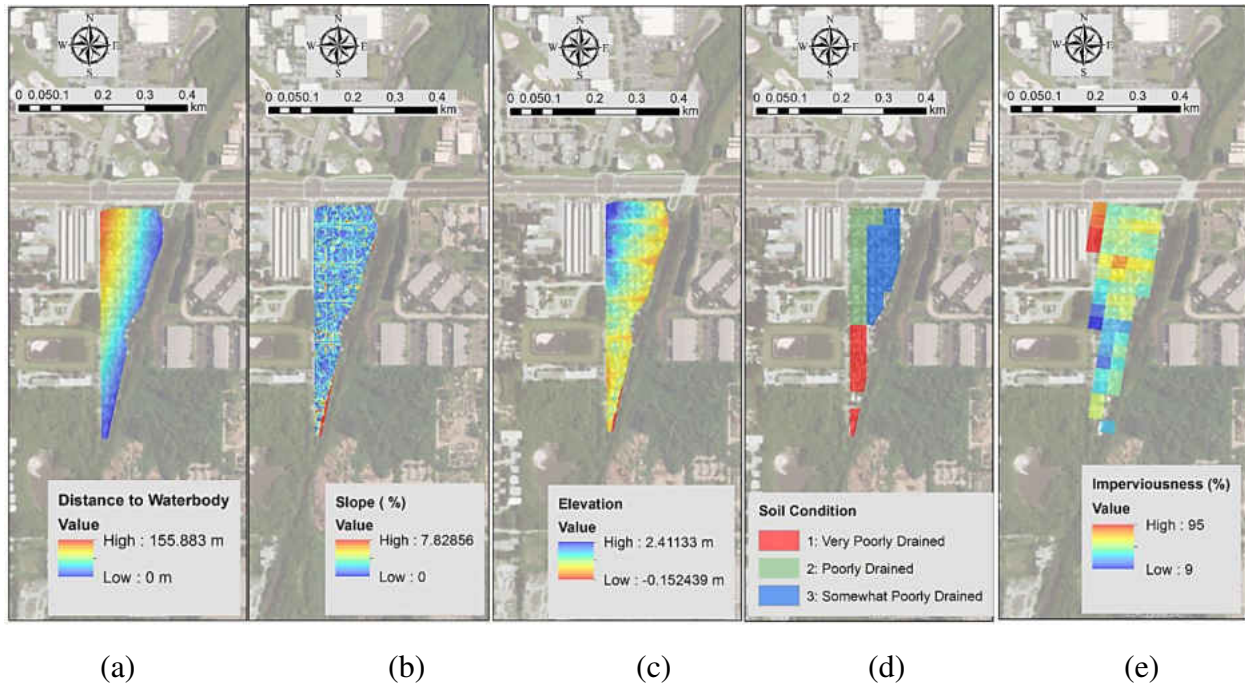
| (a) | (b) | (c) | (d) | (e) |

Figure 4-9: Non-weighted Vulnerability criterion (a) Distance, (b) Slope weight, (c) DEM, (d) Soil, and (e) Imperviousness for each vulnerability criteria for the Mariners Cove community.
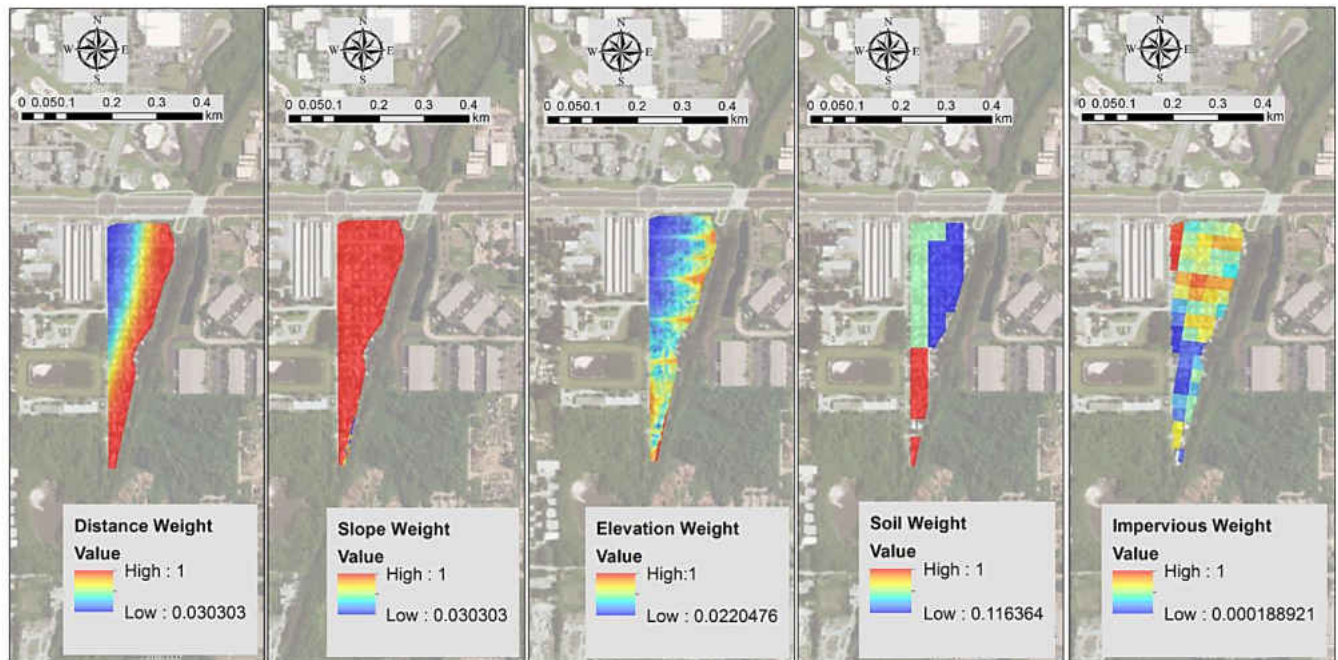
(a)   (b)   (c)   (d)   (e)

Figure 4-10: Associated weights (a) Distance, (b) Slope weight, (c) DEM, (d) Soil, and (e) Imperviousness for each vulnerability criteria for the Mariners Cove community. Source of Satellite Imagery: Esri, DigitalGlobe, GeoEye, Earthstar Geographics, CNES/Airbus DS, USDA, USGS, AeroGRID, IGN and GIS User Community.

4.4.3. Exposure

(a)   (b)   (c)   (d)

(e)   (f)   (g)   (h)
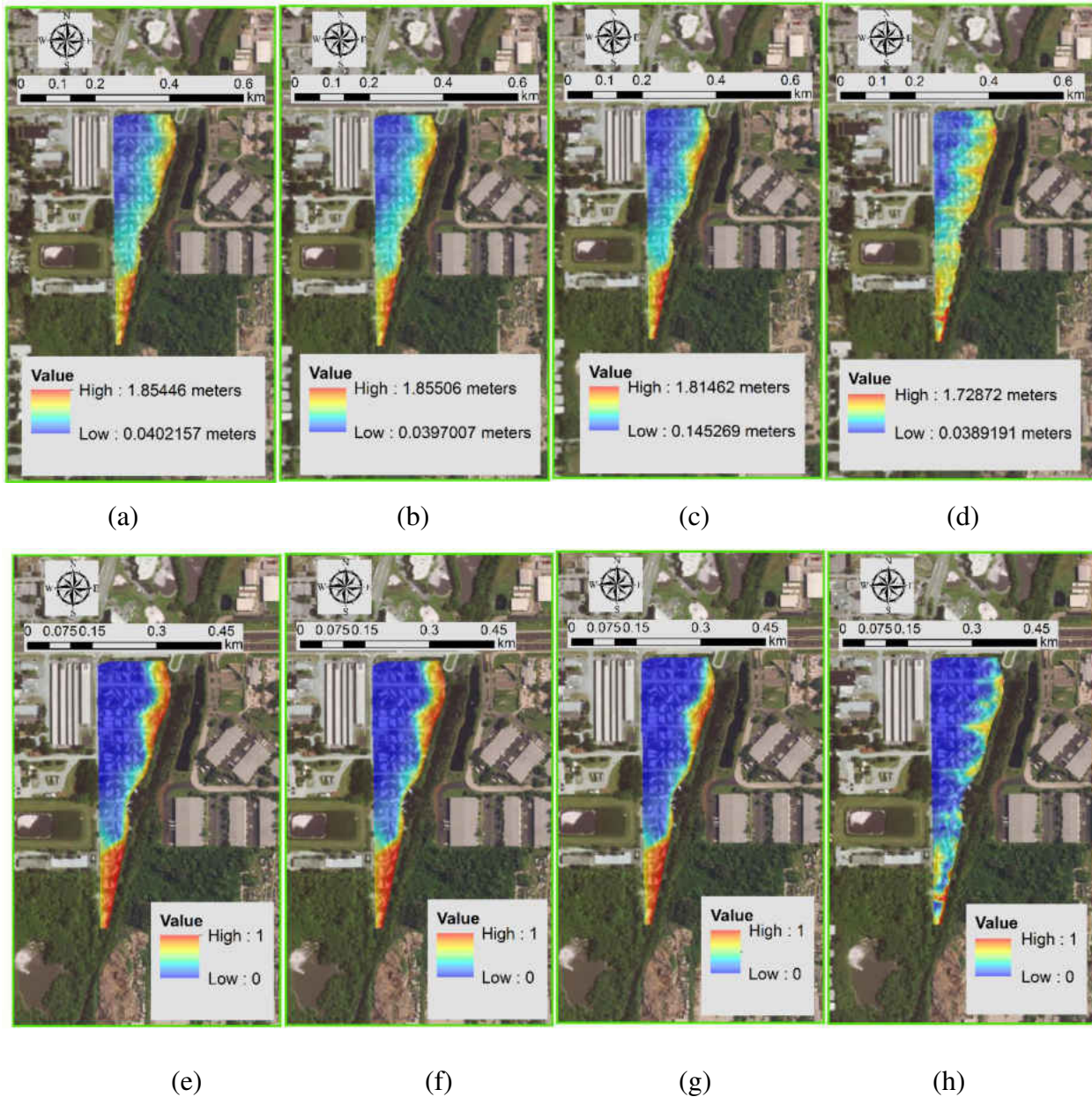
Figure 4-11: Non-normalized exposure (flood depth) for (a) no adaptive action, (b) LID Only, (c) Dredging Only and (d) Wall Only as well as normalized exposure for (e) no adaptive action, (f) LID Only, (g) Dredging Only and (h) Wall Only during Tropical Storm Debby on June 24th, 2012 Hour 18 (during max exposure).
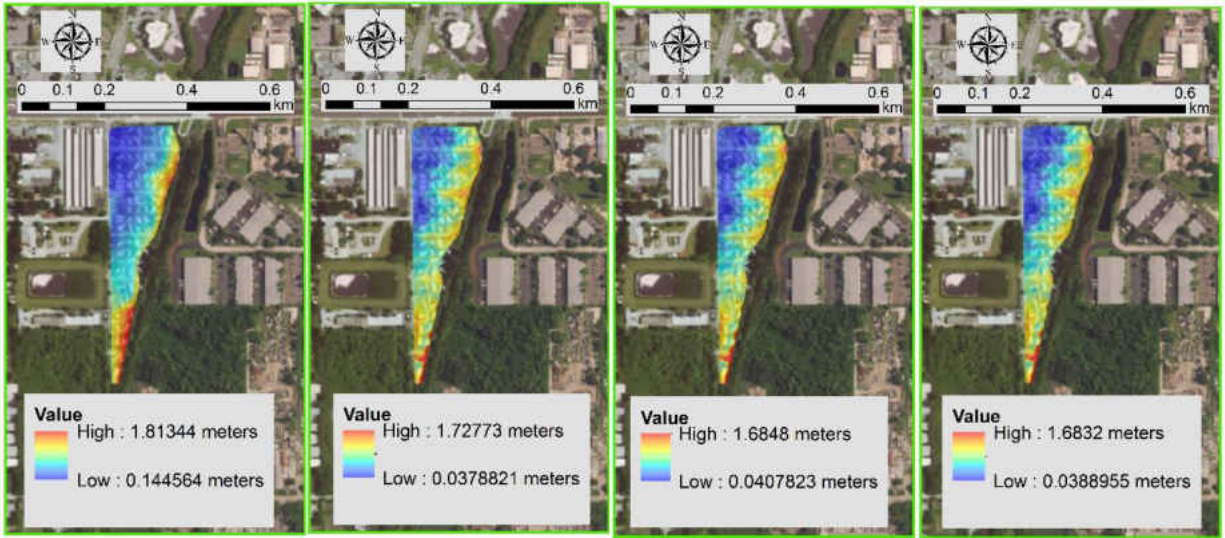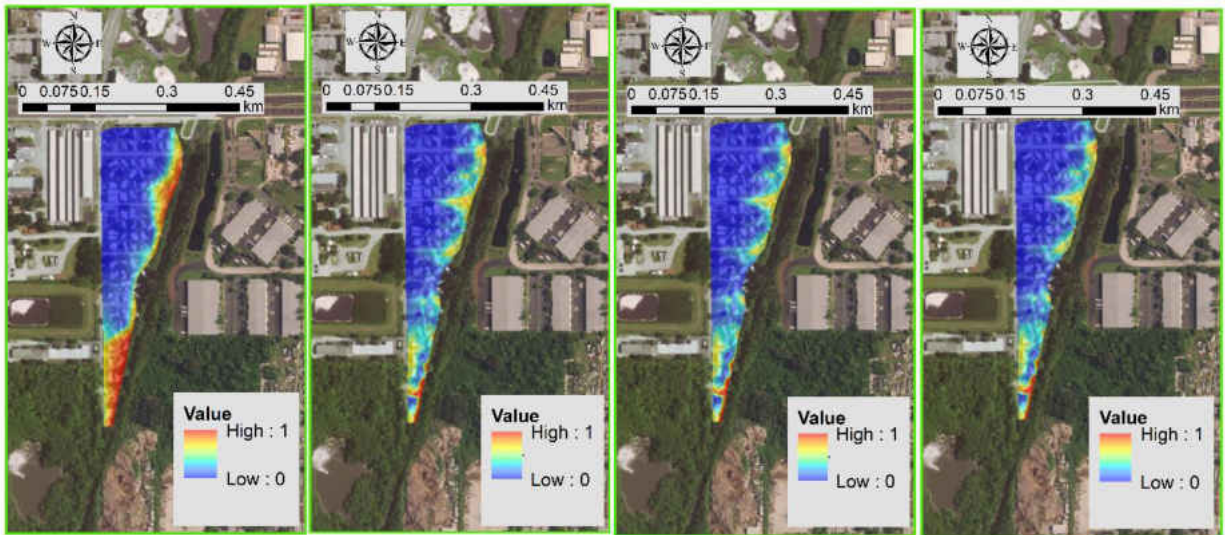
Figure 4-12: Non-normalized exposure (flood depth) for (a) LID & Dredging, (b) LID & Wall, (c) Dredging & Wall and (d) LID, Dredging & Wall as well as normalized exposure for (e) LID & Dredging, (f) LID & Wall, (g) Dredging & Wall and (h) LID, Dredging & Wall during Tropical Storm Debby on June 24th, 2012 Hour 18(during max exposure).

4.4.4.   Resilience

Table 4-10: Resilience Results

Scenario	Initial Recovery Period Post-Max Flooding T_i (hours)	Final (Full) Recovery Period Post-Max Flooding T_f (hours)	Relative Change in Time of Exposure $\dfrac{T_f - T_i}{T_i}$	Resilience $\dfrac{1}{\left[\dfrac{T_f - T_i}{T_i}\right]}$
No Action	14	120	7.57	0.132
LID Only	14	120	7.57	0.132
Dredging Only	13	99	6.61	0.151
Wall Only	13	28	1.15	0.870
LID & Dredging	13	99	6.61	0.151
LID & Wall	13	28	1.15	0.870
Dredging & Wall	12	25	1.08	0.926
LID, Dredging & Wall	12	25	1.08	0.926

4.4.5. Risk

(a)   (b)   (c)   (d)

(e)   **(f)**   **(g)**   **(h)**
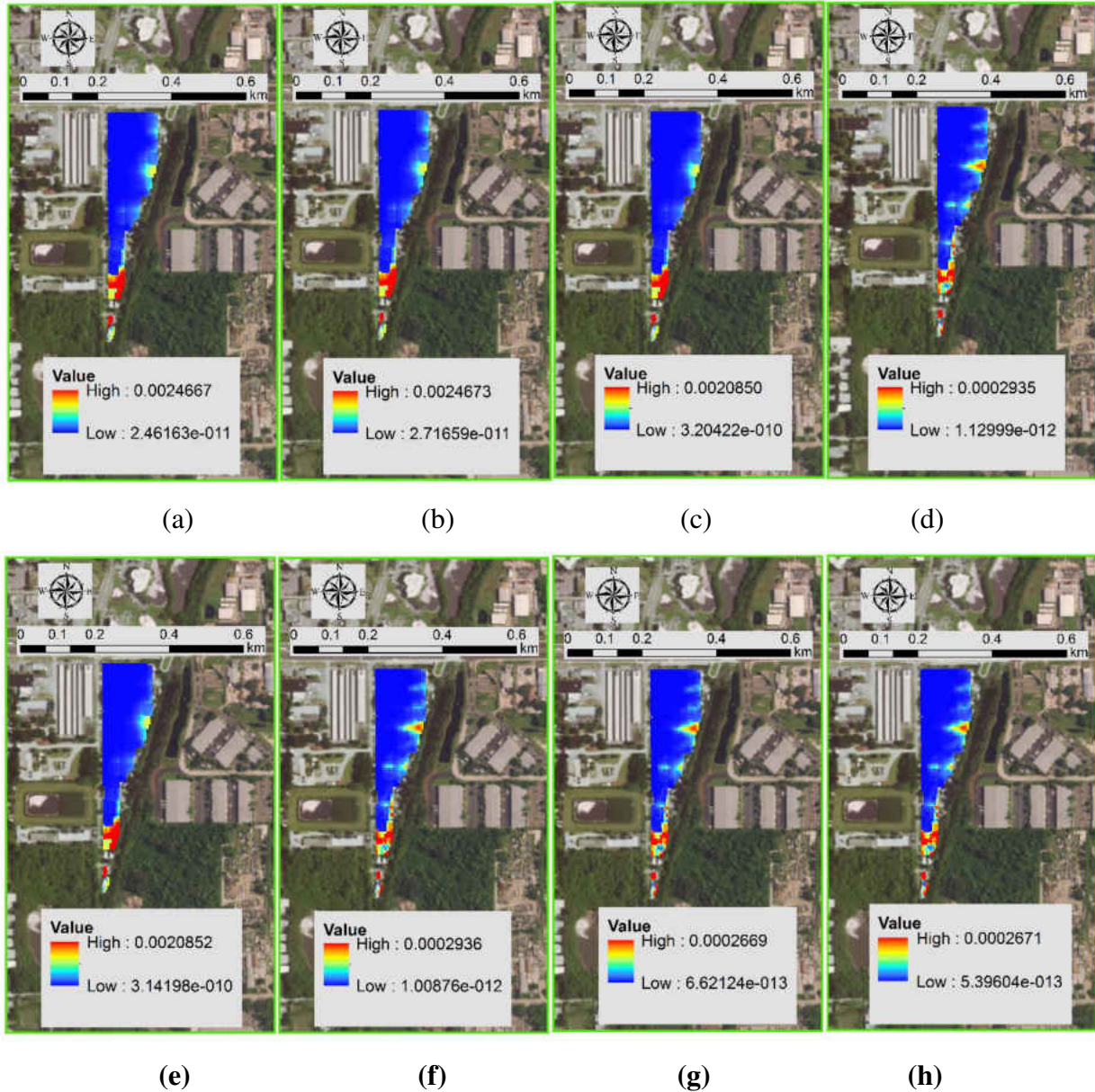
Figure 4-13: Non-normalized spatial risk values for (a) no adaptive action, (b) LID Only, (c) Dredging Only and (d) Wall Only during Tropical Storm Debby on June 24th, 2012 Hour 18 (during max exposure). Non-normalized spatial risk values for (e) LID & Dredging, (f) LID & Wall, (g) Dredging Only and (h) Wall Only during Tropical Storm Debby on June 24th, 2012 Hour 18 (during max exposure).

160
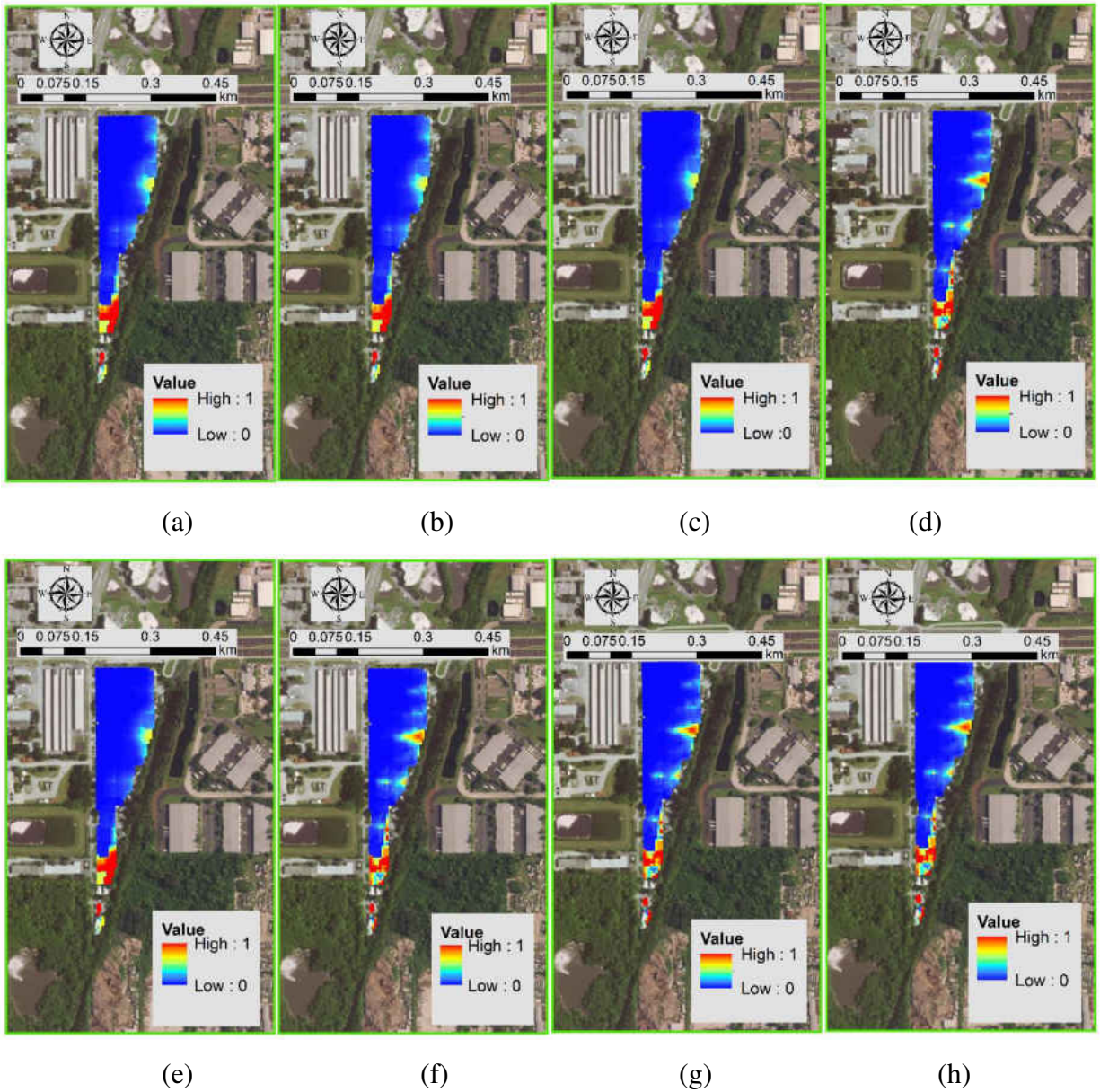
Figure 4-14:Normalized spatial risk for (a) no adaptive action, (b) LID Only, (c) Dredging Only and (d) Wall Only during Tropical Storm Debby on June 24th, 2012 Hour 18 (during max exposure). Normalized spatial risk for (e) LID & Dredging, (f) LID & Wall, (g) Dredging and Wall and (h) LID, Dredging and Wall during Tropical Storm Debby on June 24th, 2012 Hour 18 (during max exposure).

4.4.6.   Decision-Makers Criteria

Table 4-11: Non-Weighted Decision Criteria

Scenario	Initial Recovery Time (hrs.)	Final Recovery Time (hrs.)	Capital Investment Effort	Areal-Average Risk Value	Areal-Average Exposure (meters)
No Action	14	120	0	0.05	0.697
LID Only	14	120	1	0.05	0.697
Dredging Only	13	99	2	0.0456	0.662
Wall Only	13	28	2	0.0369	0.528
LID & Dredging	13	99	3	0.0456	0.661
LID & Wall	13	28	3	0.0369	0.527
Dredging & Wall	12	25	3	0.0342	0.483
LID, Dredging & Wall	12	25	3	0.0341	0.481

Table 4-12: Weighted Decision Criteria

Scenario	Initial Recovery Time	Final Recovery Time	Capital Investment Effort	Areal-Average Risk Value	Areal-Average Exposure
No Action	1.000	1.000	0.000	1.000	1.000
LID Only	1.000	1.000	0.333	1.000	1.000
Dredging Only	0.929	0.825	0.667	0.912	0.950
Wall Only	0.929	0.233	0.667	0.738	0.758
LID & Dredging	0.929	0.825	1.000	0.912	0.948
LID & Wall	0.929	0.233	1.000	0.738	0.756
Dredging & Wall	0.857	0.208	1.000	0.684	0.693
LID, Dredging & Wall	0.857	0.208	1.000	0.682	0.690
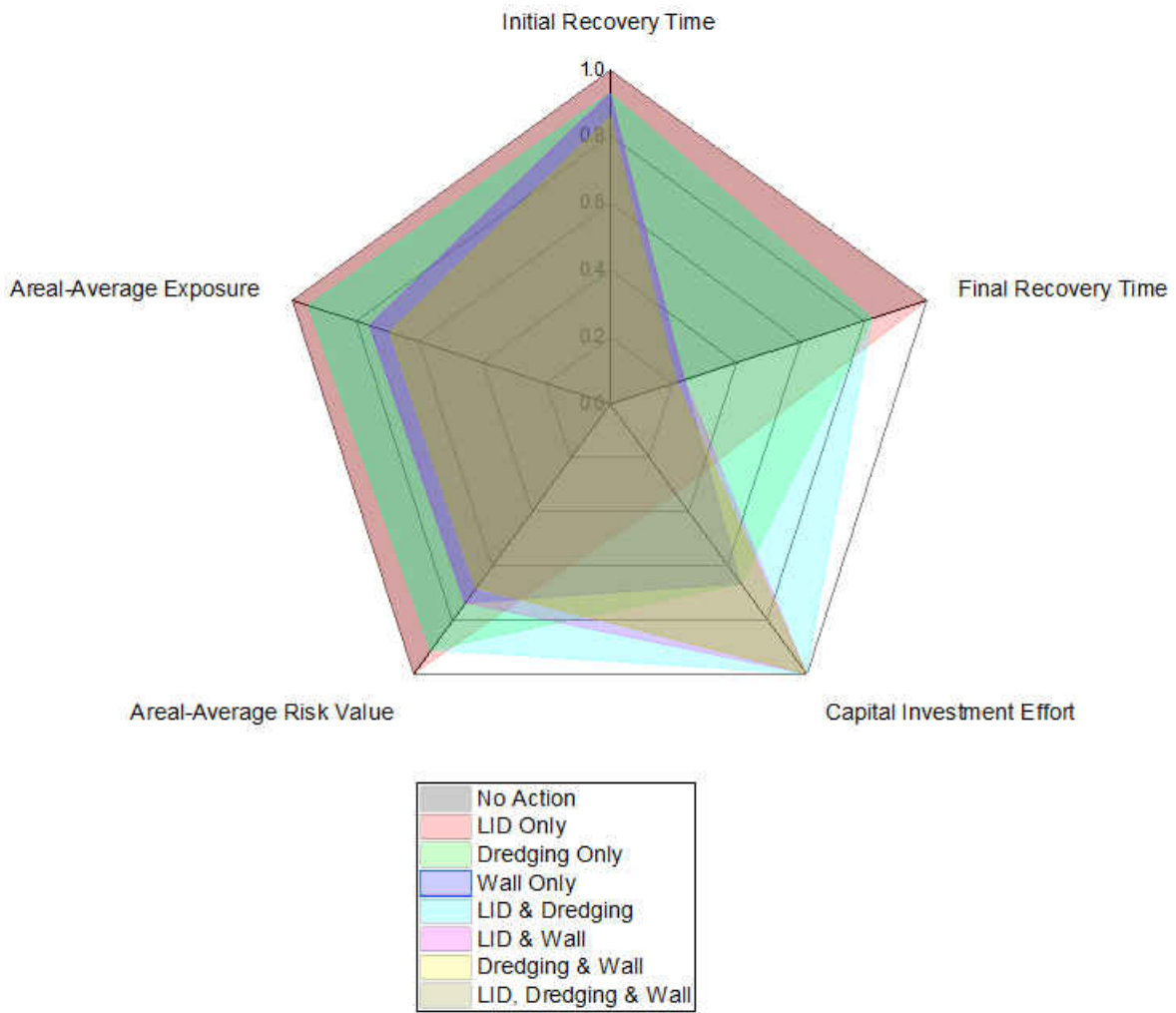
Figure 4-15: Radar plot of weighted criteria for no action and 7 adaptive measures

4.5. <u>Results & Discussion</u>

Exposure of the Mariners Cove community is presented in Figures 11 and 12 as a relation to inundation depth. Tropical Storm Debby in late June 2012 was chosen due to its associated heavy rainfall, high tides and waves. Considering the scenarios presented in Table 9, the inundation depth is higher with no adaptive measure as expected, however, incorporation of LID and dredging measures, without combined tidal wall and stormwater inlets, only offered minor reductions in inundation depths. This can be attributed to each adaptive measure offering a difference level of resilience against disturbances such as flooding. Amongst the combination of adaptive measures, the incorporation of dredging and the tidal wall with stormwater inlets provides greatest contribution to reducing the exposure magnitude or inundation depth (Figure 12c-d).

When considering spatial exposure changes, there are minor changes in exposure when incorporating adaptive measures without tidal wall and stormwater inlets. With the incorporation of the tidal wall and stormwater inlets, changes in spatial exposure are more pronounced with an unexpected result such that areas that areas near the tidal wall and stormwater inlets are slightly more exposed spatially, however, exposure magnitudes are still considerably lower compared to when no adaptive action was considered. Exposure only explains one aspect of risk that can be explained further when considering resilience, since the incorporation of resilience can essentially determine how long the exposure is felt within the area of concern. For instance, for what time period will the area of concern be exposed or inundated and how for what time period when flood water begin to recede? Answers to these questions can be provided by discussing results of the resilience metric.

165

The goal of the resilience metric is to minimize the difference between the initial recovery time and the final recovery time [i.e., the numerator ($T_f - T_i$) such that the system in question can achieve recovery in a shorter period of time such that $T_f - T_i$ is small in value]. As evident in Table 10, the combination of dredging and the tidal wall resulted in minimizing the difference between the initial recovery time and the final recovery time [i.e., the numerator ($T_f - T_i$)] such that this combination resulted in faster overall recovery or greater resilience to flood waters.

Given the eight scenarios considered, with the hazard and vulnerability components kept the same, the primary components that influenced changes in risk were exposure and resilience which are tied to the adaptive measures implemented. The expected value of risk change decreases considerably for adaptive measures incorporating the tidal wall (Figure 13). Reduction in risk magnitudes overall (Figure 13a-h), with the incorporation of adaptive measures such as LID, dredging and the tidal wall, can be attributed to an increase in flood resilience. Irrespective of changes to exposure magnitudes, resilience remains the greatest influence to risk such that increases in flood resilience (i.e., decreases the time for water to recede from the area) via incorporation of adaptive measures presented in Table 10, help to offset risk magnitudes as evident in Figure 13.

Spatially, risk does not change much, across adaptive measures, with the exception of the southwestern corner of the Mariners Cove area and the eastern boundary of the Mariners Cove area (Figure 14). The changes in risk, spatially, near the southwestern corner and eastern boundary of Mariners Cove are attributable to incorporation of the tidal wall and stormwater inlets.

166

In general, the closer south near the Mariners Cove boundary, the higher the risk. Overall, each adaptive measure offers a difference level of resilience against flood disturbances and subsequently offer differing changes in risk, more so by magnitude than spatially.

4.6. <u>Conclusion</u>

Assessing flood risk for decision making requires identifying components of risk and quantifying these components by an integrative approach. These components associated with risk include hazard, vulnerability, exposure and resilience in the form of adaptive capacity. Vulnerability, exposure and resilience are dependent on the hazard(s) considered while vulnerability is dependent on adaptive capacity, which is tied to resilience. Hence, risk can vary primarily on hazard(s) considered and the associated level of resilience for such hazard(s). Specifically for infrastructure, resilience is tied to the level of recovery given the hazard(s) considered which could be interdependent. This has implications for decision-makers such as municipalities, who may rely on risk being fixed and do not consider interdependent hazards, adaptive measures and resilience (as a function of adaptive measures and hazards). As such this study addresses approaches in considering resilience in overall flood risk management analysis and determine if coupling flood risk and engineering resilience, via adaptive measures, could improve flood impact assessment. As a result, this study notes this approach has implications for decisions makers such as municipalities and their constituents on a policy level when considering existing flood insurance methodologies.

Incorporating resilience within risk framework, as it pertains to drainage infrastructure systems, is inherently important for such systems to reduce flood risk. Particularly for engineered

drainage infrastructure systems with adaptive capacity such as LID and flood proofing structure, risk is typically considered for a low probable, damaging event for design purposes. In this study, risk is no longer fixed for an entire area but varies spatially, which could vary with hazards considered and could vary with adaptive measures adopted. With this advancement, resilience becomes an important factor for determining the performance of drainage infrastructure and flood protection during a major flood event. The resilience term was determined from observing time of water receding (i.e., time of recovery via the system). The time between the initial and final (full) water receding from an area of concern is a useful parameter for determining resilience of drainage infrastructure systems toward flooding. The shorter the time period for water to fully recede during flooding, the more resilient the system and vice-versa. It is indicative that either alternative with dredging and the tidal wall or alternative with LID, dredging and the tidal wall should be chosen as the most beneficial plan of action for the community considered. Enacting a system for which flood waters can recede within a shorter time frame can reduce exposure and subsequently reduce damage and overall risk to flooding. Our case study has fully confirmed this suite of new concept within the context of such a coupled risk and resilience framework. Future work may be extended to tackle different types of flooding events for inland cities as well.

4.7. <u>References</u>

Akaike H. 1974. A new look at the statistical model identification. IEEE Trans. Autom. Control 19: 716–722.

Ali, M.M., Mikhail, N.N., Haq, M.S., 1978: A class of bivariate distributions including the bivariate logistic. J. Multivar. Anal. 8 (3): 405–412.

Ciurean, R. L., Schroter, D., & Glade, T. (2013). Conceptual Frameworks of Vulnerability Assessments for Natural Disasters Reduction. In J. Tiefenbacher, Approaches to Disaster Management - Examining the Implications of Hazards, Emergencies and Disasters. Retrieved from http://www.intechopen.com/books/approaches-to-disaster-management-examining-the-implications-of-hazards-emergencies-and-disasters/conceptualframeworks-of-vulnerability-assessments-for-natural-disasters-reductio

Clayton, D.G., 1978: A model for association in bivariate life tables and its application in epidemiological studies of familial tendency in chronic disease incidence. Biometrika, 65 (1): 141–151

Corbella, S. and Stretch, D.D., 2013: Simulating a multivariate sea storm using Archimedean copulas. *Coastal Engineering* 76: 68-78.

De Bruijn, K.M., 2005: Resilience and flood risk management. A systems approach applied to lowland rivers. PhD thesis. Delft University of Technology, Delft, The Netherlands.

De Michele, C., Salvadori, G., Canossi, M., Petaccia, A., Rosso, R., 2005: Bivariate statistical approach to check adequacy of dam spillway. *J. Hydrol. Eng.*, 10 (1): 50–57.

De Michele, C., Salvadori, Passoni, G., Vezzoli, R., 2007: A multivariate model of sea storms using copulas. *Coastal Engineering* 54: 734-751

Favre, A.C., El Adlouni, S., Perreault, L., Thiémonge, N., Bobée, B., 2004: Multivariate hydrological frequency analysis using copulas. *Water Resour. Res*, 40 (1): W01101.

Francis, R., & Bekera, B. (2014). A metric and frameworks for resilience analysis of engineered and infrastructure systems. Reliability Engineering and System Safety, 121, 90 - 103.

Frank, M.J., 1979: On the simultaneous associativity of F(x, y) and x + y – F(x, y). Aequationes Math,19 (1): 194–226.

Gumbel, E.J., 1960: Distributions des valeurs extrêmes en plusieurs dimensions. *Publ. Inst.Stat. Univ. Paris*, 9: 171–173.

Joe, H., 1993: Parametric families of multivariate distributions with given margins. J. Multivar. Anal. 46 (2): 262–282.

Joe, H., 1997: Multivariate models and dependence concepts. Monographs on Statistics and Applied Probability Vol. 73. Chapman & Hall, London, UK.

Jones Edmunds and Associates, Inc., 2013: Floodplain Analysis, Cross Bayou Watershed Management Plan. Pinellas County Board of County Commissioners and Southwest Florida Water Management District.

Jordanger, L. A. and Tjostheim, D., 2014: Model selection of copulas: AIC versus a cross validation copula information criterion. Statistics and Probability Letters, 92(1): 249-255.

Joyce, J., Chang, N. B., Harji, R., Ruppert, T., and Imen, S., 2017: Developing a multi-scale modeling system for resilience assessment of green-grey drainage infrastructures under

climate change and sea level rise impact. Environmental Modelling and Software, 90: 1-26.

Khadka, M. S., 2008: Parameter estimation of Copula using maximum likelihood estimation (MLE) method. Oklahoma State University, ProQuest Dissertations Publishing.

Nelsen, R.B., 2006. An Introduction to Copulas, Springer Series in Statistics. Springer, NewYork, USA.

NOAA, 2016: Sea Level Trends. Accessed August 2016. [Available online at https://tidesand currents.noaa.gov/sltrends/sltrends.html

Omer. M., 2013: The resilience of networked infrastructure systems. World Scientific.

Park, J., Seager, T. P., Rao, P. S. C., Convertino, M. and Linkov, I., 2013: Integrating Risk and Resilience Approaches to Catastrophe Management in Engineering Systems. Risk Analysis, 33: 356–367. doi:10.1111/j.1539-6924.2012.01885.x

Patton, A., 2004: On the Out-of-Sample Importance of Skewness and Asymmetric Dependence for Asset Allocation, *Journal of Financial Econometrics*, 2(1): 130-168

Streamline Technologies, Inc., 2015: An Integrated Surface Water-Groundwater Model of the Cross Bayou Watershed

Trepanier, J.C., Needham, H.F., Elsner, J.B., and Jagger, T.H., 2014: Combining Surge and Wind Risk from Hurricanes Using a Copula Model: An Example from Galveston, Texas, *The Professional Geographer*, DOI:10.1080/00330124.2013.866437

Wahl, T., Mudersbach, C., Jensen, J., 2012: Assessing the hydrodynamic boundary conditions for risk analyses in coastal areas: a multivariate statistical approach based on Copula functions. *National Hazards and Earth Syst. Science*, 12, 495–510

Wahl, T., Jain, S., Bender, J., Meyers, S.D. and Mark E. Luther 2015:Increasing risk of
compound flooding from storm surge and rainfall for major US cities, Nature Climate
Change, doi:10.1038/nclimate2736

Wang, C., Chang, N.-B., and Yeh, G. (2009). Copula-based flood frequency (COFF) analysis at
the confluences of river systems. *Hydrological Process,* 23, 1471–1486.

Xu, K., Ma, C., Lian, J. and Bin, L., 2014: Joint probability analysis of extreme precipitation and
storm tide in a coastal city under changing environment. *PLoS One,* 9(10): e109341. doi:
10.1371/journal.pone.0109341.

Yodo, N. and Wang, P., 2016: Engineering Resilience Quantification and System Design
Implications: A Literature Survey, *Journal of Mechanical Design*, 138(11).

Zhang, L., Singh, V.P., 2007. Bivariate rainfall frequency distributions using Archimedean
copulas. J. Hydrol. 332 (1–2), 93–109.

Zhang Q, Li J, Singh VP, 2011: Application of Archimedean copulas in the analysis of the
precipitation extremes: effects of precipitation changes, *Theor Appl Climatol*, 107 (1–2):
255-264. doi:10.1007/s00704-011-0476-y.

CHAPTER 5: FINAL REMARKS

5.1. <u>Summary of Current Work</u>

Before risk or resilience can be undertaken, potential hazards and impacts must be assessed. Areas of concern may be more(less) at risk and/or less (more) resilient to certain combinations of hazards than others and vice-versa. The rationale for including resilience within risk is that without resilience, other components of risk such as vulnerability and exposure may have greater influence over time causing greater impacts. The information presented suggests that reducing the time of exposure can be linked to resilience. A resilient response is a response that reflects reduced time of exposure, subsequently reducing damage and overall risk. Information presented in this thesis has demonstrated that by surveying existing conditions and providing alternative courses of action, resilience can be a tangible concept for consideration in theory and in practice for risk assessment.

5.2. <u>Future Work</u>

- Impact of results on flood mapping and insurance policies (incorporation of resilience as a factor of flood insurance studies)

- Application potential in decision support framework for municipalities for emergency response

- Interdependency between drainage systems and transportation networks for advanced cascade impact assessment.

173

APPENDIX A: ICPR VALIDATION RESULTS
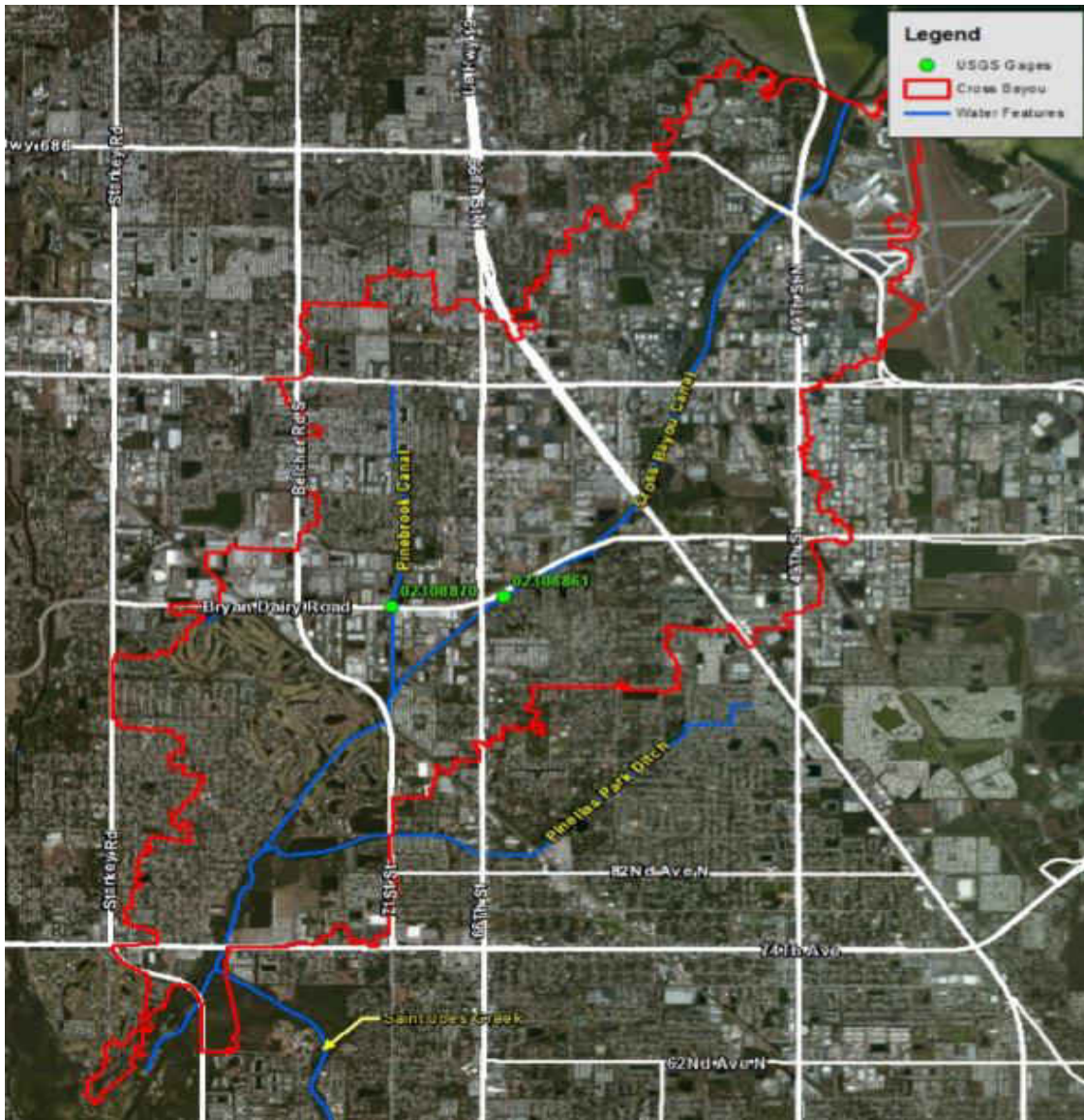
Fig.A.1. Location of USGS gauge stations for ICPR model validation (Source: Streamline Technologies, Inc., 2015)

Table A.1. USGS Gauge 02308861 Statistical Metrics

Period of Record	# of Gauge Measurements	R	R^2	ME	MAE	RMSE	N-S
01/01/2007-01/01/2014	121,954	0.841	0.708	0.101	0.224	0.305	0.624
01/01/2009-01/01/2014	86,872	0.865	0.748	0.065	0.208	0.283	0.705

Note: Gauge measurements are for stage. Six statistical metrics were considered: Correlation Coefficient (R), Coefficient of Determination (R2), Mean Error (ME), Mean Absolute Error (MAE), Root Mean Square Error (RMSE) and Nash-Sutcliffe Model Efficiency Coefficient (N-S).

Table A.2. USGS Gauge 02308860 Statistical Metrics

Period of Record	# of Gauge Measurements	R	R^2	ME	MAE	RMSE	N-S
01/01/2007-01/01/2014	122,606	0.895	0.807	0.014	0.049	0.092	0.794
01/01/2009-01/01/2014	87,539	0.910	0.827	0.025	0.050	0.096	0.815

Note: Gauge measurements are for stage. Six statistical metrics were considered: Correlation Coefficient (R), Coefficient of Determination (R2), Mean Error (ME), Mean Absolute Error (MAE), Root Mean Square Error (RMSE) and Nash-Sutcliffe Model Efficiency Coefficient (N-S).

APPENDIX B: LOW IMPACT DEVELOPMENT

Table B.1: Low Impact Development Utilized for the Purpose of Thesis

Low Impact Development	Description	Ecosystem Services
Retention basin http://www.stormwaterpa.org	▪ A recessed area within the landscape that is designed to store and retain a defined quantity of runoff, allowing it to percolate through permeable soils into the groundwater.	▪ Reduces stormwater volume, which reduces the average annual pollutant loading that may be discharged from the system. ▪ Suspended solids, heavy metals, bacteria, pesticides, and nutrients are removed as runoff percolates through the soil profile.
Treatment swales http://www.dot.ca.gov	▪ Have been used for conveyance of stormwater along roads for decades. ▪ When properly designed and maintained, swales can be used for stormwater treatment, providing retention and infiltration of stormwater.	▪ Provides reduction of stormwater volume which reduces pollutant loads. ▪ Suspended solids, oxygen demanding materials, heavy metals, bacteria, some varieties of pesticides, and nutrients may be removed as runoff percolates through the soil profile.

Low Impact Development	Description	Ecosystem Services
Pervious pavement http://nacto.org	▪ Pervious pavement systems include the subsoil, the sub-base, and the pervious pavement and include several types of designed systems such as pervious concrete, pervious aggregate products, pervious paver systems, and modular paver systems.	▪ Pervious pavement systems are retention systems and is an optional component of a treatment train to reduce stormwater volume and pollutant load from parking lots, or similar types of areas.
Greenroof/Cistern http://greencitygrowers.com	▪ A vegetated roof followed by filtrate storage in a cistern, which can be reused. ▪ The filtrate from the greenroof is collected in a cistern or, if the greenroof is part of a BMP treatment train, the filtrate may be discharged to a downstream BMP.	▪ The greenroof/cistern system functions to attenuate, evaporate, and lower the volume of discharge and pollutant load coming from the roof surface. ▪ Greenroof systems have been shown to assist in stormwater management by attenuating hydrographs,

Low Impact Development	Description	Ecosystem Services
		neutralizing acid rain, reducing volume of discharge, and reducing the annual mass of pollutants discharged.

APPENDIX C: SDSM CALIBRATION & VALIDATION

Table C.1. Predictor variables used for future rainfall projection

Center/Agency & Climate Scenario	Variable	Variable Description
Hadley Centre **CM2 AR4 A2**	h3a2p_fna	Surface airflow strength
	h3a2p_una	Surface zonal velocity
	h3a2p_vna	Surface meridional velocity
	h3a2p _zna	Surface vorticity
	h3a2p _zhna	Surface divergence
	h3a2p5_fna	500 hPa airflow strength
	h3a2p5_una	500 hPa zonal velocity
	h3a2p5_vna	500 hPa meridional velocity
	h3a2p5_zna	500 hPa vorticity
	h3a2p500na	500 hPa geopotential height
	h3a2p5zhna	500 hPa Surface divergence
	h3a2shumna	Surface specific humidity

Table C.2. SDSM Monthly Calibration Statistics

Month	R-Squared
January	0.329
February	0.477
March	0.266
April	0.559
May	0.429

Month	R-Squared
June	0.076
July	0.136
August	0.176
September	0.117
October	0.840
November	0.400
December	0.217

Note: Monthly SDSM calibration for Period of Sept 1998-Sept 2010 using log-transform of daily rainfall record for the same period and HADCM3 AR4 A2 predictor variables. R-squared represents goodness of fit of predictor variables in explaining occurrence of rainfall on a monthly basis for each station.

Observed vs. SDSM Monthly Mean Rainfall (Jan 2011–Jan 2014)

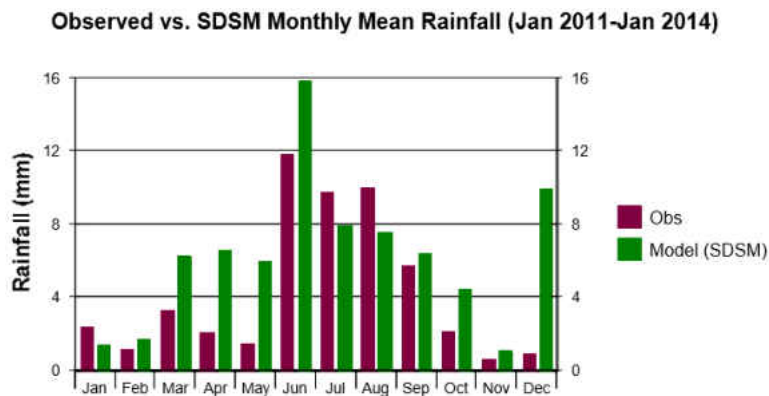**Fig. C.1: Observed vs. SDSM mean monthly rainfall for validation period (Jan 2011-Jan 2014)**

Observed vs. SDSM Monthly Variance (Jan 2011-2014)

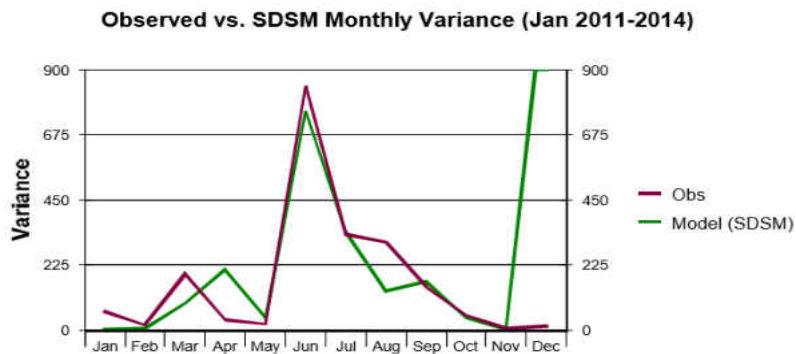**Fig.C.2: Observed vs. SDSM monthly variance for validation period (Jan 2011-Jan 2014)**

APPENDIX D: GREEN-AMPT PARAMETERS

Fig. D.1. NRCS Soil Zone Classification with Cross Bayou Watershed boundary in black

185

Table D.1. Soil Properties Used for Each NRCS Soil Zone from Figure D.1

Soil Zone	Vertical Hydraulic Cond. (m/d)	Saturated Moisture Content	Residual Moisture Content	Initial Moisture Content	Field Moisture Content	Wilting Moisture Content	Pore Size Index	Bubble Pressure (cm)	Allow Recharge	Initial Water Table(m)
1017080	7.895	0.411	0.003	0.020	0.020	0.005	0.568	4.144	Yes	0.790
1017083	7.930	0.440	0.033	0.145	0.145	0.065	0.496	2.499	Yes	0.010
1017106	20.128	0.401	0.002	0.013	0.013	0.004	0.570	4.327	Yes	1.080
1017100	7.951	0.399	0.007	0.036	0.036	0.013	0.561	4.162	Yes	0.080
1017112	7.817	0.422	0.016	0.093	0.093	0.031	0.560	3.673	Yes	0.030
1017088	11.940	0.394	0.002	0.012	0.012	0.004	0.570	4.440	Yes	0.310
1017092	4.552	0.412	0.011	0.053	0.053	0.021	0.495	3.870	Yes	0.360
1017087	7.276	0.407	0.010	0.050	0.050	0.019	0.481	4.004	Yes	0.140
1017086	7.133	0.417	0.017	0.087	0.087	0.033	0.488	3.797	Yes	0.180
1017107	6.897	0.408	0.007	0.042	0.042	0.014	0.553	3.849	Yes	0.360
1017104	6.926	0.443	0.030	0.123	0.123	0.059	0.521	3.834	Yes	0.010
1017089	1.779	0.422	0.023	0.103	0.103	0.045	0.471	3.610	Yes	0.050
1017094	6.262	0.424	0.014	0.068	0.068	0.028	0.515	3.652	Yes	0.690
1017090	6.977	0.402	0.008	0.045	0.045	0.015	0.575	4.430	Yes	0.360
1017091	7.951	0.828	0.007	0.745	0.745	0.429	0.392	22.617	Yes	0.080
1017096	20.558	0.403	0.008	0.038	0.038	0.016	0.581	4.590	Yes	1.450
1017085	5.087	0.407	0.012	0.050	0.050	0.023	0.488	4.046	Yes	0.140
1017097	6.409	0.422	0.015	0.062	0.062	0.029	0.493	3.227	Yes	0.290
1017110	6.483	0.395	0.001	0.004	0.004	0.002	0.541	4.311	Yes	0.380
1017098	7.879	0.453	0.013	0.080	0.080	0.025	0.516	2.651	Yes	0.160
1017099	6.927	0.411	0.004	0.030	0.030	0.008	0.573	4.264	Yes	0.790
1017095	7.951	0.732	0.028	0.416	0.416	0.201	0.396	5.218	Yes	0.020
1017093	7.913	0.419	0.008	0.045	0.045	0.016	0.532	3.296	Yes	0.720
1017082	7.911	0.398	0.003	0.023	0.023	0.006	0.572	4.422	Yes	1.400
1017105	6.262	0.424	0.014	0.068	0.068	0.028	0.515	3.652	Yes	2.011
1017108	5.873	0.398	0.011	0.055	0.055	0.022	0.493	4.150	Yes	0.360

Soil Zone	Vertical Hydraulic Cond. (m/d)	Saturated Moisture Content	Residual Moisture Content	Initial Moisture Content	Field Moisture Content	Wilting Moisture Content	Pore Size Index	Bubble Pressure (cm)	Allow Recharge	Initial Water Table(m)
1017103	7.723	0.667	0.025	0.371	0.371	0.180	0.418	5.473	Yes	0.020
1017109	6.262	0.424	0.014	0.068	0.068	0.028	0.515	3.652	Yes	0.003
1017111	6.262	0.424	0.014	0.068	0.068	0.028	0.515	3.652	Yes	0.003
OFFSITE	6.262	0.424	0.014	0.068	0.068	0.028	0.515	3.652	No	0.610

Note: During the initial simulations of a June 21-30, 2012 storm event for ICPR calibration, infiltration and recharge to the groundwater appeared high for pervious areas based on comparison with observed data. This resulted in lower modeled stages than observed at both of the USGS gauges. Low runoff volumes were caused by high saturated vertical conductivities based on the weighted average Green-Ampt parameters. It is believed that compaction in urban areas and "thatching" of grassed areas likely reduces the vertical conductivity at the surface. Thatching is caused by the build-up of organic matter (grass clippings) at the surface of the soils and can significantly reduce infiltration rates (Streamline Technologies, Inc., 2015). For this reason, calibrated vertical hydraulic conductivity values (Column 2) appear to be much lower and uniform than recorded by NRCS.

APPENDIX E: COPULAS ANALYSIS

Table E.1.Fitted Distributions for Hazard Variables for Target Year 2012

Variable	Fitted Distribution	Parameter(s) [location, scale, shape]
Tidal Stage	Generalized Extreme Value	[0.1836,0.1209,0.4494]
Rainfall	Generalized Extreme Value	[2.766,6.261e-04,2.190e-04]
Wind Speed	Generalized Extreme Value	[-0.1232,2.204,6.932]
Wave Height	Generalized Extreme Value	[0.2545,0.1488,0.2576]

Table E.2.Goodness of Fit Tests for Target Year 2012

Variable	# of Data points	Null Hypothesis	p-value	Chi-Squared	K-S
Tidal Stage	364	Data are consistent with proposed statistical distribution in Table 7	0.05	Rejects null hypothesis	Does not reject null hypothesis at 5% significance level
Rainfall	364	Data are consistent with proposed statistical distribution in Table 7	0.05	Does not reject null hypothesis at 5% significance level	Rejects null hypothesis

Variable	# of Data points	Null Hypothesis	p-value	Chi-Squared	K-S
Wind Speed	364	Data are consistent with proposed statistical distribution in Table 7	0.05	Rejects null hypothesis	Rejects null hypothesis
Wave Height	364	Data are consistent with proposed statistical distribution in Table 7	0.05	Rejects null hypothesis	Does not reject null hypothesis at 5% significance level

Table E.3. Tidal Stage versus Rainfall for Copulas Analysis for Target Year 2012

Tidal Stage vs. Rainfall			
Copula Family	Max. Log Likelihood Value	Dependence Parameter (θ)	AIC
Gumbel	8.55e-14	1.00	72.2
Clayton	577.7	0.100	-0.7182
Frank	-1.417e+05	0.100	-11

Table E.4. Tidal Stage versus Wind Speed for Copulas Analysis for Target Year 2012

	Tidal Stage vs. Wind Speed		
Copula Family	**Max. Log Likelihood Value**	**Dependence Parameter (θ)**	**AIC**
Gumbel	-1.405e-14	1.00	3.59-6.28i
Clayton	-67.06	0.100	4.51-6.28i
Frank	-42.22	0.100	75.8-6.28i

Table E.3. Tidal Stage versus Wave Height for Copulas Analysis for Target Year 2012

	Tidal Stage vs. Wave Height		
Copula Family	**Max. Log Likelihood Value**	**Dependence Parameter (θ)**	**AIC**
Gumbel	-4.47e-15	1.00	78.1 - 6.28i
Clayton	9.67e+02 - 1.093e+01i	0.675	-1.748 + 0.0226i
Frank	142.7	0.100	2.08

APPENDIX F: PERMISSION TO REPUBLISH MATERIAL

Attached are terms and conditions from Elsevier for republishing the following reference as supplement to Chapter 3 of this thesis:

Joyce, J., Chang, N. B., Harji, R., Ruppert, T., and Imen, S., 2017: Developing a multi-scale modeling system for resilience assessment of green-grey drainage infrastructures under climate change and sea level rise impact. Environmental Modelling and Software, 90: 1-26.

The inclusion of the aforementioned reference falls under the limited license section of the Elsevier terms and conditions regarding thesis/dissertation (line item 20) on the next page of this appendix section.

LIMITED LICENSE

The following terms and conditions apply only to specific license types:

15. Translation: This permission is granted for non-exclusive world English rights only unless your license was granted for translation rights. If you licensed translation rights you may only translate this content into the languages you requested. A professional translator must perform all translations and reproduce the content word for word preserving the integrity of the article. If this license is to re-use 1 or 2 figures then permission is granted for non-exclusive world rights in all languages.

16. Website: The following terms and conditions apply to electronic reserve and author websites:
Electronic reserve: If licensed material is to be posted to website, the web site is to be password-protected and made available only to bona fide students registered on a relevant course if:
This license was made in connection with a course,
This permission is granted for 1 year only. You may obtain a license for future website posting,
All content posted to the web site must maintain the copyright information line on the bottom of each image,
A hyper-text must be included to the Homepage of the journal from which you are licensing at http://www.sciencedirect.com/science/journal/xxxxx or the Elsevier homepage for books at http://www.elsevier.com , and
Central Storage: This license does not include permission for a scanned version of the material to be stored in a central repository such as that provided by Heron/XanEdu.

17. Author website for journals with the following additional clauses:
All content posted to the web site must maintain the copyright information line on the bottom of each image, and the permission granted is limited to the personal version of your paper. You are not allowed to download and post the published electronic version of your article (whether PDF or HTML, proof or final version), nor may you scan the printed edition to create an electronic version,
A hyper-text must be included to the Homepage of the journal from which you are licensing at http://www.sciencedirect.com/science/journal/xxxxx , As part of our normal production process, you will receive an e-mail notice when your article appears on Elsevier's online service ScienceDirect (www.sciencedirect.com).   That e-mail will include the article's Digital Object Identifier (DOI). This number provides the electronic link to the published article and should be included in the posting of your personal version. We ask that you wait until you receive this e-mail and have the DOI to do any posting.
Central Storage: This license does not include permission for a scanned version of the material to be stored in a central repository such as that provided by Heron/XanEdu.

18. Author website for books with the following additional clauses:
Authors are permitted to place a brief summary of their work online only.
A hyper-text must be included to the Elsevier homepage at http://www.elsevier.com.

All content posted to the web site must maintain the copyright information line on the bottom of each image.

You are not allowed to download and post the published electronic version of your chapter, nor may you scan the printed edition to create an electronic version.

Central Storage: This license does not include permission for a scanned version of the material to be stored in a central repository such as that provided by Heron/XanEdu.

19. Website (regular and for author): A hyper-text must be included to the Homepage of the journal from which you are licensing at http://www.sciencedirect.com/science/journal/xxxxx or for books to the Elsevier homepage at http://www.elsevier.com

20. Thesis/Dissertation: If your license is for use in a thesis/dissertation your thesis may be submitted to your institution in either print or electronic form. Should your thesis be published commercially, please reapply for permission. These requirements include permission for the Library and Archives of Canada to supply single copies, on demand, of the complete thesis and include permission for UMI to supply single copies, on demand, of the complete thesis. Should your thesis be published commercially, please reapply for permission.